STUDY OF UNZIPPING TRANSITIONS OF AN ADSORBED POLYMER AND BLOCK COPOLYMER DNA BY A PERIODIC FORCE

RAMU KUMAR YADAV

A thesis submitted for the partial fulfillment of the degree of Doctor of Philosophy

Department of Physical Sciences

Indian Institute of Science Education and Research Mohali
Knowledge city, Sector 81, SAS Nagar, Manauli PO, Mohali 140306, Punjab, India.

August 2022

This thesis is dedicated to my family.

Declaration

The work presented in this thesis has been carried out by me under the guidance of Dr. Rajeev Kapri at the Indian Institute of Science Education and Research Mohali. This work has not been submitted in part or in full for a degree, a diploma, or a fellowship to any other university or institute. Whenever contributions of others are involved, every effort is made to indicate this clearly, with due acknowledgement of collaborative research and discussions. This thesis is a bona fide record of original work done by me and all sources listed within have been detailed in the bibliography.

Ramu Kumar Yadav

(Candidate)

In my capacity as the supervisor of the candidate's thesis work, I certify that the above statements by the candidate are true to the best of my knowledge.

Dr. Rajeev Kapri

(Supervisor)

Acknowledgements

I would like to thank and express my deep gratitude to my thesis supervisor, Dr. Rajeev Kapri for his continuous support, guidance and suggestions from the beginning to the date. He has been always there whenever I needed him. He has always helped and encouraged me during my PhD. It is because of his guidance, my PhD went well.

I would also like to thank my doctoral committee, Dr. Abhishek Chaudhuri, Dr. Sanjeev Kumar and Dr. Yogesh Singh for supporting and helping me in IISER Mohali. Dr. Abhishek has always given me some valuable suggestions and helped me to understand many things related to my research. Thanks to the Library, Computer centre and Administrative staff of IISER Mohali for their cooperation. I am grateful to all faculty members and staffs of IISER Mohali for their direct or indirect support.

I would like to thank Dr. M Suman Kalyan for all the discussions I have done with him. I have learned a lot from him. I also thank Dr. Rajneesh Perhate. I wish to thank Andri Sharma. She has always been very friendly and supportive.

I am thankful to my school teachers Shambhu Sharan and Nathu Chauhan for their teaching and support to me. Nathu Chauhan sir always encouraged me to do study. I want to thank my physics teacher of class 11th and 12th, Parshuram Shukla, a very excellent teacher and an inspiration to me. He is one of the reason that I am studying physics today. I also thank Prof. Dhruwa Chand Srivastava for believing in me and supporting me in MSc. I am grateful to all my teachers who have taught me.

When it comes to friendship I would like to thank Shyam for 14 years of friendship and academic togetherness. Discussion with him about the every spectrum of life has made my journey of life enjoyable. I can not forget to thank my friends at IISER Mohali. They are Avinash, Sudhanshu, Sumit, Arnob, Shekhar, Anirban, Jyotsana, Anshu, Ankit Singh, Amit, Anzar, Aslam, Jaskaran, Deepak, Mayank, and Shubhendu. My other friends whom I am thankful to are Anuj, Vivek and Shailesh.

I wish to thank my brothers, sisters, cousins, nephews, brother in law, sister in laws, and all other relatives and well wishers for their support. The love and

support I get from my parents and family can not be expressed in words. These people have always supported me mentally and boosted my morale so that I can work fearlessly. I thank my brother Vinod Kumar Yadav for his support. Lastly, I would like to give a very special thank to my eldest brother Ashok Kumar Yadav for his constant support and encouragement. He has been very enthusiastic towards my academic success and achievements.

Abstract

This thesis aims to study the the dynamic transitions in unzipping of an adsorbed polymer from a surface (or wall), a homopolymer double stranded DNA (dsDNA), and the block copolymer dsDNA subjected to an external periodic pulling force. The unzipping transition, in the presence of a static pulling force, is well studied and is a first-order phase transition. The polymer unzips from the surface, and the DNA unzips to two single strands, only when the pulling force exceeds a critical value which depends on temperature. For the static force case the results do not depend on the DNA sequence. In the presence of a periodic force, it is found that the DNA, or the adsorbed polymer, can be unzipped from a zipped state to an unzipped state dynamically, either by varying the frequency of the periodic force keeping the amplitude fixed, or by varying the amplitude of the force at a constant frequency. The force-distance isotherms obtained from the time series of extension between the end monomers of the DNA (or the distance between the surface and the end monomer of the polymer) show hysteresis whose area acts as a dynamical order parameter. It is found that, at fixed force amplitude, the area of the hysteresis loop first increases, reaches to a maximum at some frequency that depends on the force amplitude, and then decreases as the frequency of the periodic force is increased. The area of the loop is found to scale differently at higher and the lower frequencies. The thesis studies how the dynamical order parameter behaves for various types of surfaces and various sequences for the block copolymer DNA. The thesis also studies the Stochastic Resonance phenomena in the unzipping of a homopolymer and block copolymer DNA by a periodic force.

Contents

List of Publications

1. **Ramu Kumar Yadav** and Rajeev Kapri, *Physical Review.* E, **103**, 012413 (2021), *Unzipping of a double-stranded block copolymer DNA by a periodic force.*

2. Ramu Kumar Yadav, arXiv:2207.11140 (2022), **Study of unzipping transitions in an adsorbed polymer by a periodic force**, Pre-print.

3. **Ramu Kumar Yadav**, M. Suman Kalyan, Rajeev Kapri, and Abhishek Chaudhuri, *Stochastic Resonance as a measure of dynamical transitions in periodically driven DNA* (to be submitted).

Chapter 1

Introduction

Polymers play a significant role in our life, and their use touches many aspects of human life. Because they fulfill the demands of modern life, our survival in this time is very hard without polymers. Over time, we are becoming more dependable on polymer. The term polymer in Greek means 'many parts' and refers to large molecules whose structure comprises multiple repeating units known as monomers, bound together by covalent chemical bonds. The polymer can have identical structural units (homopolymer) or different (heteropolymer). Broadly, polymers are of two types: naturally occurring polymers and synthetic polymers. Those found in plants and animals are natural polymers. Some of the well-known natural polymers are rubber, cellulose, etc., whereas plastics, nylon, polyethylene, to name a few, are synthetic polymers produced by a process known as polymerization [1]. A polymer can be produced from a monomer through a process called polymerization. For example, ethylene, which is a monomer, polymerizes to form polyethylene, a polymer.

$$nCH_2 = CH_2 \xrightarrow{polymerisation} -[-CH_2 - CH_2-]_n-$$

The type of polymerization mechanism used depends on the type of functional groups attached to the reactants. Biopolymers like proteins and nucleic acids play essential roles in biological processes. Polymers can also be classified based on the structure of the monomer chain. This category has the following classifications: linear, branched, or network polymers. In a linear polymer, the monomers are arranged linearly to form a long chain known as a backbone. The backbone

chain may have hundreds or thousands of monomers. Whereas in a branched-chain polymer, linear chains of a polymer form branches giving it a tree-like structure. Henceforth, by a polymer, we shall mean a linear polymer. A polymer contains a large number of single bonds around which rotations are possible, and various conformational states can exist. As a result, a polymer molecule can have a huge number of conformational states, and statistical methods can be used to explore the conformation of a polymer chain. The main interest is to know the global properties of the polymer, which remain valid for a large class of polymer chains. For this purpose, we need to omit the details of the polymer structure as much as possible and extract simple and universal features from it [2]. The simplest model used to describe a polymer is an ideal chain (or *freely-jointed chain*). It only assumes a polymer as a random walk and neglects any interactions among monomers. In this model, a chain consists of N links, each of length a, which can point in any direction independent of each other. The size of the polymer is given by the root mean square of the end to end vector $\vec{r}$ [2, 3]

$$R \sim \langle r^2 \rangle^{1/2} \sim N^{2\nu} \tag{1.1}$$

with $\nu = 1/2$. But, for real polymers, there is an excluded volume effect, i.e., two monomers cannot occupy the same space. This is a long-range (along the chain but short-range in space) interaction that swells the polymer. A model which takes care of excluded volume effect is a self-avoiding walk (SAW) on a lattice and is a suitable candidate to study real polymers. The size of the polymer is again given by Eq. (1.1) but with an exponent $\nu = 3/(d+2)$ in $d-$dimensions, obtained by Flory within a mean field approach. In one-, two- and three-dimensions, the values of ν are 1, 3/4 and 3/5, respectively, which are very close to the experimentally [4, 5] observed values and the numerical simulations [6].

1.1 Directed Polymer

A polymer configuration can be seen as a trajectory of a particle moving between two points. If all the trajectories between these points do not contain loops or overhangs, then these configuration are of a directed polymer. Formally, a directed polymer (DP) in $D = d + 1$ dimensions is a polymer which grows in a preferred direction and can have transverse fluctuations in d dimensions. A discretized ver-

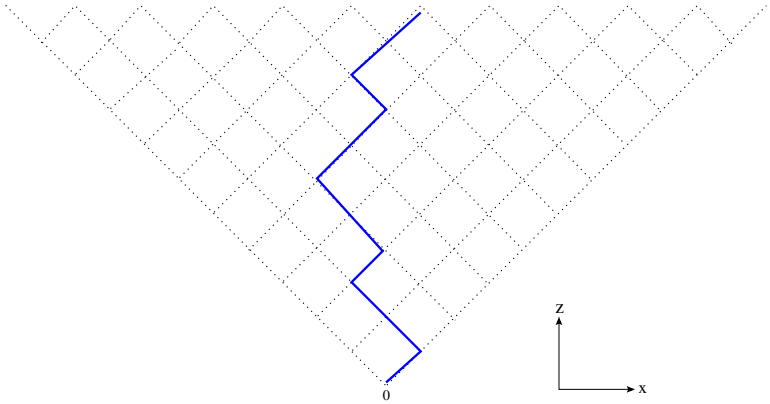

Figure 1.1: Schematic diagram of a DRW on a $D = 1 + 1$ square lattice. The walk is directed towards the diagonal (z direction) of the square but can have transverse fluctuations along x-direction.

sion of this is a directed random walk (DRW) on a lattice and can be defined as follows: If we choose $\vec{z}$ as a preferred direction, then for a DRW, the projection of each step on $\vec{z}$ is non zero [7] . For example, in $D = 1 + 1$, a directed walk that takes steps only along the positive diagonal of a square lattice can be mimicked as a directed polymer. A DRW , on a square lattice of $D = 1 + 1$ dimension, is illustrated in Fig. 1.1. Since there are two possible steps at each lattice point, therefore a polymer of length N has total 2^N configurations. In general, a directed polymer of length N in $D = d + 1$ dimensional hypercubic lattice has $(2d)^N$ configurations. A free DP or a DRW in continuum, is described by the Hamiltonian [8]

$$H_0 = \gamma \int_0^N \left(\frac{\partial \mathbf{r}(z)}{\partial z} \right)^2 dz, \tag{1.2}$$

where $\mathbf{r}(z)$ is the d-dimensional position vector of a monomer at a length z along the contour of the polymer from one end $z = 0$ and γ is the elastic constant. The above Hamiltonian represents purely entropic contribution which arises due to various conformation of the polymer. The partition function for the polymer is given by the path integral

$$Z(\mathbf{r}, z) = \int_{\mathbf{0},0}^{\mathbf{r},z} \mathcal{D}\mathbf{r}(z) e^{-\beta H_0}, \tag{1.3}$$

or equivalently, in differential form, by a Schrodinger equation (Diffusion equation) in imaginary time [3, 7]

$$\frac{\partial Z(\mathbf{r}, z)}{\partial z} = D\nabla^2 Z(\mathbf{r}, z), \tag{1.4}$$

where $D = 1/4\beta\gamma$ s the thermal diffusion constant. Its solution

$$Z(\mathbf{r}, z) = \frac{1}{\sqrt{4\pi D z}} \exp\left(\frac{-r^2}{2Dz}\right), \tag{1.5}$$

gives a normalized probability distribution of the position vector $\mathbf{r}$ at length z from the end at $(\mathbf{0}, 0)$. For a polymer of length N , the above distribution gives

$$\langle \mathbf{r} \rangle = 0, \qquad \langle r^2 \rangle = N, \tag{1.6}$$

where $\langle \cdots \rangle$ denotes thermal averaging. The transverse size of the polymer is therefore given by

$$R_{\perp,N} \sim \langle r^2 \rangle^{1/2} \sim N^{2\nu_\perp} \quad \text{with} \quad \nu_\perp = 1/2. \tag{1.7}$$

Along the z direction the polymer advances with a constant speed, therefore, the longitudinal size of the polymer is equal to its length

$$R_{\parallel,N} \sim N^{2\nu_\parallel} \quad \text{with} \quad \nu_\parallel = 1. \tag{1.8}$$

The DRW on a two dimensional lattice was studied numerically by Chakrabarti and Manna [9] and analytically by Szpilka [10]. The exponents $\nu_\perp = 1/2$ and $\nu_\parallel = 1$ are obtained by Cardy [11] using the field-theoretical description (in analogy with the work of de Gennes [12] on the self avoiding walk problem) and by Privman and Svrakic [13] using the generating function techniques in $d \geq 2$. These exponents are independent of dimensionality.

1.1.1 Applications as a model system

The DP model has many vital applications in statistical physics. For over five decades, it has been used (both in a pure as well as in a random medium) to understand a variety of interesting physical situations where one is concerned with the statistical fluctuations exhibited by an essentially linear elastic object, such as longitudinally stretched polymers in a gel matrix, vortex lines in ceramic superconductors, growing surfaces, morphology, and statistics of self-affine fractal tear lines in paper, domain walls in $2d$ dirty magnets, dislocation lines in disordered solids, spin glasses, etc. (see Halpin-Healy and Zhang [14] and references therein). By the

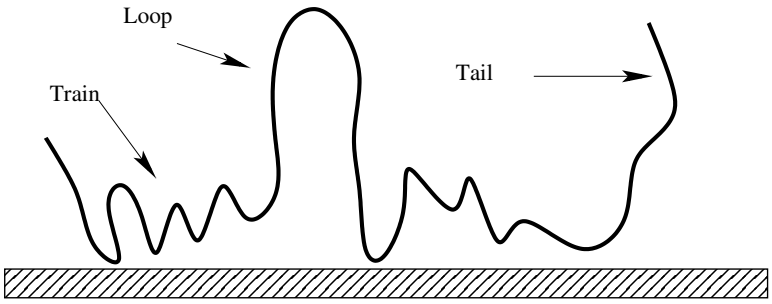

Figure 1.2: Schematic representation of an adsorbed polymer chain at the solid-liquid interface.

passage of time, its application has been growing. The DP model has also been used to study the homopolymer DNA unzipping transition [15, 16, 17, 18, 19, 20, 21], and block copolymer DNA unzipping transition [22], which is the first step towards biological processes like DNA replication and RNA transcription. Recently, the DP model has been adapted in the study of stochastic resonance in the unzipping of DNA.

1.2 Polymer Adsorption

Polymers in solution may readily get adsorbed onto various surfaces where there is an attractive interaction between segments of the polymer and the surface, which overcompensates for the conformational entropy loss of the polymer upon adsorption. This is one of the most important phenomena and has enormous implications in many processes such as lubrication, adhesion, surface protection, coating of surfaces, wetting, vortex lines, biology, etc [23]. The adsorption process of polymers onto a surface is largely governed by the prevailing conditions under which polymer, solvent, and surface interact. The adsorption process depends on the type of surface on which the polymer is adsorbed, with its internal structure. There are three different kinds of surfaces where polymers are adsorbed. The surface can either be penetrable (to be called soft-wall) or it can be impenetrable (hard-wall). Furthermore, a soft-wall can be either homogeneous or heterogeneous. For the former case, the polymer has the same affinity on either side of the wall, whereas it has different affinities for the heterogeneous case. An adsorbed polymer chain on the interface of solid-liquid is represented in Fig. 1.2. A review of polymer adsorption can be seen in Netz and Andelman [24].

1.2.1 Adsorption-desorption transition

In the above section, we have defined the physical situation under which a polymer gets adsorbed onto an attractive surface. This adsorbed polymer needs to be desorbed from the surface, which can be done by increasing the temperature. At low temperatures, the polymer remains in an adsorbed phase because it gains energy due to attraction with the wall, whereas at high temperatures, the desorbed phase dominates and the polymer gains entropy. This competition between the energy and the entropy (to minimize the total free energy) causes a phase transition known as the adsorption-desorption transition. This happens at a critical temperature T_d, which is known as the desorption temperature [25] . The adsorption-desorption transition of a polymer, up to an extent, is similar to the denaturation transition of a double-stranded DNA (dsDNA), where the two strands of the DNA get separated at melting temperature T_M. The transition is monitored by a physical quantity, $\langle m \rangle$, which is the fraction of monomers adsorbed on the surface. Above the critical temperature T_d, polymer favors to being in desorbed phase with $\langle m \rangle = 0$. Below the critical temperature T_d, the fraction $\langle m \rangle$ is finite and increases as temperature T decreases. At low T, the polymer is in a completely adsorbed phase with fraction $\langle m \rangle = 1$. At critical temperature

$$\langle m \rangle \sim N^{\phi}, \tag{1.9}$$

where ϕ is the crossover exponent. In $d = 2$, the value $\phi = 1/2$, has been obtained exactly using the conformal invariance and numerically by using Monte Carlo simulations and transfer matrix studies [7]. The adsorption-desorption transition has been studied over six decades [26, 27, 28, 29, 30, 31, 32, 33, 34]. The scaling arguments were given by deGennes [27] which were supported by the mean-field calculations [23]. The exact solutions for the Gaussian (non self-avoiding) polymer were found by Rubin [26], and for the self-avoiding directed polymers by Privman et al. [28, 29] in two and three dimensions.

1.2.2 Unzipping transition

An adsorbed polymer can also be removed from the surface by applying a pulling force (see the Fig. 1.3). The adsorption-desorption transition induced by force is known as unzipping transition. When a pulling force g is applied on one end of the

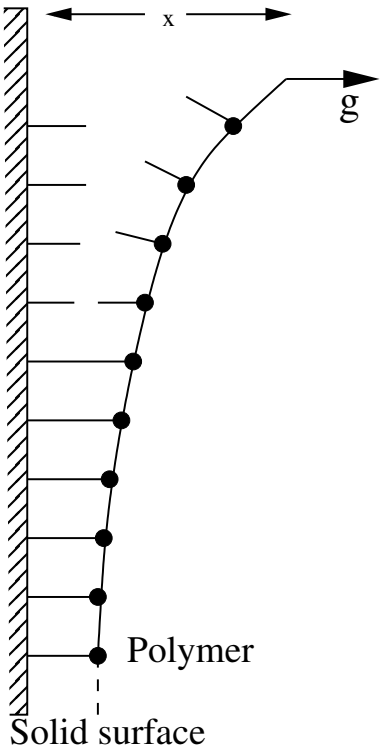

Figure 1.3: Schematic diagram of unzipping of an adsorbed polymer by a force g.

polymer keeping the other end fixed, it is found that the polymer unzips from the surface if the force exceeds a critical value g_c [35, 36, 37, 38, 39, 40]. The polymer remains in an adsorbed phase below this critical force, while above it, the polymer is in the unzipped phase. The unzipping of an adsorbed polymer from the surface is a first-order phase transition. The unzipping transition of a directed polymer is studied by Kapri and Bhattacharjee [35] by using generating function and the exact transfer matrix techniques in a pure as well as in a random medium. Whittington et. al. [36] studied the unzipping of a directed copolymer and Mishra et al. [38] used exact enumeration to study the unzipping of a self-avoiding polymer.

1.3 Copolymer

A copolymer is a polymer that is made up of more than one species of monomer. Several commercially essential polymers are copolymers. For example, polyethylene-vinyl acetate (PEVA), nitrile rubber, and acrylonitrile butadiene styrene (ABS) are copolymers. Schematic diagram of PEVA is shown in Fig. 1.4. The process of forming a copolymer by the use of multiple species of monomers is known as copoly-

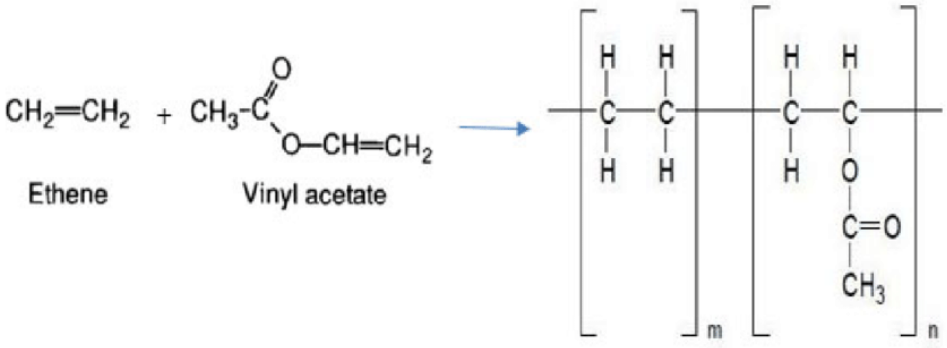

Figure 1.4: Monomer and structure of Poly(ethylene-co-vinyl acetate)(PEVA) copolymer.

merization. It is frequently used to improve or modify specific properties of plastics. A homopolymer is a polymer that is formed only from one type of monomer unit. Copolymers derived from copolymerization of two monomer species are sometimes called bipolymers. Copolymers can be built in various patterns. They are categorized based on their structures. Single chain copolymers are known as linear copolymers, whereas those having polymeric side chains are called branched copolymers. On the basis of the arrangement of the monomers on the main chain, the linear copolymers can be further divided into several categories such as block copolymers, statistical copolymers, alternating copolymers, periodic copolymers, gradient copolymers, and stereoblock copolymers. Whereas a branched copolymer is a polymer in which the monomers form a branched structure. Some essential types of branched copolymers are star, comb, grafted, and brush copolymers [41].

1.3.1 Block Copolymer

When more than one homopolymer unit is attached chemically, the resulting single-chain macromolecule is called a block copolymer [41]. The intermediate non-repeating unit at which the two homopolymer chains are attached is known as a junction block. There are two homopolymer blocks in a diblock copolymer, whereas a triblock copolymer contains three different blocks of homopolymers. A famous example of such a block copolymer is acrylonitrile butadiene styrene, commonly referred to as SBS rubber. Automobile tires are made up of SBS rubber. The blocks in SBS rubber are polystyrene and polybutadiene (StyreneButatineStyrene). An example describing the structure of a block copolymer which is made up of the monomers 'A' and 'B' is provided below.

$$-A-A-A-A-B-B-B-B-A-A-A-A-B-B-B-B-$$

is a block copolymer where $-A-A-A-A-$ and $-B-B-B-B-$ groups are the blocks.

1.4 DNA: The genetic information carrier of life

1.4.1 DNA structure

DNA is known as Deoxyribonucleic Acid, which is a genetic material that is inside all living organisms. It is an organic compound with a unique molecular structure. It is a very long, double-stranded polymer, where each strand contains a sequence of nucleotides and its two complementary polymeric chains twisted about each other in the form of a regular right-handed double helix [42]. There are three components in a nucleotide: sugar, phosphate, and nitrogen base. In a polymeric chain of nucleotides, the sugar of each nucleotide is attached by a phosphate group to the sugar of the adjacent nucleotide. The sugar and phosphate groups are always attached together by the same chemical bonds, known as the sugar-phosphate backbone.The two strands run in opposite directions. The sugar and the phosphate are the same for each nucleotide, whereas there are four possible bases in the DNA alphabet: cytosine (C), guanine (G), adenine (A), and thymine (T). The two strands in the molecule are held together by hydrogen bonds between the bases according to the Watson-Crick pairing scheme, shown in Fig. 1.5. Adenine (A) on one chain is always paired with thymine (T) on the other chain, and, likewise, guanine (G) is always paired with cytosine (C). An important feature of Watson-Crick pairing is that the base pairs have exactly the same geometry. The two strands are complementary to each other. It means, if one knows the sequence of one strand, the sequence of the other can be figured out, as the bases will be those that form hydrogen bonds with the bases in the first strand. Formally, this is known as double-stranded DNA(dsDNA). But, DNA molecule is not always double-stranded helical structures, sometimes they occur in single-stranded form called ssDNA. Even though both have the same chemical composition and can act as genetic material, they also show some characteristics differences.

Two factors primarily responsible for the stability of the DNA double helix are

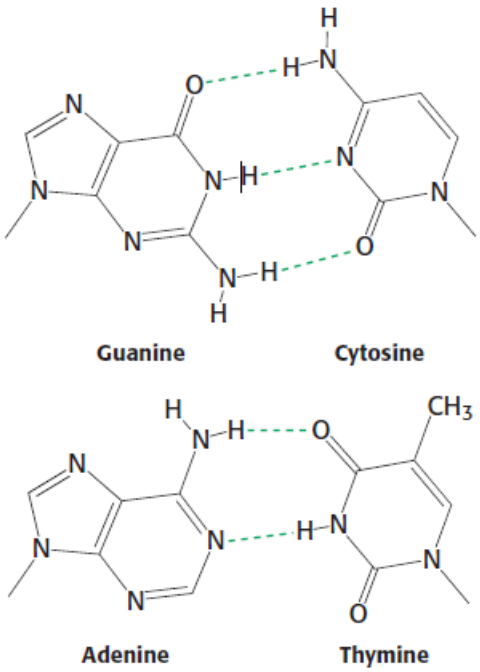

Figure 1.5: The DNA base pairs. Dashed lines represent the hydrogen bonds.

base pairing between complementary strands and stacking interaction between adjacent bases. The hydrogen bonds between complementary bases are a fundamental feature of the DNA double helix, which contributes to the thermodynamic stability of the helix and the specificity of base pairing. However, hydrogen bonds are not the only force that stabilizes the double helix. Another significant contribution comes from stacking interactions between the bases. The bases are flat, relatively water-insoluble molecules, and they tend to stack above each other roughly perpendicular to the direction of the helical axis [42]. The structure of the dsDNA is shown in Fig. 1.6.

DNA is a hereditary material responsible for carrying and transmitting genetic information that passes from one generation to the next. Apart from being responsible for inheriting genetic instructions in all living organisms, DNA also plays a crucial role in producing proteins. Each strand of the DNA double helix carries the same information – their base sequences are complementary. This information can be read only if the strands of the DNA come apart, which is essential in the biological processes like DNA replication and RNA transcription [45]. In the following, we briefly introduce these processes.

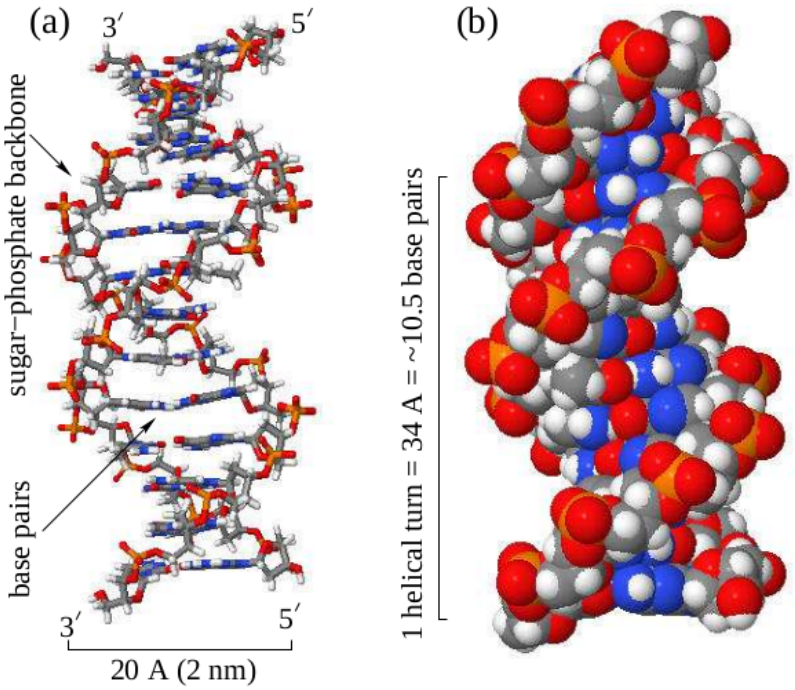

Figure 1.6: Structure of the B-DNA Duplex CGCGGTGTCCGCG in solution. (a) The stick model, and (b) the space filling model. The coordinates are taken from the protein data bank [43] (PDB key 1LAI [44]) and plotted using Jmol: An open-source Java viewer for three-dimensional molecular structures (http://www.jmol.org/).

Summary of DNA replication

DNA replication is one of the most important processes in biology. DNA encodes all the information that is passed on to the next generation of cells, and it must be rapidly and faithfully copied when the time comes for cells to divide. The replication of DNA is executed by molecular machines called DNA polymerase, which travel along the DNA molecule as it replicates it. DNA replication is semi-conservative, where each strand in the DNA double helix acts as a template for the synthesis of a new, complementary strand. The basic mechanisms of DNA replication are similar across organisms. During the process, the two parental strands of DNA separate, and each acts as a template to direct the synthesis of a new complementary daughter strand following the normal base pairing rules (A with T; G with C). The two new double-stranded molecules then pass to the two daughter cells at cell division. The point at which separation of the strands and synthesis of new DNA takes place is called the replication fork (or Y-fork). The

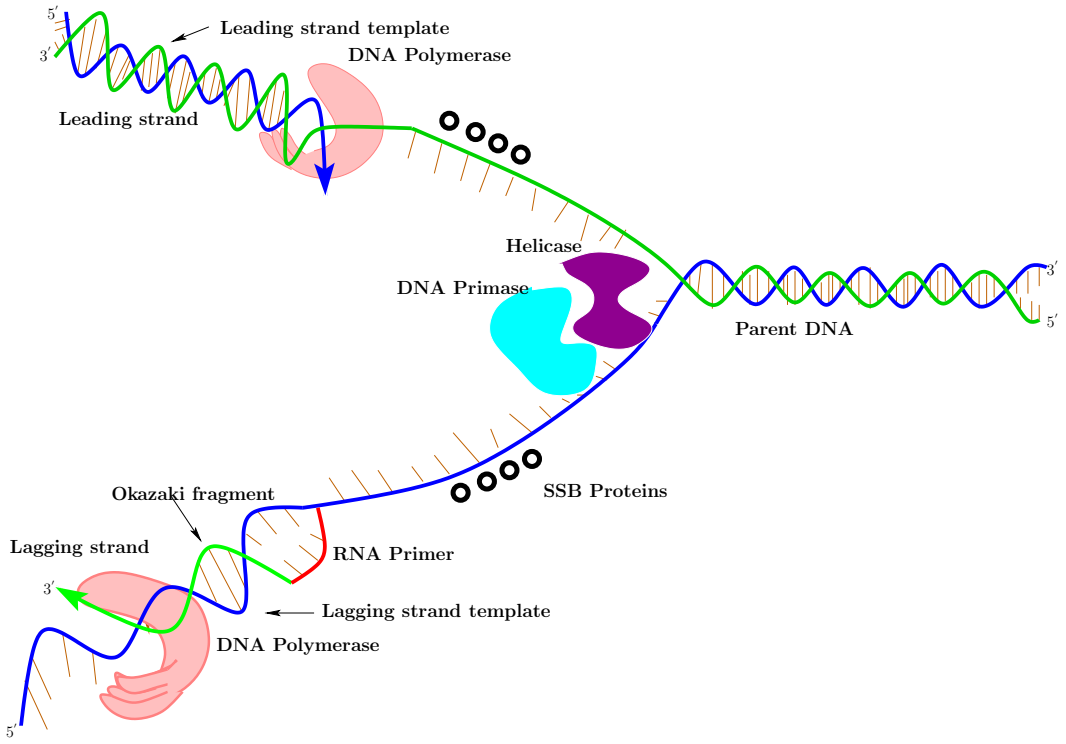

Figure 1.7: Schematic representation of DNA replication.

schematic diagram of DNA replication is shown shown in Fig. 1.7. Several studies suggest that the force acting at the junction of the Y-fork on the DNA is periodic in nature [46, 47, 48, 49]. Molecular motors like helicases are driven by adenosine triphosphate (ATP) in a living system. The periodic hydrolysis of ATP to adenosine diphosphate (ADP) can generate a continuous push and pull type of motion. These chemomechanical cycles suggest that biological machines act like repetitive force generators, and it is believed that biomolecules in many physiological conditions experience forces with periodic signatures. For example, it has been postulated that DNA-B, a ringlike hexameric helicase, pushes through the DNA like a wedge and produces unidirectional motion and strand separation [50]. The active rolling model and the inchworm model are two mechanisms which suggest that plasmid copy reduced (PcrA) helicase goes through a cycle of pulling the dsDNA part of the DNA and then moving on the ssDNA part during the ATP hydrolysis [51]. Similarly, the viral RNA helicase NPH-II hops cyclically from the double-stranded to the single-stranded part of the DNA and back during the ATP hydrolysis cycle [52].

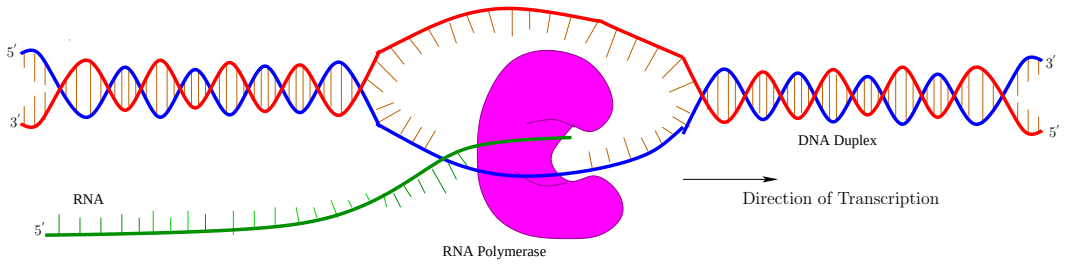

Figure 1.8: Schematic diagram showing the unzipping of dsDNA by RNA polymerase during RNA transcription.

Summary of RNA transcription

RNA transcription is a cellular process in which RNA is synthesized using DNA as a template. It is the first step of gene expression that involves the formation of an RNA molecule from DNA. The genetic information flows from DNA to protein, and this flow of information takes place in a sequential process of transcription and translation [53]. Only one strand of DNA is copied during the process of transcription, known as the template strand, and the RNA formed is called the mRNA. RNA polymerase is the enzyme involved in transcription. It uses single-strand DNA to synthesize a complementary RNA strand. RNA polymerase binds to specific DNA sequences called promoters to initiate RNA synthesis, resulting in local DNA unwinding. The position of the first synthesized base of the RNA is called the start site. RNA polymerase moves along the DNA and sequentially synthesizes the RNA chain. DNA has unwound ahead of the moving polymerase, and the helix is reformed behind it. RNA synthesis always occurs in a fixed direction, from the 5′- to the 3′-end of the RNA molecule. RNA polymerase recognizes the terminator sequence on the DNA that causes no further ribonucleotides to be incorporated. These sequences often contain self-complementary regions, which can form a stem-loop or secondary hairpin structure in the RNA product. These cause the polymerase to pause and subsequently cease transcription [42]. A schematic diagram of RNA transcription is shown in Fig. 1.8.

1.4.2 Block copolymer DNA

DNA can be particularly designed and conjugated with synthetic polymers to produce DNA block polymers, named as DBCs [54]. DBCs behave like DNA and polymers since they are made out of DNA segments. As a result of incorporating the DNA segment into the block copolymer, DBCs will have several unique qualities not found in traditional block copolymers, such as exact chemical structure segment, specialized self-assembly driving force, and molecular recognition, etc. Although the first DBC was synthesized in the late 1980s [55], this new material class has gotten much attention and has been a popular candidate for novel nanostructure design and construction in the last two decades [56, 57].

1.5 Melting of DNA

The hydrogen bonds between the bases of the complementary strands in the dsDNA can be easily broken to form two separate strands of the DNA. This process is known as melting of DNA. This can be carried out in various ways:

1. By chemical agents in neutral pH, known as chemical denaturation.
2. By increasing the temperature of the solution of DNA, known as thermal denaturation or melting of dsDNA.
3. By applying an external pulling force on the two strands of dsDNA. This process is known as DNA unzipping.

1.5.1 Chemical denaturation of DNA

Compounds, such as urea (H_2NCONH_2) and formamide ($HCONH_2$), can cause the denaturation of DNA at neutral pH by disrupting the hydrophobic forces between the stacked bases. Urea and formaldehyde contain functional groups that can form H-bonds with the electronegative centers of the N-bases. At the high concentrations (8M urea or 70% formamide) of the denaturant, the competition for H-bonds favor interactions between the denaturant and the N-bases rather than between complementary bases. As a result, the two strands separate. The dsDNA

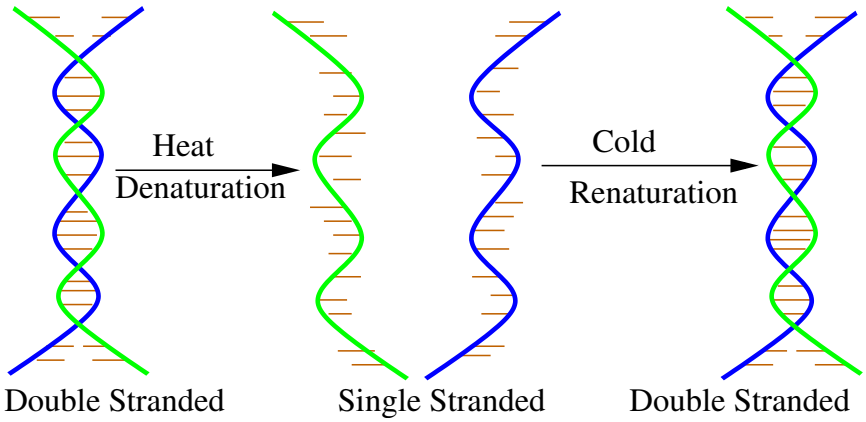

Figure 1.9: Schematic diagram showing thermal denaturation of a double-stranded DNA into two single strands and vice-versa.

can also be denatured by the extreme pH conditions. In the acidic medium, the ring nitrogens of A, G, and C get protonated by the acid while the ring nitrogens of G and T get deprotonated in the alkaline medium. This changes their electronic configuration, so they no longer donate electrons to the aromatic rings. Therefore, the bases are no longer planar or aromatic. The protonation state of the non-ring nitrogens are also changed. This affects the specific hydrogen bonding between the base pairs, with the result that the double-stranded structure breaks down; that is, the DNA becomes denatured [45]. The pH of melting depends on the mole fraction of GC pairs on the DNA. Larger the mole fraction of GC pairs, the higher the pH of melting.

1.5.2 Thermal denaturation

When a DNA solution is heated enough, the dsDNA unwinds, and the hydrogen bonds that hold the two strands together weaken and finally break. This process is known as DNA denaturation. The denaturation (melting) of the DNA is a cooperative phenomenon. The melting of the ends of the DNA and a more mobile AT-rich internal region will destabilize adjacent areas in the helix, leading to a progressive and concerted melting of the whole structure at a well-defined temperature known as the denaturation or melting temperature (T_m). At T_m, 50% base-pairs of the DNA are broken. The amount of strand separation, or melting, is measured by the absorbance of ultraviolet (UV) light passed through a solution of the DNA. Nucleic acids absorb maximum UV light at a wavelength of $\lambda_{max} = 260$ nm because of the electronic structure of their bases. The absorbance at 260 nm (A_{260}) is greatest

for isolated nucleotides, intermediate for ssDNA, and least for the dsDNA. When two strands of DNA come together, the close proximity of the bases in the strands quenches some of this absorbance. When the two strands separate, this quenching disappears, and the absorbance rises 30% to 40%. The melting temperature T_m is a function of the G+C content of the DNA sample and ranges from 80°C to 100°C for long DNA molecules. While the ratio of G (Guanine) to C (Cytosine) and A (Adenine) to T (Thymine) in an organism's DNA is fixed, the GC content (percentage of G +C) can vary considerably from one DNA to another. Because G-C pairs form three hydrogen bonds, while A-T pairs form only two, the higher the percentage of GC content, the higher its T_m. Thus, A double-stranded DNA rich in G and C needs more energy to denature than the one rich in A and T, thus having higher melting temperature (T_m). However, this complete separation of DNA strands by thermal denaturation is reversible. When the solution of denaturated DNA is slowly cooled, the single strands often meet their complementary strands and renature to a regular double helix. A schematic diagram showing the thermal denaturation and renaturation of DNA is shown in Fig. 1.9. For a review on the thermal denaturation of DNA, see Ref. [58]. In experimental study, it is customary to obtain the differential melting curves, i.e., dA_{260}/dT vs T. These curves either show a single peak or several peaks whose positions and heights depend on the sequence length, composition and the salt concentration. For very short sequences (about $10^2 - 10^3$ base pairs), the melting curve shows a single peak indicating a sudden denaturation of the two strands. This peak is quite broad and gets rounded due to the strong finite-size effects. For chains of intermediate lengths ($\approx 10^3 - 10^4$ base pairs) there are several peaks of typical width of about 0.5°C or less. These peaks are the signatures of sharp transitions of cooperatively melting regions. For very long chains ($\approx 10^6$ base pairs), there is again only a single broad peak covering about 15°C to 20°C, which is the overlap of many individual peaks associated with the denaturation of single domains. On the theoretical side, the DNA denaturation has been studied over six decades and various models have been proposed [18, 59, 60, 61, 62, 63, 64, 65, 66, 67, 68, 69, 70, 71, 72, 73, 74]. These studies are based either on the Poland Sheraga model [60] or the Peyrard Bishop model [62]. All these models agree that the thermal denaturation of the DNA is a phase transition, but the order of the transition depends on the model used. Some models [18, 59, 60, 61, 62] predict thermal denaturation is a continuous transition while the others [63, 64] predict it is a discontinuous transition.

1.5.3 Force induced unzipping

The separation of the strands of a dsDNA into two single strands, either by increasing the temperature (around $80 - 100°C$) or in extreme pH conditions cannot be relevant processes in the physiological conditions ($37°C$ and at neutral pH) found in living organisms. Instead, in biological processes, like DNA replication and RNA transcription, it is found that the enzymes and other proteins exert mechanical force on the DNA to separate the two strands apart. This separation by a mechanical force is known as unzipping transition [15]. In the last two and half decades, the advent of single-molecule manipulation techniques have made it possible to apply a piconewton force on a single DNA molecule to study the unzipping transition. In the following subsections, we review the theoretical and experimental studies done so far to understand the unzipping transition.

Theoretical studies

The simple coarse-grained models have been used to study DNA unzipping theoretically. In these models, the two strands of the DNA are described as two interconnected polymeric chains. These chains are either defined on a lattice as a self-avoiding walks [19, 20, 21, 22], or in the continuum as worm like chain [75, 76, 77, 78, 79, 80]. A constant pulling force is applied at one end of the DNA, which pulls apart it's two strands. These simple models can be solved analytically and predict the universal properties of the unzipping transitions, such as the order of transition, phase diagram etc. quite well. The two important models worth mentioning are Poland Scheraga (PS) model [60, 81, 82], and the Peyrard–Bishop–Dauxois (PBD) model [62, 83, 84, 85] whose simple extensions are used extensively to study the unzipping transition.

Consider a homopolymer DNA of length N which is under the influence of an applied pulling force $\mathbf{g}$ at one end ($z = N$) while the other end ($z = 0$) is kept fixed. The Hamiltonian of dsDNA in the continuum can be written as [15]

$$\begin{aligned} H_D &= H_0 + H_{\mathbf{g}} \\ &= \int_0^N dz \left[\frac{1}{2} \left(\frac{\partial \mathbf{r}_1(z)}{\partial z} \right)^2 + \frac{1}{2} \left(\frac{\partial \mathbf{r}_2(z)}{\partial z} \right)^2 + V(\mathbf{r}(z)) \right] - \int_0^N \mathbf{g}.\frac{\mathbf{r}(z)}{z} dz \end{aligned} \tag{1.10}$$

where $\mathbf{r}_i(z)$ is the d-dimensional position vector of a monomer at a length z along the contour of the ith strand from the anchored end, $V(\mathbf{r}(z))$ is the binding potential, and $\mathbf{r}(z) = \mathbf{r_1}(z) - \mathbf{r_2}(z)$ is the relative coordinate. By mapping Eq. (1.10) to a non-Hermitian quantum Hamiltonian [86, 87, 88]

$$H_q(g) = \frac{1}{2}(p + ig)^2 + V(\mathbf{r}) \tag{1.11}$$

with p as momentum, Bhattacharjee [15] found that the dsDNA unzips to two single strands if the pulling force exceeds a critical value. The separation between the strands of DNA shows a discontinuous increase as g approaches g_c from below, which implies that the unzipping is a first-order phase transition. The above model has been generalized to study the unzipping for the heterogeneous DNA case [89, 90, 91, 92, 93, 94, 95]. The unzipping of DNA can be studied in two different ensembles: (1) fixed force ensemble, and (2) fixed distance ensemble. In the fixed force ensemble, a constant pulling force g is applied on the strands of the DNA, whereas in the fixed distance ensemble, the separation x between the strands is kept constant. A class of exactly solvable models for a homopolymer DNA in $D = d+1$ dimensions are studied by Merenduzzo *et al.* [17, 18], and the phase diagram of unzipping have been obtained in the force-temperature plane. The phase diagrams contain two different phases of the dsDNA named as the zipped and the unzipped phases. In the zipped phase, the DNA is a double-stranded chain i.e., the hydrogen bonds between the base pairs are not broken; however, in unzipped phase, the hydrogen bonds between the base pairs are broken, and the strands of the DNA get separated from each other like a zipper. In these models, the existence of a cold unzipping transition was observed towards low temperatures, where the critical pulling force increases with increasing temperature. The dynamics of dsDNA in unzipping transition has also been studied [18, 96]. Based on such models, a phase coexistence based mechanism [97] and a front propagation [98] for helicase motion is proposed. These models have also been extended to investigate the transcription of RNA by applying a force pulling at an intermediate point [99, 100, 101, 102]. In these studies, in addition to the usual zipped and the unzipped phases, a new phase, which was called the eye phase, appeared in the phase diagram. The eye phase resembles the transcription bubble produced at the initiation of RNA transcription. The complete phase diagram of DNA unzipping was observed by Kapri et al. [99] in both the fixed distance and the fixed force ensembles. The phase diagrams are found to be independent of the ensemble used for the end case but showing strong ensemble dependence for the intermediate point. Using exact enumeration, Giri and

Kumar [103] studied the effect of saturation of hydrogen bonding on a dsDNA. They found the eye phase and ensemble dependence even for the DNA of finite lengths. They also studied pulling direction dependence on the phase diagrams and obtained various intermediate phases [104]. The nature of the unzipping transition is found to be the same even after introducing the semiflexibility of the DNA strands [105] The role of single-strand binding proteins on DNA unzipping has also been studied by modeling the nature of binding by a randomly oriented force [106, 107]. It was found that the DNA unzips, even in the absence of a constant pulling force at the end, to two singles strands if the force fluctuation is increased. The transition, however, in this case, becomes continuous. The possible applications of DNA unzipping have also started coming up. There are some studies [108, 109, 110] that see mechanical unzipping as a potential tool for DNA sequencing.

Over the past one decade, unzipping of biomolecules by a periodic force has drawn some attention. If biomolecules are subjected to a periodic forcing, they can unbind and rebind with a hysteresis in their force-distance isotherms. The study of hysteresis in unbinding and rebinding of biomolecules can provide useful information on the kinetics of conformational transformations, the potential energy landscape, controlling the folding pathway of a single molecule, and in force sensor studies[111, 112, 113, 114, 115]. In recent years, the behavior of a dsDNA under a periodic force has been studied using Langevin dynamics simulation of an off-lattice coarse-grained model for a short homo-polymer DNA chains [75, 76, 77, 78, 79] and Monte Carlo simulations on a relatively longer chains of directed self-avoiding walk (DSAW) model of a homo-polymer dsDNA [19, 20, 21], and a block copolymer DNA [22] on a 2-dimensional square lattice. In both type of studies, a dynamical phase transition was found to exist, where the DNA can be taken from the zipped state to an unzipped state with an intermediate dynamic state. It was found that the area of the hysteresis loop, A_{loop}, which represents the energy dissipated in the system, depends on the frequency of the periodic force for the homo-polymer chains, however for block copolymer DNA, A_{loop} depends on the frequency of periodic force as well as the block copolymer DNA sequence and on the base pair type on which the periodic force is acting. At higher frequencies, it decays with frequency as $A_{loop} \sim 1/\omega$, whereas at lower frequencies, it scales with the amplitude g_0 and frequency ω of the oscillating force as $A_{loop} \sim g_0^{\alpha}\omega^{\beta}$. The values of exponents α and β are however found to be different in these studies. In a recent study [80], using Langevin dynamics simulations on longer double-stranded DNA chains, the value of exponents has been obtained. These values are same as the exponents

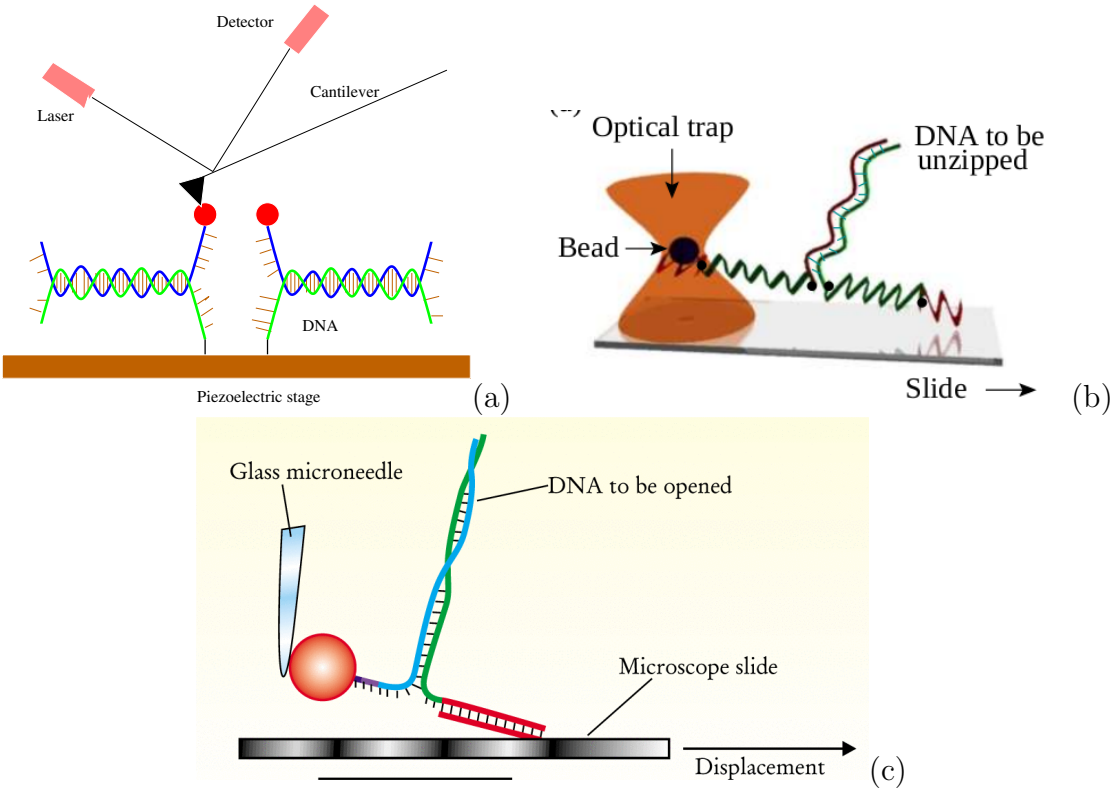

Figure 1.10: Schematic diagrams of various experimental setups used to study DNA unzipping. (a) Atomic force microscope (AFM), (b) Laser optical tweezers (LOTs), (c) Glass microneedle. They all work in the fixed-distance ensemble.

obtained in Monte Carlo simulation studies of a directed self-avoiding walk model of a homopolymer DNA [20] and the block copolymer DNA [22].

Experimental Studies

In this section, we briefly introduce a few single-molecule micro-manipulation techniques used to study DNA unzipping. The developments of these techniques have opened up the possibility of applying a mechanical force in the pico-newton range on a single DNA molecule. These studies have revealed information about the unzipping kinetics, thermodynamic information, and sequence-dependent effects [116, 117, 118, 119, 111, 120, 121, 122]. Similar to theoretical studies, the DNA unzipping experiments are also done either in the fixed distance or in the fixed force ensembles.

The various experimental techniques used to probe DNA unzipping are shown schematically in Figs. 1.10 and 1.11.

1. *Fixed distance ensemble:* The various techniques which work in the fixed distance ensembles are atomic force microscope (AFM), laser optical tweezers (LOTs), and glass microneedles. The schematic diagrams of these experimental techniques are shown in Figs. 1.10(a), 1.10(b) and 1.10(c), respectively.

   Optical Tweezers use light to manipulate microscopic objects. The working principle of LOT is based on the optical gradient force generated by a focused beam of light acting on an object with an index of refraction higher than that of the surrounding medium. The radiation pressure from a focused laser beam can trap small objects. In the biological sciences, these instruments have been used to apply forces in the pN range and to measure displacements in the nm range of objects ranging in size from 10 nm to over 100 mm. For more information on optical tweezers and its applications see Ref. [123].

   Microneedle (MNs) device consists of needles of micron size, which are arranged on a small patch. In the glass microneedle set-up, a calibrated glass microneedle tip acts as a force lever whose deflection can be resolved with great precision to give a force resolution of the order of 0.1 pN. It can be done by analyzing a videotape of the microscope image recorded during the opening experiment [124, 125, 126].

   To perform DNA mechanical unzipping experiment using LOT and glass microneedle, a specific DNA construction has to be designed, in which linker arms prolongate the strands of the DNA to be unzipped to reduce as far as possible non-specific interaction between the DNA to be unzipped and the apparatus used to perform such experiments (e.g., the microscope slide and the bead). These linker arms consist of dsDNA, which contain, close to one of their extremities, multiple, modified base pairs. One type of linker is modified with biotin groups to react to streptavidin-coated bead, and the other type is modified with digoxigenin groups to react to anti-digoxigenin coated microscopic slides [124, 125, 126, 116]. The bead is either held in an optical trap [116] or attached with the glass microneedle tip [124, 125, 126], and the microscope slide is laterally displaced, which leads to a progressive opening of the double helix. The force is obtained from a measurement of the bead position within the trap, or the deflection of the tip of the microneedle under microscope, which is measured on the video imageas a function of this displacement. Optical tweezers have also been used to study RNA transcription [127], folding-unfolding transitions in single titin molecules [128], folding-unfolding kinetics in RNA molecules [129, 130], for the detection of

the position and dynamic nature of Protein-DNA interactions [131] etc. Recently, optical tweezers has been used to investigate stochastic resonance (SR) in single DNA hairpins driven by oscillatory mechanical forces [132]. For recent advances of OTs in single-molecule manipulation see Ref. [133].

Atomic Force Microscopy, or AFM, is a high-resolution form of scanning probe microscopy that employs a sharp tip in a raster motion to measure and visualize materials at the atomic- and nano-scales. The AFM is based on the principle that a very soft cantilever with a tip that is moved to the vicinity of a surface can sense the roughness of the surface and deflect by an amount which is proportional to the proximity of the tip to the surface (Fig. 1.10(a)). AFMs can be used to apply mechanical force on the dsDNA [134, 135, 136, 137]. At the same time, AFMs can be used to sweep surfaces and take images of the DNA molecule. The surface is coated with the DNA molecules to be unzipped, and the AFM tip is coated with molecules that can bind to the DNA. By moving the tip to the substrate, contact between the tip and one of the strands of the DNA molecules adsorbed on the substrate is made. The tip is now pulled back at a constant speed, and its deflection is measured. This measures the force acting on the DNA as a function of its extension, known as the force-extension curve. Depending upon the stiffness of the cantilever, the AFM can measure forces in the (20 pN - 10 nN) range. Other than DNA unzipping, AFMs have also been used for the unfolding of individual titin molecule [138], identification of binding mechanisms in single molecule-DNA complexes [139] etc. In recent past, AFMs has been used to measure the elasticity of dsDNA [140].

2. *Fixed force ensemble:* Magnetic tweezers (MTs) are devices used for studying the mechanical properties of biomolecules like DNA or proteins in single-molecule experiments. It works in the fixed-force ensemble. MT is based on the principle that a magnetized bead experiences a force in a magnetic field gradient. A single molecule is tethered to a surface at one end and attached to a magnetic bead at the other; the bead is manipulated with the help of an external magnetic field. The DNA is pulled by moving the translation stage that supports the magnets, and the bead's position is recorded [117, 118]. MTs can also be used to generate torque [141, 142]. MT has been used to study the elasticity of DNA molecules [143, 144, 145], unfolding RNA molecules [146], unwinding by RNA polymerase [147], etc. Almost two decades ago, Danilowicz et al. [117, 118] used MT to study the mechanical unzipping of lambda

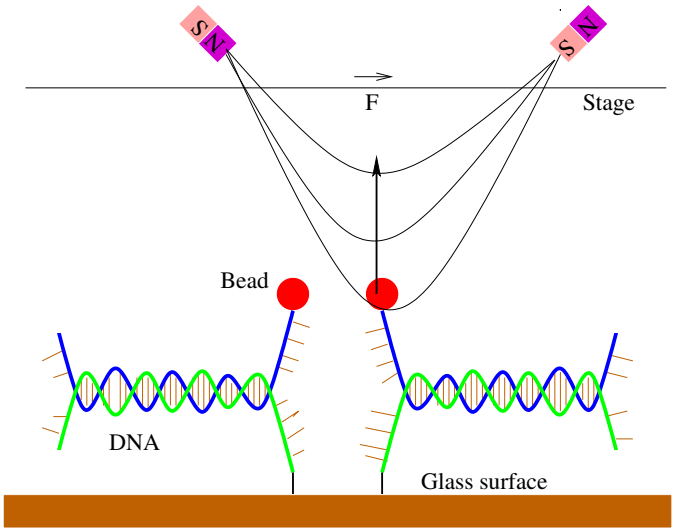

Figure 1.11: Schematic diagrams of Magnetic tweezers (MTs). It works in the fixed-force ensemble

phage DNA and obtained the unzipping phase diagram for a range of temperatures [118]. They have also measured the hysteresis in the unzipping and rezipping of dsDNA [111]. The schematic diagram of the basic set-up is shown in Fig. 1.11.

1.6 Stochastic Resonance

Stochastic resonance (SR) is one of the many interesting phenomena arising from the interplay between the noise and the nonlinearity in externally driven systems. When SR is triggered, the response of a system embedded in a noisy environment acquires an enhanced sensitivity towards small external time-dependent forcing. The concept of SR was first coined in 1981 by Benzi *et al.* [148] in an attempt to understand the climatic changes during the ice ages. SR has been studied in a large variety of systems, including climate dynamics [148, 149], colloidal particles [150, 151, 152], biological systems [132, 153, 154, 155], and quantum systems [156, 157]. With an advent of single-molecule manipulation techniques, it is now possible to measure SR at the level of individual molecules. Using the optical tweezers, the first experimental study of SR in single DNA hairpins, has been done in recent past [132].

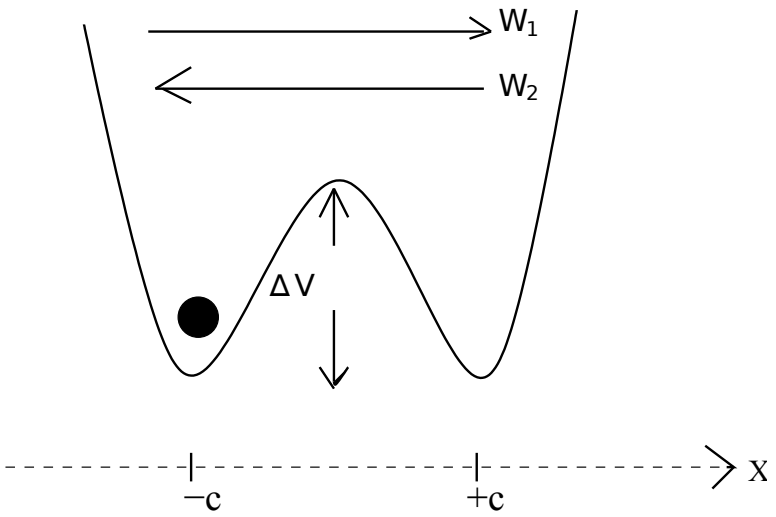

Figure 1.12: Classical particle in the symmetric double well potential $V_0(x)$. Particle transits between the two wells due to thermal noise, with the Kramers transition rate $W = W_1 = W_2$ given by Eq. 1.12.

1.6.1 Theoretical understanding

A. Standard example: a classical particle in the double well

The mechanism of stochastic resonance is straightforward to explain. Consider a heavily damped particle of mass m and viscous friction γ, moving in a symmetric double-well potential $V_0(x)$ (see Fig. 1.12). The particle is subject to a random force which is induced by the coupling to a heat bath. The fluctuating force causes the particle to transit between the two potential minimas at $x = -c$ and $x = +c$, respectively. If the parameter κ measures the strength of the noise and ΔV is the height of the potential barrier separating the two minimas, then in the case $\kappa < \Delta V$, the rate of transition between the two potential wells from $x = -c$ to $+c$, is given by Kramers formula [158]

$$W = \langle \tau \rangle^{-1} = \frac{\sqrt{|V_0''(0)|V_0''(c)}}{2\pi} \exp\left(\frac{-2\Delta V}{\kappa}\right), \tag{1.12}$$

τ is the inverse of the transition rate, i.e. the mean passage time from $x = -c$ to $+c$. The transition rate depends on noise strength, κ, the height, ΔV , of the potential barrier and the curvature at the extrema. Let us now add a small periodic

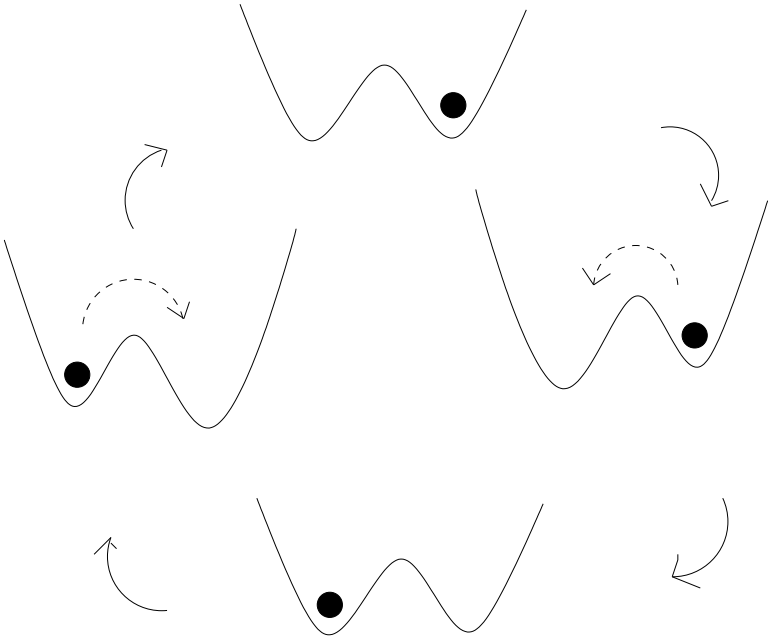

Figure 1.13: In the presence of an optimal degree of noise, stochastically activated transitions between the two metastable states are most likely after one half-cycle of the periodic injected signal. As a result, at non-vanishing noise strength, the response is optimally synced with the external modulation of the double-well potential. .

modulation of the potential

$$V(x,t) = V_0(x) + V_1 \frac{x}{c} \sin(\omega_s t). \tag{1.13}$$

Here by 'small' we mean $V_1 < \Delta V$, such that the driving does not cause deterministic transitions between two wells. Since the modulation is linear in x, it does affect the height of the barrier seen by the particle but not the second derivatives in the Kramers rate (Eq. 1.12). If the modulation frequency, ω_s, is not too large, we get

$$W_{1,2}(t) = \frac{\sqrt{|V_0''(0)|V_0''(c)}}{2\pi} \exp\left(\frac{-2}{\kappa}(\Delta V \pm V_1 \sin(\omega_s t))\right) \tag{1.14}$$

for the two rates W_1 (from $-c$ to $+c$) and W_2 (vice versa). Hence, at a certain phase of the driving, the probability to go from state 1 to state 2 is increased, whereas the opposite transition is decreased.

The SR can now be illustrated using the preceding description. When the noise is small, the average residence time in the two states is much longer than the driving period $2\pi/\omega_s$. Consequently, the individual transitions occur at unpredictable

times. However, when the noise level is increased to a certain point, we see almost a periodic transitions: the particle usually jumps from state 1 to state 2 and back once per modulation period. The transitions are most likely to occur at those instants of time when the corresponding transition rates, $W_{1,2}$, are maximized and the average residence times in both the metastable states is equal to the half of the modulation period [see Fig. 1.13]. As the noise strength increases further, too many transitions are activated by the noise during one cycle of the periodic drive, and the cooperation between the signal and the noise is lost again. This is the SR effect: the system's response is most regular at a finite, non-vanishing noise level!

B. General model: Two-state model

In the two-state model, the system can be found in one of the two metastable states at any given time. The dynamics within the states is completely neglected. The output variable of the system can have only two values:

$$x = \begin{cases} -c & \text{in state 1} \\ +c & \text{in state 2} \end{cases} \tag{1.15}$$

The dynamics of the system can be described in terms of two transition rates W_1 and W_2. These rates indicate the probability that the system will move from state 1 to state 2 ($W_1\Delta t$) or state 2 to state 1 ($W_2\Delta t$) within a short time interval Δt. The transition rates depend on the strength of the noise (more noise enhances the transition rates), the amplitude and frequency of the external signal.

Given $W_1(t)$ and $W_2(t)$, the time evolution of the probabilities $p1$ and p_2 of finding the system in state 1 or 2 is given by

$$\dot{p_1} = -W_1(t)p_1 + W_2(t)p_2, \tag{1.16}$$

$$\dot{p_2} = W_1(t)p_1 - W_2(t)p_2. \tag{1.17}$$

Using the conservation of total probability, $p_1 + p_2 = 1$, these equations reduce to

$$\dot{p_1} = -(W_1 + W_2)p_1 + W_2. \tag{1.18}$$

In the limit $t \to \infty$, the above equation has the unique asymptotic periodic solution

$$p_1(t)^{(as)} = \frac{1}{1-\exp(-\langle W\rangle t_S)} \int_0^{t_S} dt' W_2(t-t') \exp\left(-\int_{t-t'}^{t} dt'' W(t'') \right) \quad (1.19)$$

Where $W(t) = W_1(t) + W_2(t)$ and $\langle W\rangle$ is the average of $W(t)$ over the driving period. Therefore the asymptotic ensemble average of the output variable,$x(t)$, is

$$\langle x(t)\rangle^{(as)} = -cp_1(t)^{(as)} + cp_2(t)^{(as)} = c(1-2p_1(t)^{(as)}) \quad (1.20)$$

This is the main quantity in quantitative characterization of SR for the two-state model.

C. Quantifying SR

The power spectrum of the output variable, $x(t)$, is used to measure SR. It exhibits a strong peak ('signal peak') at the signal frequency, ω_s. The area under this peak, known as output signal power, is the measure of SR. Often the signal-to-noise ratio (SNR) is also used. It is defined by the height of the signal peak divided by the height of the background noise at frequency ω_s. When the output signal power (or the SNR) reaches a maximum as a function of noise strength, we term it as SR.

Power spectrum: The power spectrum, $P(\Omega)$, of the position $x(t)$ of the particle in the double well, is defined as [159]:

$$P(\Omega) = \frac{1}{2\pi t_{max}} \left| \int_0^{t_{max}} dt\, x(t) \exp(-i\Omega t) \right|^2. \quad (1.21)$$

In the limit $t_{max} \to \infty$, the Wiener-Khintchine theorem [160] expresses the power spectrum,

$$P_\infty(\Omega) = 4 \int_0^\infty d\tau C(\tau) \cos(\Omega\tau), \quad (1.22)$$

in terms of the autocorrelation function,

$$C(\tau) = \frac{1}{t_s} \int_0^{t_s} dt\, \langle x(t+\tau)x(t)\rangle^{(as)}. \quad (1.23)$$

The brackets $\langle\cdots\rangle^{as}$ denote an average over the stochastic realization of the noise in the asymptotic limit. For large time differences $\tau \to \infty$, we can factorize the

correlation $\langle x(t+\tau)x(t)\rangle = \langle x(t+\tau)\rangle\langle x(t)\rangle$, indicating the fact that at large τ the only correlation between $x(t+\tau)$ and $x(t)$ is due to periodic drive. In this limit, the autocorrelation function approaches a periodic function of τ, which permits us to write its Fourier transform (Eq. 1.22) as a sum of δ peaks at integer multiples of the driving period and of a smooth background $P_N(\Omega)$:

$$P_\infty(\Omega) = \sum_{n=-\infty}^{\infty} S_n \delta(\Omega - n\omega_s) + P_N(\Omega). \tag{1.24}$$

The weights, S_n, of the signal peaks are given by

$$S_n = \frac{2\pi}{t_s^2} \left| \int_0^{t_s} dt \, \langle x(t)\rangle^{as} \exp(-i\omega_s n t) \right|^2, \tag{1.25}$$

where $\langle x(t)\rangle^{as}$ is the periodic asymptotic limit of the expectation value of $x(t)$. The weight, S_1, of the main signal peak at $\Omega = \omega_s$ is called the output signal power. It is the stronger the 'more periodically' the transitions between the two metastable states occur and can therefore be regarded as a quantitative measure of SR. In other words, the SNR,

$$SNR = \frac{P(\omega_s)}{P_N(\omega_s)}, \tag{1.26}$$

can be used also for this purpose.

Power spectrum in the two-state model: The output signal power, for two-state model, is obtained by inserting the Eq. 1.20 into Eq. 1.25. The noise background, without modulation has Lorentzian shape

$$P_N^{[\text{no signal}]}(\Omega) = 4c^2 \frac{W}{\Omega^2 + W^2}, \tag{1.27}$$

with $W = W_1 + W_2$.
Now let us add small modulation and assume that assume that the rates vary symmetrically and sinusoidally under periodic forcing

$$W_1(t) = \frac{1}{2}\langle W\rangle - \epsilon \sin(\omega_S t), \tag{1.28}$$

$$W_2(t) = \frac{1}{2}\langle W\rangle + \epsilon \sin(\omega_S t). \tag{1.29}$$

Using these both equations in to Eq. 1.19, we get

$$p_1(t)^{(as)} = \frac{1}{2} + \epsilon \frac{\sin(\omega_S t - \phi)}{\sqrt{\langle W \rangle^2 + \omega_S^2}}, \tag{1.30}$$

where ϕ is the phase difference between drive and response. This equation, via Eqs. 1.20 and 1.25, gives us the output signal power which is is proportional to the squared amplitude of the periodic response:

$$S_1 = \frac{4\pi c^2 \epsilon^2}{\langle W \rangle^2 + \omega_S^2}. \tag{1.31}$$

This expression is valid generally for all symmetric two-state systems with sinusoidally modulated transition rates.

After dividing S_1 by the level, $P_N(\omega_S)$, of the noise spectrum at $\Omega = \omega_S$ (see Eq. 1.27), we get

$$\text{SNR} \propto \frac{\epsilon^2}{\langle W \rangle}. \tag{1.32}$$

For a more detail description of SR, see the review in Ref. [159].

1.7 Summary of Monte Carlo simulation

In this section, we give a brief summary about Monte Carlo simulation which has been adopted to study the problems in this thesis. First, we describe how the estimates for the observables are done by using the Monte Carlo simulation. There are many textbooks on Monte Carlo simulations. One such textbook which describes MC simulations in details is given in Ref. [161].

The states of the system, which is in equilibrium with a reservoir at inverse temperature $\beta = 1/k_B T$ (k_B is Boltzmann constant), are sampled according to the Boltzmann probability distribution

$$p_\mu = \frac{1}{Z} e^{-\beta E_\mu}, \tag{1.33}$$

where E_μ is the energy of the system in state μ and Z is the partition function

which is given by

$$Z = \sum_{\mu} e^{-\beta E_{\mu}}. \tag{1.34}$$

The expectation value $\langle X \rangle$ of an observable X is given by

$$\langle X \rangle = \frac{\sum_{\mu} X_{\mu} e^{-\beta E_{\mu}}}{\sum_{\mu} e^{-\beta E_{\mu}}}. \tag{1.35}$$

Monte Carlo techniques work by choosing a subset of states at random from some probability distribution p_{μ} which is to be specified. If we choose $\{\mu_1 ... \mu_M\}$ as M such states, then the best estimate of the quantity X is given by

$$X_M = \frac{\sum_{i=1}^{M} X_{\mu_i} p_{\mu_i}^{-1} e^{-\beta E_{\mu_i}}}{\sum_{j=1}^{M} p_{\mu_j}^{-1} e^{-\beta E_{\mu_j}}}. \tag{1.36}$$

We call X_M as the estimator of X. The estimator X_M becomes more and more accurate estimate of $\langle X \rangle$ as the sample size M increases and in the limit $M \to \infty$ we have $X_M = \langle X \rangle$.

The essence of the idea behind Monte Carlo simulation is that if we can pick M states from those states which make important contributions to the sums in Eq. (1.35) and ignore contributions from all other states. Importance sampling is used to accomplish this where instead of picking our M states in such a way that every state of the system is as likely to get chosen as every other, we pick them so that the probability that a particular state μ gets chosen is $p_{\mu} = Z^{-1} e^{-\beta E_{\mu}}$. Then the estimator for $\langle X \rangle$, Eq. (1.36), becomes

$$X_M = \frac{1}{M} \sum_{i=1}^{M} X_{\mu_i}. \tag{1.37}$$

In Monte Carlo simulations, the states are generated by using the mechanism of Markov process. Markov process generates a new state ν of the system from a given state μ in random fashion. The probability of generating the state ν given μ is referred as transition probability $P(\mu \to \nu)$ for the transition from μ to ν. The transition probabilities should satisfy the following two conditions: (i) they should not vary over time, and (ii) should depend only on the properties of the current states μ and ν, and not on any other states the system has passed through. The

transition probabilities $P(\mu \to \nu)$ should also satisfy

$$\sum_{\nu} P(\mu \to \nu) = 1, \tag{1.38}$$

because given a state μ of the system, Markov process must generate some state ν. There is a finite probability that the system can stay in the original state μ, therefore $P(\mu \to \mu)$ need not to be zero.

We choose the Markov process in such a way that when it runs for long enough time starting from any state of the system, it eventually reaches to equilibrium producing the states with their correct Boltzmann probabilities. It should be possible for our Markov process to reach any state of the system from any other state, when we run it for long enough time. This requirement is called *condition of ergodicity*. We also have to ensure that the states we generate after the system reaches to the equilibrium are generated according to the Boltzmann probability distribution, rather than any other distribution. We call it *condition of detailed balance* which tells that in equilibrium the transition probabilities must satisfy

$$\frac{P(\mu \to \nu)}{P(\nu \to \mu)} = \frac{p_\nu}{p_\mu} = e^{-\beta(E_\nu - E_\mu)}. \tag{1.39}$$

If we satisfy the Eqs. (1.38) and (1.39) along with the condition of ergodicity then the states generated by our Markov process in the equilibrium are according with Boltzmann distribution. The Metropolis algorithm satisfies all the necessary requirements which we will discuss next.

1.7.1 Metropolis algorithm

If μ and ν are two states generated by a Markov process such that $E_\mu < E_\nu$, then the Metropolis algorithm chooses the transition probabilities between the states μ and ν according to

$$P(\mu \to \nu) = \begin{cases} e^{-\beta(E_\nu - E_\mu)} & \text{if } E_\nu - E_\mu > 0 \\ 1 & \text{otherwise.} \end{cases} \tag{1.40}$$

We implement the above rule to study the problems in this thesis.

1.8 Outline of the Thesis

Finally, we present an outline of the work done in this thesis. We have considered three problems, and we give the central ideas of these problems as follows:

In chapter 2, we study the dynamic transitions in the unzipping of an adsorbed polymer from a surface (or the wall) which is subjected to a periodic force on one end (free end) while keeping its other end fixed. We consider three different type of the walls:

1. The surface is impenetrable, i.e., the polymer is allowed to stay only on one side of the wall. We refer such a surface as *hardwall* in the thesis.

2. The surface is penetrable, i.e., the polymer is allowed to cross the surface, and the polymer has an equal affinity on either sides of the surface. We call such a surface as *softwall*.

3. The surface is penetrable but the polymer has different affinities on either sides of the surface. This can be thought of as an interface between the two immiscible liquids in which the polymer has different degrees of solubility.

We shall obtain the results for the static force case using the Monte Carlo simulations and shall compare them with the analytical results obtained earlier using the generating function technique to verify the validity of our simulation. We shall also discuss the results obtain for the dynamic force case. In this case force-distance isotherms show the hysteresis.

In chapter 3, we study the unzipping of a double-stranded block copolyer DNA by a periodic force. We shall obtain the phase diagram for the static force case using the generating function technique and exact transfer matrix method. We will see that the results obtain for the static force case are independent of DNA sequence. Then we shall show that when DNA is subjected to a periodic force it unbinds and rebinds with a hysteresis in its force-distance isotherm. We will show that the results thus obtain for the periodic case depend on the DNA sequence.

Chapter 4 is devoted to the study of the stochastic resonance phenomenon in the unzipping of a homo-polymer DNA and a block copolymer DNA by periodic force. We shall measure the output signal(OS), which is resonance quantifier. We shall see how the OS shows a peak when it is plotted as a function of the frequency of the applied force confirming the occurrence of stochastic resonance in periodically driven DNA.

Chapter 2

Dynamic Transitions in Unzipping of an Adsorbed Polymer

In this chapter, we study the dynamic transitions in the unzipping of an adsorbed polymer on a surface (or wall) by a pulling force. We consider three different types of walls:

1. In the first type of wall, the polymer is allowed to stay only on one side of the wall, i.e., the wall is impenetrable. We refer such a surface as *hard-wall*.
2. In the second type of wall, the polymer is allowed to cross the surface, and it has equal affinity on both the sides of the surface. We call such a surface as *soft-wall*.
3. In the third type of wall, the polymer is allowed to cross the surface, but it has different affinities on either sides of the surface. This can be thought of as an interface between two immiscible liquids in which the polymer has different degree of solubility.

Let us first define our model.

2.1 Model

We model the polymer by a directed self-avoiding random walk in $d = 1 + 1$ dimensional square lattice. The walk starts at the origin O, and is restricted to go towards the positive direction of the diagonal axis (z direction). The directional nature of the walks takes care of the self-avoidance. We put an attractive wall along z-axis at $x = 0$. Whenever a monomer is on the wall, polymer gains an energy $-\epsilon(\epsilon > 0)$. One end of the polymer is always kept anchored to the wall at the origin, and other end monomer is subjected to a time-dependent periodic force $g(t)$, which acts along the transverse direction (x direction) and is given by

$$g(t) = g_0 \sin(\omega t), \tag{2.1}$$

where g_0 is the amplitude and ω is the angular frequency. Throughout the chapter, by frequency we mean the angular frequency.

The three different possibilities for the wall, as mentioned above, can be modeled by assigning a repulsive potential $V(> 0)$ on one side of the wall, say $x < 0$. In the two extreme limits, i.e., (i) for $V = 0$, the wall behaves as a softwall, and (ii) for $V = \infty$, it behaves like a hardwall. All other values of V, the wall acts like an interface between the two immiscible liquids with different affinities with the polymer. The schematic diagram of the model is shown in Fig. 2.1. For the static case, i.e., $\omega = 0$, this model has been solved analytically using generating function and exact transfer matrix techniques and exact phase diagram has been determined [35]. However, for the dynamic case, i.e., $\omega \neq 0$, the model cannot be solved analytically. We perform Monte Carlo simulations using the Metropolis algorithm. The polymer chain undergoes Rouse dynamics that consists of local corner-flip or end-flip moves [3]. It does not violate mutual avoidance with hard wall. The elementary move consists of selecting a random monomer from the chain and flipping it. If the move results in the adsorption of the monomer on the wall, it is always accepted as a move. The opposite move, i.e., desorption of the monomer from the wall, is chosen with the Boltzmann probability $\eta = \exp(-\Delta E/k_B T)$, where ΔE is the energy difference between two states. The move involving movement of monomer from one desorbed state to another is always accepted. The time is measured in units of Monte Carlo steps (MCSs). One MCS consists of N flip attempts, which means that on average, every monomer is given a chance to flip. Throughout the simulation, the detailed balance is always satisfied

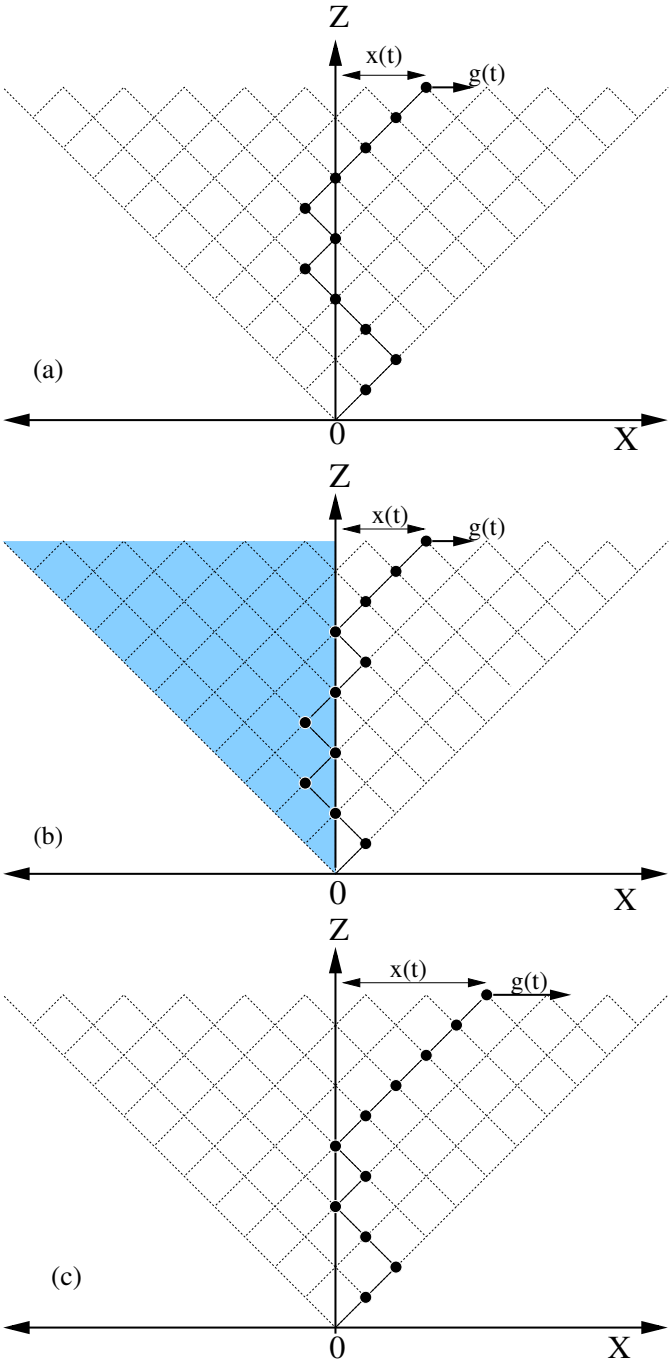

Figure 2.1: Schematic diagram of a directed polymer adsorbed on a surface (along z-axis) at $x = 0$. (a) Soft-wall: polymer is allowed in the whole region. (b) Wall separating two different types of media: polymer is allowed in whole region, however there is an extra repulsive potential $V(> 0)$ on side $x < 0$. (c) Hard-wall: polymer is not allowed in the region $x < 0$. One end of the polymer is anchored at the origin (O), and the chain on the free end is subjected to a time-dependent periodic force with frequency ω and amplitude g_0.

and the algorithm is ergodic in nature. It is always possible, from any starting polymer configuration, to reach any other configuration by using the above moves. We have checked that we get the same results from a completely stretched polymer configuration. Before taking any measurements, we let the simulation run for $400\pi/\omega$ in lower frequency regime, and $4000\pi/\omega$ in higher frequency regime, to achieve the stationary state.

We report quantities in the dimensionless units. The quantities having dimensions of energy are measured in units of ϵ, and the quantities that have dimensions of length are measured in terms of the lattice constant a. The time is measured in units of MCS. We have taken $k_B = 1$, $\epsilon = 1$ and $a = 1$.

2.1.1 Quantities of interests

The various quantities that are of interest to us are:

- *Displacement of end monomer from the wall:* The displacement, $x(t)$, of the end monomer of the polymer from the wall is the response to the oscillating force $g(t)$. The displacement $x(t)$ is monitored as a function of time t for various force amplitudes g_0 and frequency ω.

- *Dynamical order parameter:* The time averaging of $x(t)$ over a complete period,
$$Q = \frac{\omega}{2\pi} \oint x(t)dt. \tag{2.2}$$
The quantity Q can be used as a dynamical order parameter [162].

- *Force-distance isotherms:* From the time series $x(t)$, we can obtain the extension $x(g)$ as a function of force g. On averaging it over many cycles of the periodic force, we can obtain the average extension $\langle x(g)\rangle$ as a function of g. The average extension, $\langle x(g)\rangle$, depends on the frequency ω of the oscillating force. At higher frequencies, the system does not get enough time to get equilibrated and therefore the $\langle x(g)\rangle$ is not same for the forward and backward paths. This results in a hysteresis loop in force-extension plane.

- *Area of the hysteresis loop:* The area of hysteresis loop, A_{loop}, which is defined by
$$A_{loop} = \oint \langle x(g)\rangle dg, \tag{2.3}$$

depends upon the frequency ω and the amplitude g_0 of the driving force and can serve as an another candidate for the dynamical order parameter.

2.2 Results and Discussions

In this section, we discuss the results obtained in our simulations for both the static and dynamic cases. Let us first discuss the static force case briefly.

2.2.1 Static Case

In the static limit, this model has been solved analytically using the generating function and exact transfer matrix techniques [35]. We first briefly mention the generating function technique and obtain the exact phase diagrams for all the three cases. We then validate our Monte Carlo simulation results by obtaining the force-distance isotherms for various system sizes and then extract the critical unzipping force values at various temperatures using finite-size scaling. We then compare them with the analytical results.

A. Phase diagram

The directed nature of our model makes it possible to calculate the partition function for the polymer via a recursion relation. The generating function technique can then be used to obtain the phase boundary. In this method, the singularities of the generating function are determined. The singularity nearest to the origin gives the phase of the polymer and the phase transition occurs whenever the two singularities cross each other. The method is described as follows: Let $\mathcal{Z}_n(x)$ represents the partition function, in the fixed-distance ensemble, of a polymer of length n with separation x between the nth monomer and the wall. Let each lattice site on one side (say $x < 0$) of the wall has a repulsive potential $V (V > 0)$. The soft-wall and the hard-wall are then the limiting cases for $V \to 0$ and $V \to \infty$, respectively. In the presence of potential V, the recursion relation satisfied by the

partition function is given by

$$\mathcal{Z}_{n+1}(x) = \begin{cases} [\mathcal{Z}_n(x+1) + \mathcal{Z}_n(x-1)]e^{-\beta V} & \text{for } x < 0 \\ \mathcal{Z}_n(x+1) + \mathcal{Z}_n(x-1) & \text{for } x > 0 \\ [\mathcal{Z}_n(x+1) + \mathcal{Z}_n(x-1)]e^{\beta\epsilon} & \text{for } x = 0. \end{cases} \tag{2.4}$$

If the above recursion relation is iterated N times with an initial condition $\mathcal{Z}_0(x) = e^{\beta\epsilon}\delta_{x,0}$, we get the partition function of a polymer of length N. The generating function for the partition function $\mathcal{Z}_n(x)$, can be taken to be of the form (ansatz)

$$\hat{\mathcal{Z}}(z,x) = \sum_n z^n \mathcal{Z}_n(x) = \begin{cases} \eta^x(z)K(z) & \text{for } x > 0 \\ \eta'^{-x}(z)K(z) & \text{for } x < 0. \end{cases} \tag{2.5}$$

When the ansatz Eq. (2.5) is used in the above recursion relation (Eq. (2.4)), we obtain $\eta = (1 - \sqrt{1-4z^2})/2z$, $\eta' = (1 - \sqrt{1-4z^2e^{-2\beta V}})/2ze^{-\beta V}$ and $K(z) = 1/\{1 - [\eta' + \eta]ze^{\beta\epsilon}\}$. The singularities coming from η and η' are $z_1 = 1/2$ and $z_1' = 1/2\exp(-\beta V)$, respectively, and $K(z)$ has the singularity

$$z_2 = \frac{1}{2}\sqrt{1 - \left(1 - \frac{2e^{-\beta\epsilon}(1 - e^{-\beta V}e^{-\beta\epsilon})}{1 + e^{-\beta V}(1 - 2e^{-\beta\epsilon})}\right)^2}, \tag{2.6}$$

which depends on both the adsorption energy, ϵ, and the potential V. In the large length limit, the relevant partition function in fixed-distance ensemble is approximated as $\mathcal{Z}_N(x) \approx \eta^x(z_2)/z_2^{N+1}$ for $x > 0$, with free energy $\beta F = N \ln z_2 - x \ln \eta(z_2)$. The force needed to maintain the separation x is given by $g = \partial F/\partial x$. The phase boundary, in a fixed-distance ensemble, is then given by

$$g(T) = -k_B T \ln \eta(z_2). \tag{2.7}$$

The zero force melting takes place at $T_c = \infty$ for the soft-wall and $T_c = \epsilon/\ln 2$ for the hard-wall case. There is a nonzero T_c for any $V < \infty$.

In the fixed-force ensemble, there is an additional force-dependent singularity, $z_3(\beta g_0) = [2\cosh(\beta g_0)]^{-1}$, which comes from the generating function

$$\mathcal{G}(z, \beta g_0) = \sum_{n=0}^{\infty} z^n \sum_x \mathcal{Z}_n(x) e^{\beta g_0 x}. \tag{2.8}$$

The phase boundary comes from equating the two singularities $z_2 = z_3$ and is

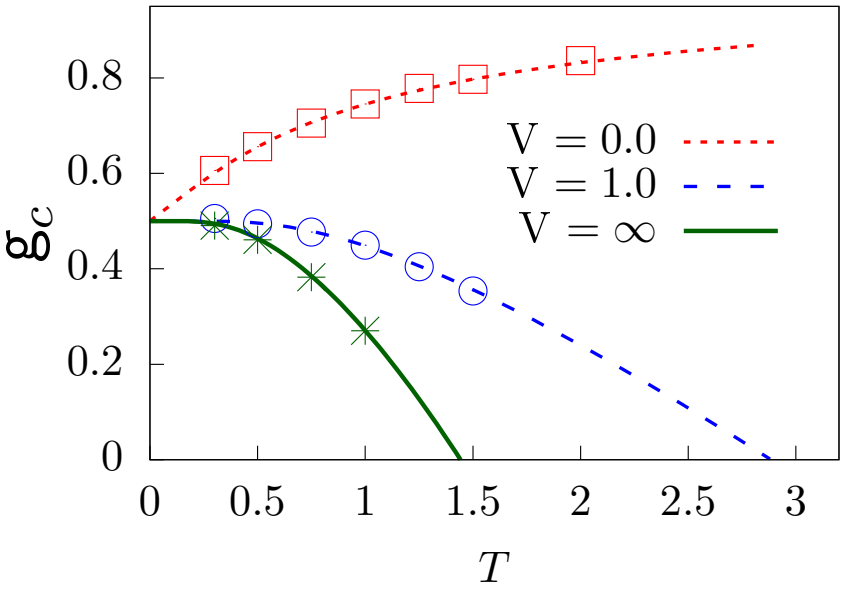

Figure 2.2: Critical unzipping force g_c as a function of temperature T for soft-wall ($V = 0.0$), wall separating two different types of media ($V = 1.0$), and hard-wall ($V = \infty$). The lines are the exact results obtained from the generating function approach, and the points are obtained by using finite-size scaling of the force-distance isotherms as obtained from the Monte Carlo simulations.

given by

$$g_c(T) = T \cosh^{-1}\left[\left\{1 - \left(1 - \frac{2u(1-vu)}{1+v(1-2u)}\right)^2\right\}^{-1/2}\right], \tag{2.9}$$

with $u = e^{-\beta\epsilon}$, and $v = e^{-\beta V}$. This phase boundary obtained in the fixed-force ensemble (Eq. (2.9)) is identical to the phase boundary obtained in the the fixed-distance ensemble (Eq. 2.7). In the limits $V \to 0$ and $V \to \infty$, the above equation simplifies to the phase boundaries for the soft-wall and hard-wall cases, respectively

$$g_c(T) = \begin{cases} T \tanh^{-1}\left[1 - e^{-\beta\epsilon}\right] & \text{for soft-wall} \\ T \tanh^{-1}\left[1 - 2e^{-\beta\epsilon}\right] & \text{for hard-wall.} \end{cases} \tag{2.10}$$

The phase boundary separating the adsorbed and the unzipped phases for all the three cases: hard-wall ($V \to \infty$), soft-wall ($V \to 0$) and the wall separating two different media ($V = 1.0$) are shown in Fig. 2.2 by lines. The region below the phase boundary represents the adsorbed phase while above it represents the unzipped phase. From Eq. 2.9, we obtained the critical force as $g_c(T = 0.5) = 0.6557....$, $0.4959....$ and $0.4636....$ for soft-wall, wall separating two media ($V = 1.0$) and

hard-wall, respectively, at temperature $T = 0.5$ used in this study.

B. Force-distance isotherms

We perform Monte Carlo simulations on the model to obtain the force g vs average extension, $\langle x \rangle$, of the end monomer of the polymer from the wall. Every data point in the force-distance isotherms is obtained by equilibrating the system for 2×10^5 MCSs and then averaged over 10^4 different realizations.

In Fig. 2.3, we have plotted the scaled extension $\langle x \rangle / N$, as a function of constant pulling force g for the polymer of various lengths $N = 128, 256$, and 512 at $T = 0.5$ obtained by using Monte Carlo simulations for (i) the soft-wall [Fig. 2.3(a)], (ii) the wall separating two different media [Fig. 2.3(c)], and (iii) the hard-wall [Fig. 2.3(e)]. From the figure, we can clearly see the existence of the zipped and the unzipped phases. The polymer is in the zipped phase at lower g values with $\langle x \rangle / N \approx 0$, and in the unzipped phase with $\langle x \rangle / N \approx 1$ when the external pulling force g exceeds a critical value g_c. Furthermore, with the increase in the chain length N, the transition becomes sharper. In the thermodynamic limit, $N \to \infty$, it would become a step function at a critical value g_c. The critical value of the force, g_c, is obtained by using the finite-size scaling on polymer lengths $N = 128, 256$, and 512

$$\langle x \rangle = N^d \mathcal{F}\Big((g - g_c) N^{\phi} \Big), \tag{2.11}$$

where d and ϕ are the critical exponents. The data shows a very nice collapse for the values:

1. $g_c = 0.65 \pm 0.02$, $d = 0.96 \pm 0.05$, and $\phi = 1.0 \pm 0.02$ for the soft-wall case,
2. $g_c = 0.49 \pm 0.02$, $d = 0.93 \pm 0.10$, and $\phi = 1.0 \pm 0.02$ for the wall separating two different media case, and
3. $g_c = 0.46 \pm 0.02$, $d = 0.90 \pm 0.10$, and $\phi = 1.0 \pm 0.02$ for hard-wall case.

The data-collapse obtained using the above exponents are shown in Figs. 2.3(b), 2.3(d), and 2.3(f) for the soft-wall, the wall separating two different media, and the hard-wall cases, respectively. The critical force values are obtained by using the above method at various temperatures are plotted by points in Fig. 2.2. They

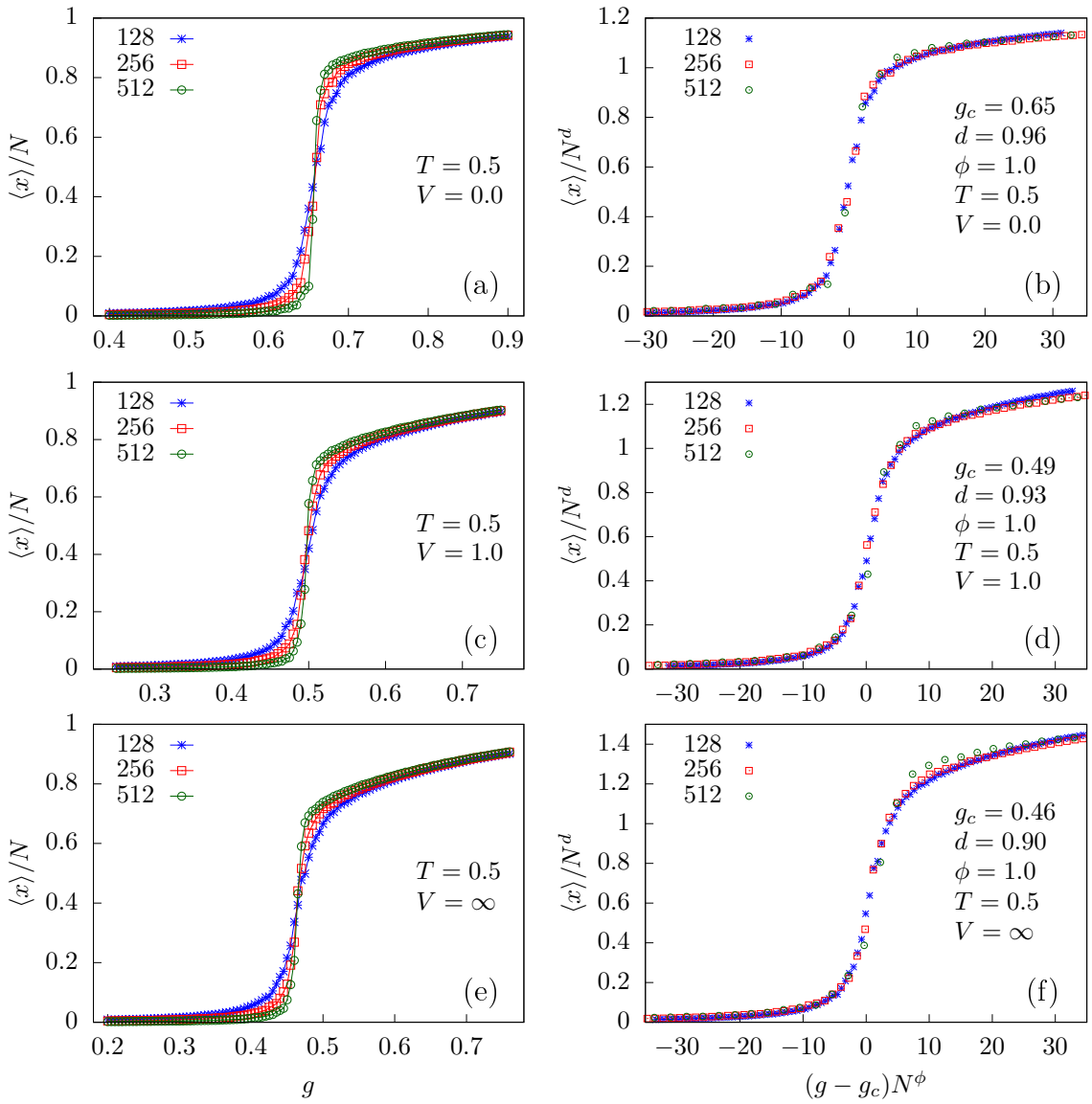

Figure 2.3: Scaled extension $\langle x\rangle/N$, as a function of constant pulling force g, obtained using Monte Carlo simulations, for different chain lengths $N = 128, 256$, and 512 at $T = 0.5$ for (a) soft-wall . (b) $\langle x\rangle/N^d$ as a function of $(g-g_c)N^\phi$ showing a nice collapse of data for $g_c = 0.65 \pm 0.02$, $d = 0.96 \pm 0.05$, and $\phi = 1.0 \pm 0.02$. (c) For wall separating two different types of media. (d) data collapse of (c) for $g_c = 0.49 \pm 0.02$, $d = 0.93 \pm 0.10$, and $\phi = 1.0 \pm 0.02$. (e) For hard-wall case. (f) Collapse of data shown in (e) for $g_c = 0.46 \pm 0.02$, $d = 0.90 \pm 0.10$, and $\phi = 1.0 \pm 0.02$.

are found to match the analytical results [Eq. 2.9] obtained using the generating function technique. Let us now use our Monte Carlo simulations to the dynamic case.

2.2.2 Dynamic Case

In the previous section, we have seen that for the static force case, the exact results are available due to the generating function technique. However, for the dynamic force case, where the polymer is subjected to an oscillating force, the exact results are not available. We therefore use the Monte Carlo simulations, to study the unzipping of polymer subjected to an oscillatory force. We will discuss results for all the three types of walls as defined at the beginning of the chapter.

The oscillating force $g(t)$ defined in Eq. (2.1) has both the positive and negative cycles. For the soft-wall and the wall separating two different media, the polymer can cross the wall and therefore both the positive and negative cycles are used in pulling the polymer. However, for the hard-wall case, the polymer cannot cross it and remains adsorbed on the wall during the negative cycle of the force. Therefore, for the hard-wall case, we take the absolute value of the force $g(t)$ to convert the negative cycles also to positive cycles and define

$$g_h(t) = g_0|\sin(\omega_h t)|, \tag{2.12}$$

where ω_h is the frequency of the force $g_h(t)$. On comparing Eqs. (2.1) and (2.12), we see that for same time period, the frequency of the force for the hard-wall case is $\omega_h = \omega/2$. Henceforth, we will remember this and drop the subscript h from both ω and force $g(t)$.

A. Extension

The response of an oscillating force $g(t)$ is seen in the extension $x(t)$ of the end monomer of the polymer from the wall. In Fig. 2.4, we have plotted the time variation of the scaled extension, $x(t)/N$, for the polymer of length $N = 128$ as a function of time t along with the time variation of the external force $g(t)$, at force amplitude $g_0 = 1.2$, for two different frequencies $\omega = 1.42 \times 10^{-2}$ and 6.28×10^{-4} for the soft-wall ($V = 0.0$), the wall separating two different media ($V = 0.5$), and the hard-wall ($V = \infty$) at temperature $T = 0.5$. The magnitude of the force rises from 0 to a peak value of g_0, which is greater than the critical force g_c required to unzip the polymer at equilibrium, and then falls back to 0 in both the positive and negative cycles. The scaled extension $x(t)/N$ follows the force $g(t)$ with a lag and

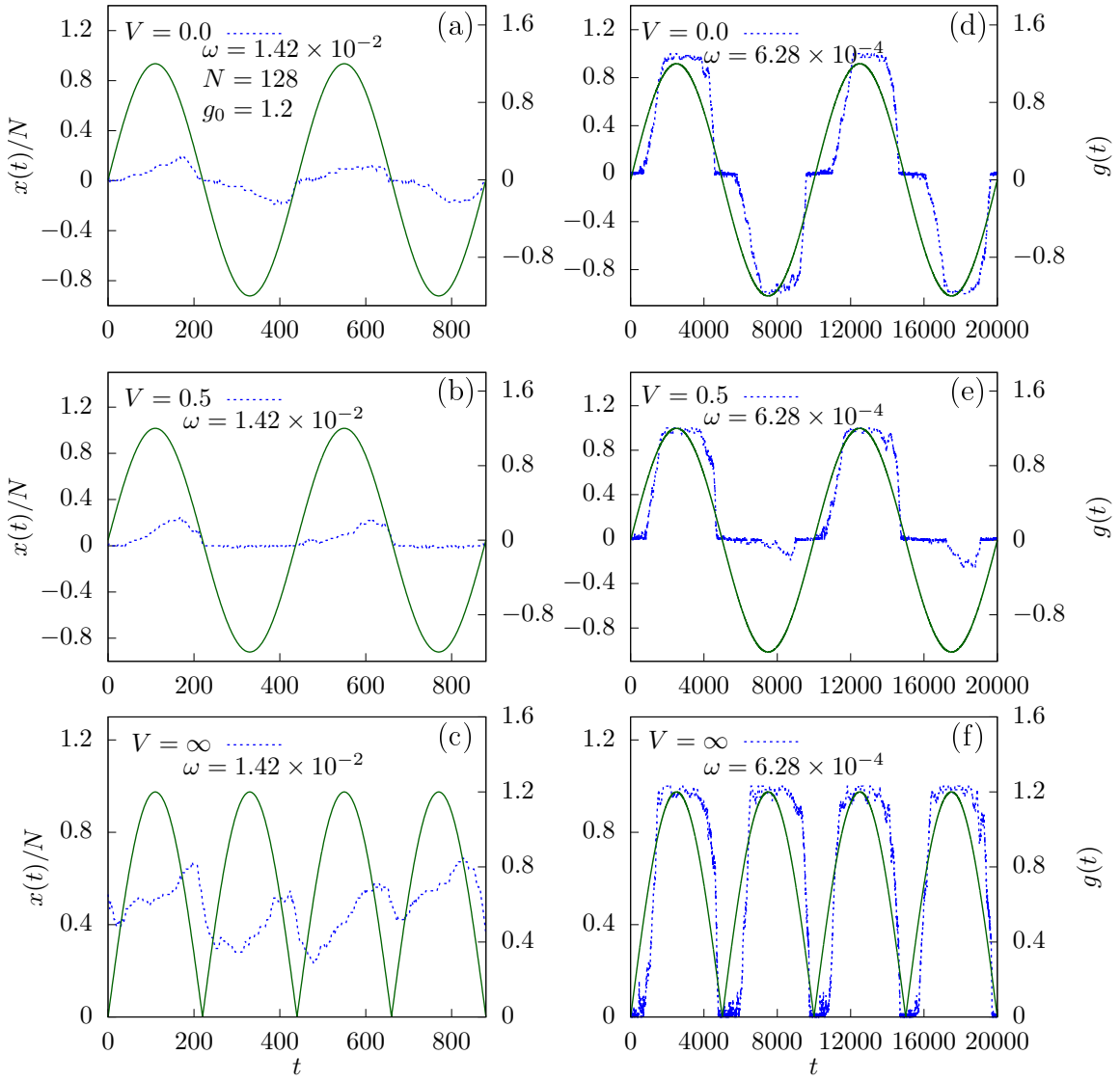

Figure 2.4: The scaled extension $x(t)/N$ from the wall of end monomer of the polymer of length $N = 128$ as a function of time t when it is subjected to a periodic force of amplitude $g_0 = 1.2$ at frequency $\omega = 1.42 \times 10^{-2}$. For the (a) soft-wall ($V = 0.0$), (b) wall separating two different media ($V = 0.5$), and (c) hard-wall ($V = \infty$). Plots (d), (e), and (f) are same as plots (a), (b), and (c) at frequency $\omega = 6.28 \times 10^{-4}$. The time variation of force, $g(t)$, is represented by solid lines.

its value depends on the frequency of the oscillating force. At a higher frequency, $\omega = 1.42 \times 10^{-2}$, the force changes very rapidly and the polymer does not get enough time to relax. Therefore, fewer number of monomers are unzipped from the wall resulting in smaller scaled extension. For the soft-wall case, since the polymer experiences similar environment on either sides of the wall, the scaled extension is

almost symmetrical in the positive and the negative cycles of the pulling force $g(t)$ [Fig. 2.4(a)]. However, this is not the case for the wall separating the two different media. In this case, the polymer feels a repulsive potential ($V = 0.5$) on side $x < 0$ and prefers to remain adsorbed on the wall. On the other side of the wall $x > 0$, the potential is $V = 0$. Therefore, the scaled extension is not the same for both the positive and negative cycles of the force [see Fig. 2.4(b)]. For the hard-wall case, the polymer is unable to cross the wall at $x = 0$ and only a positive scaled extension is observed, which is shown in Fig. 2.4(c). When the force is oscillating at a lower frequency, $\omega = 6.28 \times 10^{-4}$, the polymer gets enough time to relax and attains a fully stretched configuration in the response to the oscillating force. This results a larger scaled extension [see Figs. 2.4(d) – 2.4(f)]. However, the extension is still smaller for the negative cycle of the force in case of the wall separating the two media because the force pulls only a few monomers from the wall due to the presence of a repulsive potential $V = 0.5$ [see Fig. 2.4(e)]. The time series of extension $x(t)$ accumulated for many different cycles can be used to obtain various quantities.

B. Hysteresis loops

In the preceding subsection, we have seen that the response, $x(t)$, of the system during the rise of the magnitude of the force from 0 to g_0 and fall of the magnitude of the force from g_0 to 0 is not the same in both the positive and the negative cycles of the force. At a given temperature, we can obtain the average extension $\langle x(g) \rangle$ as a function of force g by averaging $x(t)$ over a significant number of cycles. The force-distance isotherms thus obtained show hysteresis loops.

In Fig. 2.5, we have plotted average extension $\langle x(g) \rangle$, averaged over 10^4 cycles, as a function of force g for a polymer of length $N = 128$ at five different frequencies $\omega = 1.57 \times 10^{-2}$, 1.57×10^{-3}, 1.57×10^{-4}, 4.18×10^{-5}, and 1.57×10^{-5} at two force amplitudes $g_0 = 1.0$, and 2.5 for the soft-wall ($V = 0.0$), wall separating two different media ($V = 1.0$), and the hard-wall ($V = \infty$), respectively. The values of the force amplitude g_0 is always chosen higher than the critical force g_c needed to unzip the polymer from the wall. The force-distance isotherms for all the three cases show hysteresis loops of various shapes and sizes. At $T = 0.5$, the force amplitude $g_0 = 1.0$ is slightly above the phase-boundary, $g_c = 0.6557\ldots, 0.4636\ldots$, and $0.4959\ldots$, for the soft-wall, the hard-wall and the wall separating the two different

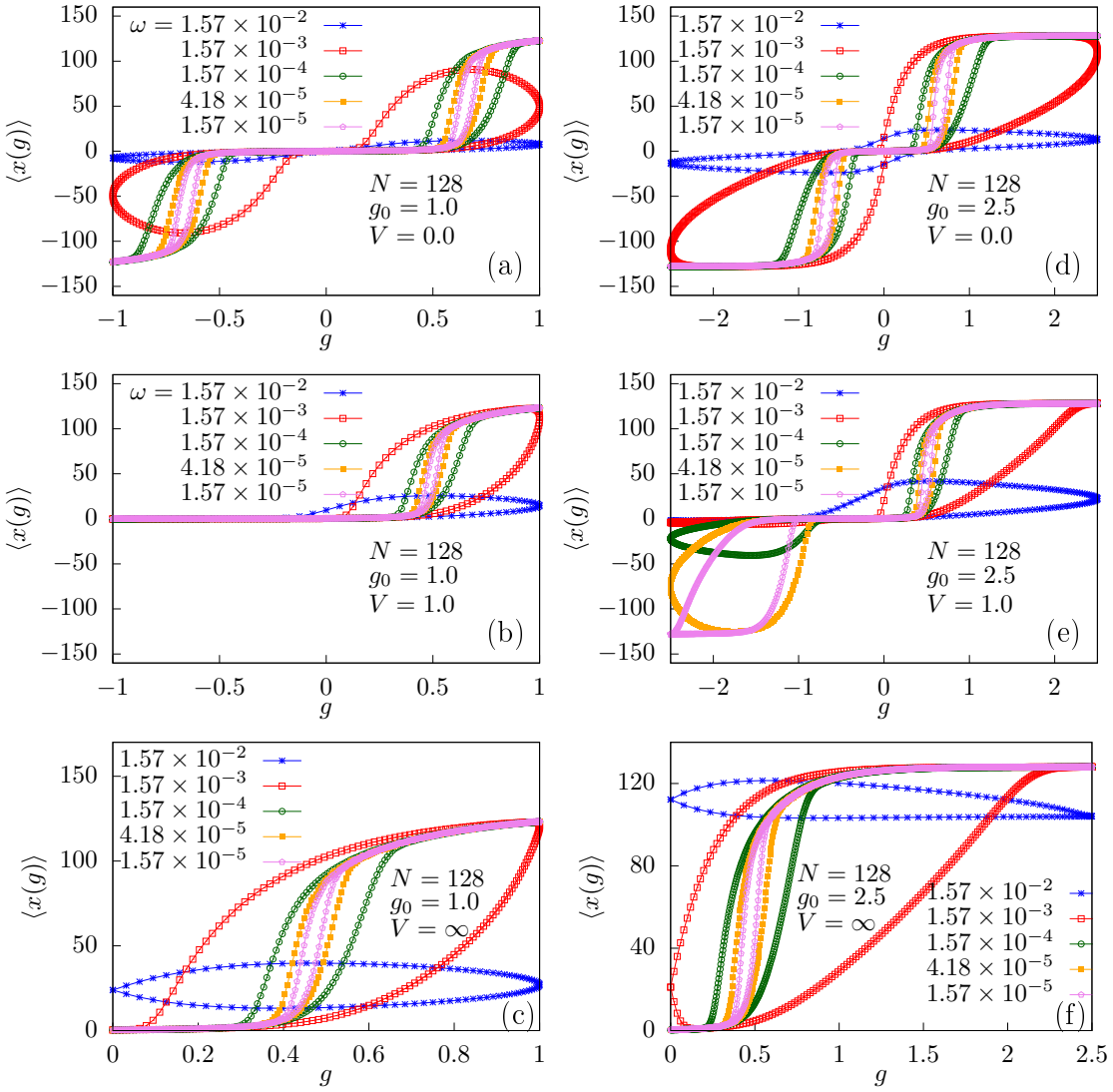

Figure 2.5: The force g vs extension $\langle x(g)\rangle$ curves averaged over 10^4 cycles of a polymer of length $N = 128$ for the various frequencies for (a) soft-wall, (b) wall separating two different type of media, and (c) hard-wall at force amplitudes $g_0 = 1.0$. Plots (d), (e) and (f) are the same as the plots (a), (b) and (c) respectively, at $g_0 = 2.5$. The line joining the points in these plots is just a guide for the eye.

media, respectively, and most of the monomers are adsorbed on the wall. For the soft-wall and the wall separating two different media, the polymer can penetrate the wall to gain the configurational entropy and due to this extra entropy, the stationary state of the polymer for the soft-wall case is an adsorbed state. At any finite temperature, the value of the critical force needed to unzip it from the wall is more than at it is at $T = 0$ (see Eq. (2.9)). Similarly, for the wall separating the two media, the critical force depends on the strength of the repulsive potential V and for smaller values V the phase diagram shows a reentrance region at lower

temperatures [35]. When the polymer is subjected to an oscillating force with a higher frequency, $\omega = 1.57 \times 10^{-2}$, the force changes very rapidly and it can only unzip a few monomers from the wall. Therefore, we obtain a small hysteresis loop for all the three cases [Fig 2.5(a)-2.5(c)]. For the soft-wall case, as the polymer experiences similar environment on both sides of the wall, the loop is divided about $\langle x(g)\rangle = 0$ into two equal and symmetrical parts. Whereas, in case of the wall separating two different media having different affinities for the polymer, the fast changing force, during the negative cycle, is unable to pull the monomers from the wall against the repulsive potential $V = 1.0$, in the region $x < 0$. Therefore, during the negative cycle of the force, the extension $\langle x(g)\rangle$ remains 0 with no hysteresis. In contrast, for the hard-wall case, at any finite temperature, few monomers of the adsorbed polymer at the free end are unzipped to gain the configurational entropy, and therefore, the stationary state of the polymer is a partially zipped state. Therefore, the average extension $\langle x(g)\rangle$ of the polymer even at $g = 0$ is finite (see Fig. 2.5(c)). When the frequency is decreased to a relatively lower value, $\omega = 1.57 \times 10^{-3}$, the polymer gets relatively more time to relax. As a result more number of monomers are separated from the wall and the area of hysteresis loop increases. For the soft-wall case, we get two symmetrical loops for the positive and the negative cycles of the oscillating force [see Fig. 2.5(a)]. In case of the wall separating two different media, the polymer remains adsorbed on wall with no hysteresis in the negative cycle of the force [see Fig. 2.5(b)]. In the positive cycle of the force loop looks similar to the loop obtained for the hard-wall case as shown in Fig. 2.5(c). At this frequency, the polymer gets fully unzipped at the maximum force value for the hard-wall and the wall separating two different media, resulting in larger loop area. As the frequency is decreased further, the polymer now has ample time to relax and therefore, the isotherms for the forward and backward paths begin to retrace each other at higher an lower force values but with a small hysteresis loop at intermediate forces. The area of the hysteresis loop decreases with the decrease in the frequency.

The force-distance isotherms for the higher force amplitude $g_0 = 2.5$ are shown in Figs. 2.5(d) – 2.5(f). The force amplitude $g_0 = 2.5$ is far far above the phase-boundary for all the three cases. For the soft-wall and the wall separating two different type of media, the stationary state is still the adsorbed polymer on the wall (i.e., $\langle x(g)\rangle = 0$ at $g = 0$). The shape of loops for the soft-wall case are similar to the loops obtained for the lower force amplitude $g_0 = 1.0$ but with larger area (Fig. 2.5(d)). In case of the wall separating two different types of the media

(Fig. 2.5(e)), the polymer remains adsorbed on the wall during the negative cycle of the force at higher frequencies $\omega = 1.57 \times 10^{-2}$ and 1.57×10^{-3} even for force amplitude $g_0 = 2.5$ resulting no hysteresis loop. During the positive force cycle, the loops are similar to $g_0 = 1.0$ case with slightly higher loop area. However, on decreasing the frequency to a value, $\omega = 1.57 \times 10^{-4}$, the polymer gets enough time to relax and at higher force values it can overcome the repulsive potential $V = 1.0$ on $x < 0$ and explore the region during the negative cycle of the pulling force. This results in a hysteresis loop in the region $x < 0$ (see Fig. 2.5(e)) which was absent for $g_0 = 1.0$ [Fig. 2.5(b)]. The loops thus obtained in the positive and negative cycles are not symmetric. For the hard-wall case, the stationary state at $g_0 = 2.5$ is an unzipped state. This can be seen by larger a value for $\langle x(g) \rangle$ at $g = 0$ at a higher frequency 1.57×10^{-2}. Under the influence of an oscillating force, at this frequency, few monomers at the anchored end of the the completely stretched polymer gets adsorbed on the hard-wall in the backward cycle and are unzipped in the forward cycle resulting in a smaller hysteresis loop (see Fig. 2.5(f)). On decreasing the frequency, more and more number of monomers will get adsorbed on the wall resulting in hysteresis loops of varying shapes and area. In the next section, we will see that this change of the stationary state from a partially zipped state at lower force amplitude $g_0 = 1.0$, to an unzipped state for higher force amplitude $g_0 = 2.5$ will give oscillatory behavior in the loop area.

C. Loop Area

In this subsection, we explore the behavior of the hysteresis loop area, A_{loop} (defined by Eq. (2.3)), of the curves discussed in the previous subsection. We determine the area of the hysteresis loops using the trapezoidal method. In this method the abscissa is divided into equally spaced intervals and the area of the curve is then the sum of the trapezoids formed by these intervals. In our study, the force $g(t)$ changes as a sine function (Eqs. (2.1) and (2.12)) resulting in a non-uniformly spaced intervals. To make evenly spaced intervals, we divide the force interval $g \in [0, g_0]$ into 1000 equal intervals for both the rise and fall of the force, in the positive as well as in the negative cycles, and then interpolate the value of $\langle x(g) \rangle$ at the end points of these intervals using cubic splines from the GNU Scientific Library [163]. On these intervals, the loop area, A_{loop}, is then numerically calculated using the trapezoidal rule.

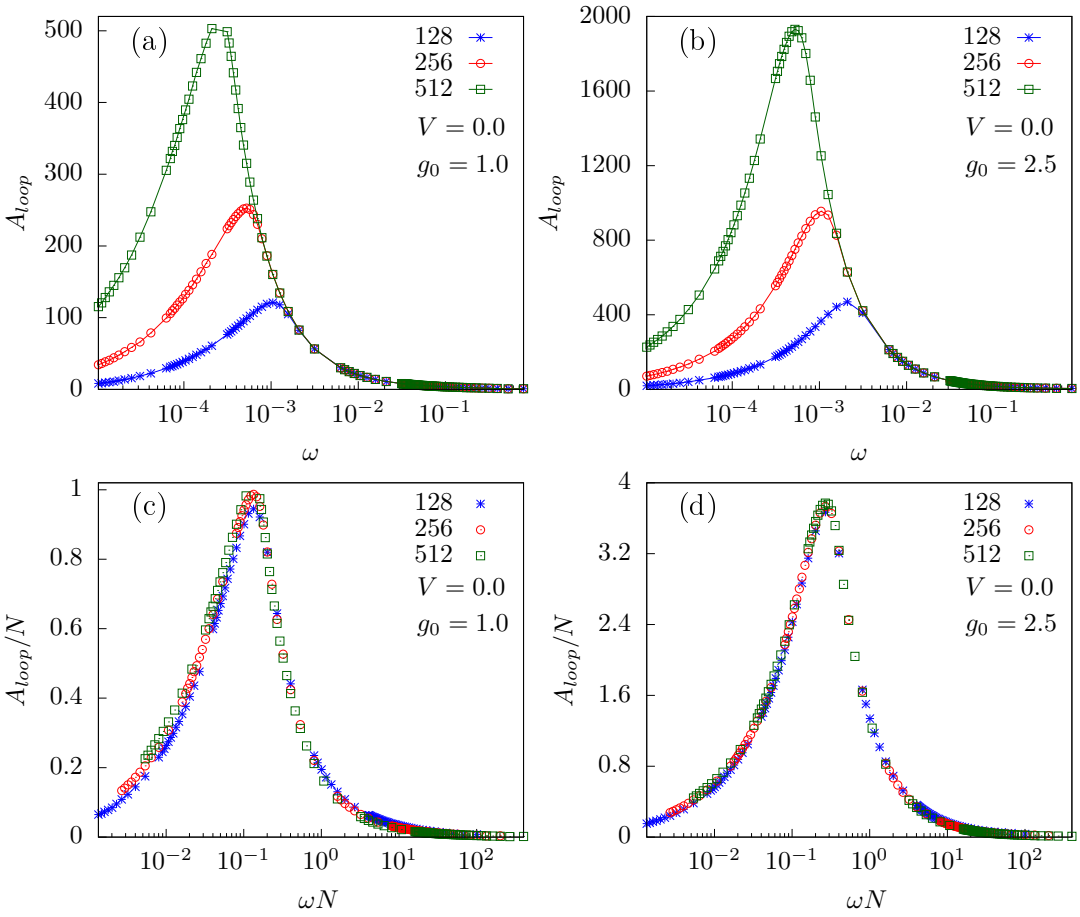

Figure 2.6: Area of the hysteresis loop A_{loop} as a function of frequency ω, in a semilog scale, for the polymer of lengths $N = 128, 256$, and 512 at force amplitudes (a) $g_0 = 1.0$ and (b) $g_0 = 2.5$ when it is adsorbed on a soft-wall ($V = 0.0$). Plots (c) and (d) are A_{loop}/N vs ωN of the data shown in (a) and (b), respectively. The line joining the points in these plots is just a guide for the eye.

In Figs. 2.6(a) and 2.6(b), we have plotted A_{loop} as a function of frequency ω for the polymer of three different lengths $N = 128, 256$, and 512 at two different force amplitudes $g_0 = 1.0$ and 2.5 for the soft-wall case ($V = 0$). We find that the loop area A_{loop} depends non-monotonically on the frequency ω of the periodic force. At very high frequencies, the area of the loop is almost zero. As the frequency of the pulling force decreases, the loop area started increasing. It reaches a maximum value at a specific frequency ω^*, to be called as resonance frequency, and then begins to decrease as the frequency is decreased further. At ω^*, the natural frequency of the polymer matches with the frequency of the externally applied force and we obtain the maximum loop area. In the limit $\omega \to 0$, the loop area $A_{loop} \to 0$. At higher force amplitudes (e.g., $g_0 = 2.5$), loop area shows similar behavior as

for $g_0 = 1.0$ but with larger magnitudes. We can also see that the frequency ω^* also depends on the amplitude g_0 of the oscillating force. From these figures, it is obvious that the resonance frequency, $\omega^*(g_0)$, at which the area of the hysteresis loop is maximum, depends on length N of the polymer. The frequency $\omega^*(g_0)$ decreases as the length of the polymer increases and in the thermodynamic limit $N \to \infty$, we have $\omega^*(g_0) \to 0$. This suggests that A_{loop} satisfies the scaling of the form,

$$A_{loop} = N^{\delta} \mathcal{Y}(\omega N^{z}), \tag{2.13}$$

with δ and z as critical exponents. On plotting A_{loop}/N data for various chain lengths as a function of ωN (i.e., for exponents $\delta = 1.00 \pm 0.05$ and $z = 1.00 \pm 0.05$), we obtain a nice collapse. The data collapse for $g_0 = 1.0$ and $g_0 = 2.5$ is shown in Figs. 2.6(c) and 2.6(d), respectively. The above scaling (Eq. 2.13) with exponents $\delta = 1$ and $z = 1$ implies that the loop area scales as $A_{loop} \sim 1/\omega$ in the high-frequency regime (i,e., $\omega \to \infty$).

The loop area A_{loop} as a function of ω for the wall separating two different media, with $V = 1$ for $x < 0$, are shown in Fig. 2.7(a) and 2.7(b) for two different force amplitudes $g_0 = 1.0$ and 2.5, respectively. For lower force amplitude, $g_0 = 1.0$, the A_{loop} curve behaves similarly as the soft-wall case but with slightly lower A_{loop} values at ω^* (see Fig. 2.6(a)). The A_{loop} curves at higher force amplitude $g_0 = 2.5$ (Fig. 2.7(b)) are very different from the soft-wall case (see Fig. 2.6(b)). In the present case a new peak starts emerging on decreasing the frequency from ω^*. This new peak appears because of the hysteresis loops emerging for the negative cycle of the force at lower frequencies for higher force amplitude (see Fig. 2.5(e)). The A_{loop} keeps on increasing till the frequency ω^{**} (say), where it reaches another maximum, and then decreases on decreasing the frequency further to $\omega \to 0$. From Figs. 2.7(a) and 2.7(b), we can see that both ω^* and ω^{**} decreases as N is increased, and in the thermodynamic limit $N \to \infty$, both $\omega^* \to 0$ and $\omega^{**} \to 0$. The above finite-size scaling form (Eq. 2.13) is applicable for this case also. In Figs. 2.7(c) and 2.7(d), we have plotted A_{loop}/N vs ωN for various chain lengths at force amplitudes $g_0 = 1.0$ and 2.5, respectively. The nice data collapse obtained for both force amplitudes again implies that $A_{loop} \sim 1/\omega$ in the high-frequency regime.

The loop area A_{loop} as a function of ω for the hard-wall ($V = \infty$ for $x < 0$) are shown in Fig. 2.8(a) and 2.8(b) for two different force amplitudes $g_0 = 1.0$ and 2.5, respectively. For lower force amplitude, $g_0 = 1.0$, the A_{loop} curve for this case also behaves similarly as the soft-wall, and the wall separating two different type of

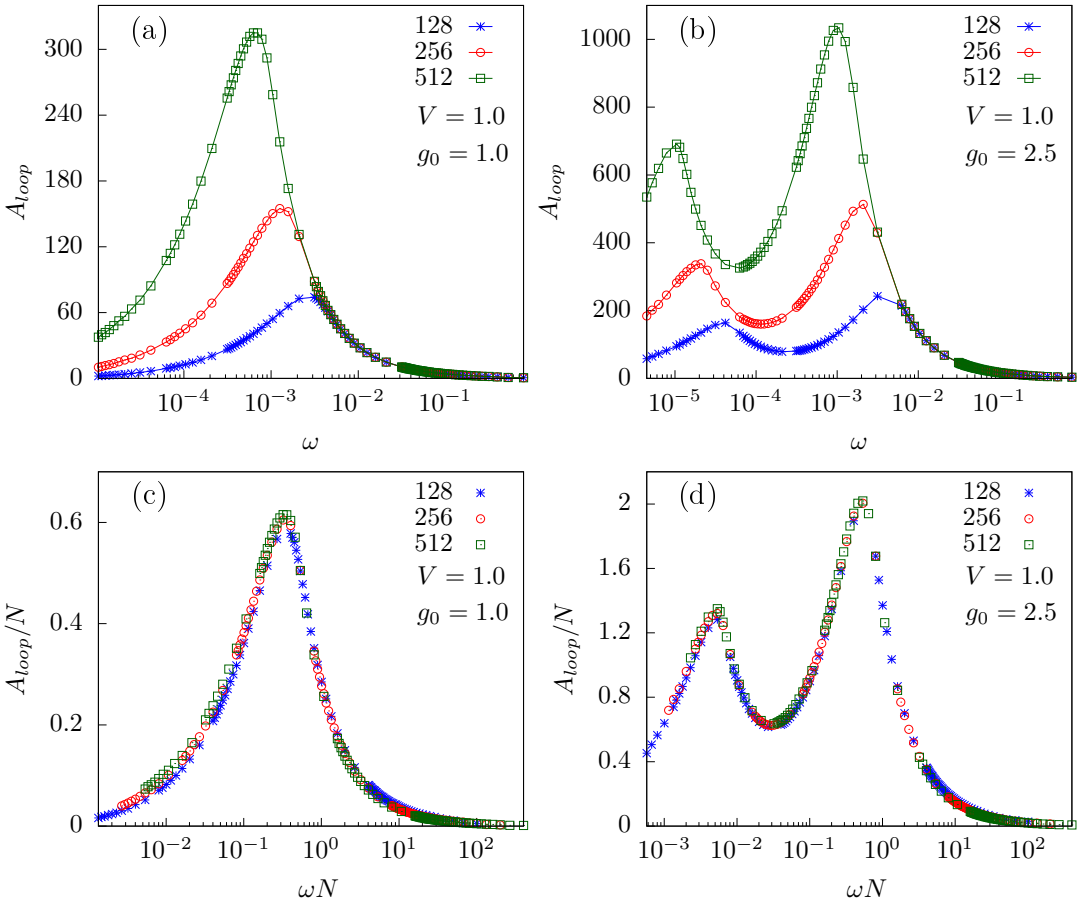

Figure 2.7: Area of the hysteresis loop A_{loop} as a function of frequency ω, in a semilog scale, for the polymer of lengths $N = 128, 256$, and 512 at force amplitudes (a) $g_0 = 1.0$ and (b) $g_0 = 2.5$ when it is adsorbed on wall separating two different media ($V = 1.0$). Plots (c) and (d) are A_{loop}/N vs ωN of the data shown in (a) and (b), respectively. The line joining the points in these plots is just a guide for the eye.

media cases (see Figs. 2.6(a) and 2.7(a)). However, for higher force amplitudes (e.g., $g_0 = 2.5$), the A_{loop} curves show oscillatory behavior in the higher frequency regime. These oscillations are similar to the A_{loop} observed for a homopolymer DNA [20] and a block copolymer DNA [22] subjected to a periodic force. The secondary peaks, which are seen only for the hard-wall case at higher force amplitudes, are possible due to the stationary state of the polymer(unzipped configuration) for the hard-wall case at these amplitudes. For all other cases, the stationary state of the polymer is an adsorbed (or zipped) configuration (see previous section). Therefore, whenever the force drops below the critical value during the fall and the rise of the force, few monomers of the polymer at the anchored end get adsorbed on the wall and unzipped giving rise to small loop area. On decreasing the frequency, more

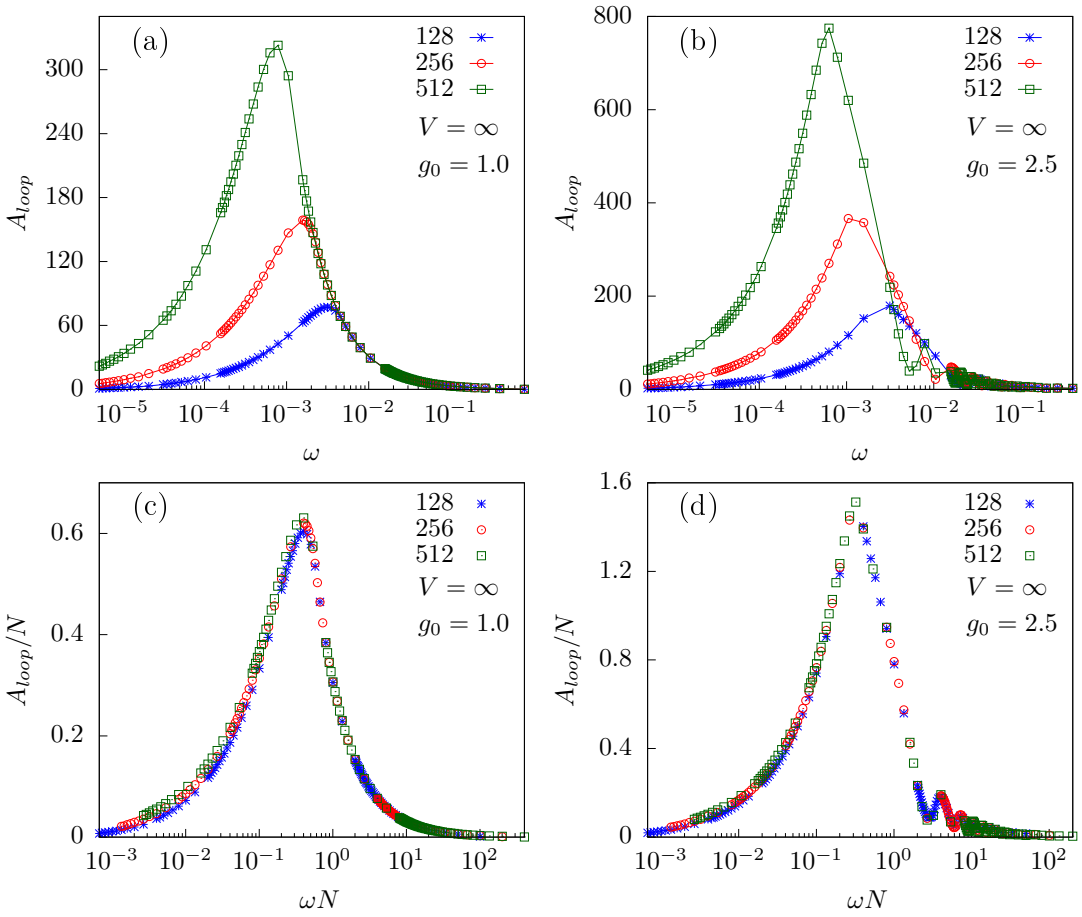

Figure 2.8: Area of the hysteresis loop A_{loop} as a function of frequency ω, in a semilog scale, for the polymer of lengths $N = 128, 256$, and 512 at force amplitudes (a) $g_0 = 1.0$ and (b) $g_0 = 2.5$ when it is adsorbed on a hard-wall ($V = \infty$). Plots (c) and (d) are A_{loop}/N vs ωN of the data shown in (a) and (b), respectively. The line joining the points in these plots is just a guide for the eye.

number of monomers take part in this zipping and unzipping process resulting in increase in loop area. It is observed that the number of secondary peaks increases as the length N of polymer increases. These secondary peaks are higher Rouse modes, whose frequencies are given by $\omega_p = (2p-1)\pi/2N$, with $p = 1, 2, ...$ as integers. The finite-size scaling form given in Eq. (2.13) is applicable for this case too. When A_{loop}/N is plotted as a function of ωN for various chain lengths a nice data collapse is obtained for force amplitudes $g_0 = 1.0$ and 2.5. The collapse is shown in Figs. 2.8(c) and 2.8(d), respectively. This again implies that $A_{loop} \sim 1/\omega$ in the high-frequency regime.

To obtain the scaling behavior in the low-frequency regime (i.e., $\omega \to 0$), we have plotted in Fig. 2.9, the area of hysteresis loop, A_{loop}, as a function of $\omega^{\beta}(g_0 - g_c)^{\alpha}$ for

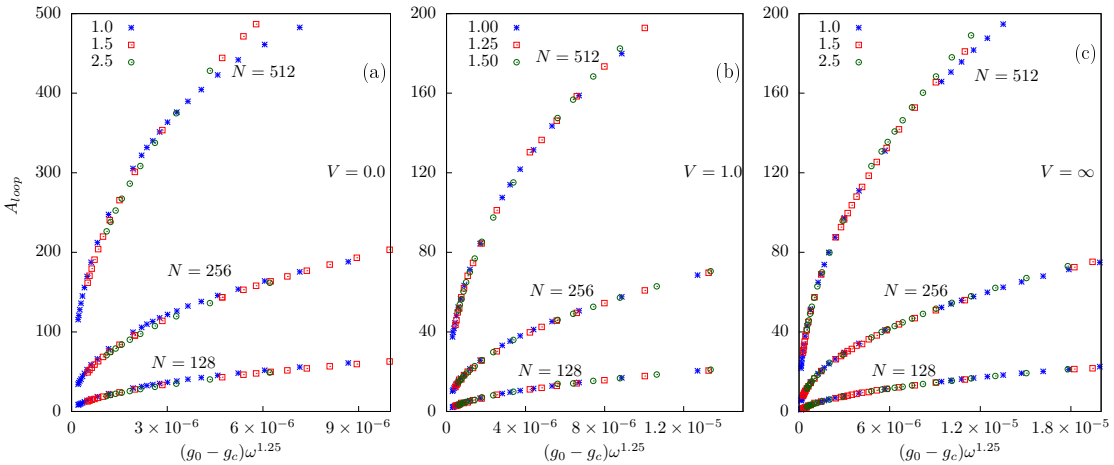

Figure 2.9: A_{loop} as a function of $(g_0 - g_c)\omega^{1.25}$ for the polymer of lengths $N = 128, 256$, and 512 at various force amplitudes for (a) soft-wall ($V = 0.0$), (b) wall separating two different media ($V = 1.0$), and (c) hard-wall ($V = \infty$).

the polymer of lengths $N = 128, 256$, and 512 at force amplitudes $g_0 = 1.0, 1.5$, and 2.5 for (i) the soft-wall ($V = 0.0$) [Fig. 2.9(a)], (ii) the wall separating two different media ($V = 1.0$) [Fig. 2.9(b)], and (iii) the hard-wall ($V = \infty$) [Fig. 2.9(c)] cases. In the above expression g_c is the critical force, needed to unzip the polymer adsorbed from the wall for the static force case at temperature $T = 0.5$. An excellent data collapse is obtained for the values of the exponents $\alpha = 1.00 \pm 0.05$ and $\beta = 1.25 \pm 0.05$ in all the three cases. The values of these exponents are found to be similar to the exponents obtained in the the Monte Carlo simulation studies of a homopolymer DNA [20] and a block copolymer DNA [22] subjected to a periodic force. In both these studies the DNA is also modelled, same as the polymer model studied in this chapter, by a directed self-avoiding walk in (1+1)-directions. In a recent study, it was shown by Langevin dynamics simulations of a longer DNA chain in 2-dimensions that these exponents remain the same [80].

D. Order parameter

In the previous sections, we have studied the response of the polymer by keeping the force amplitude g_0 fixed and varying the frequency ω of the oscillating force. It was found that the polymer can be taken from the zipped configuration to an unzipped configuration by varying ω at constant g_0. However, such a transition is also possible by keeping the frequency fixed and varying the force amplitude. Let

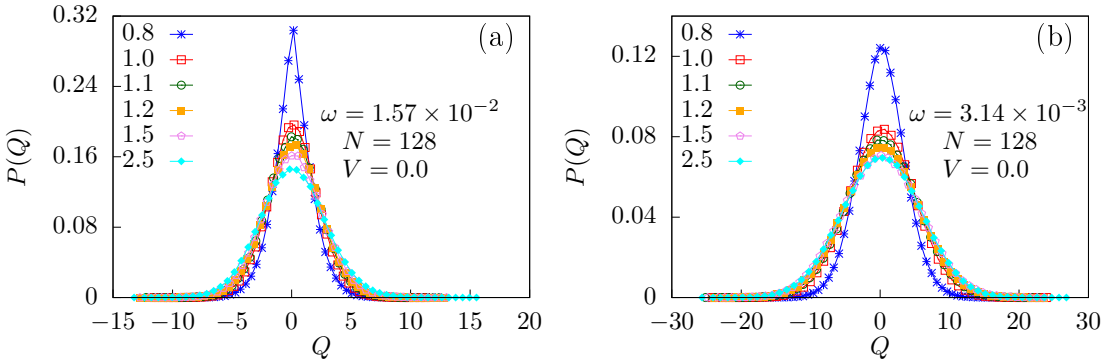

Figure 2.10: The normalized probability distribution $P(Q)$ of order parameter Q of a polymer of length $N = 128$ at various force amplitudes $g_0 = 0.8, 1.0, 1.1, 1.2, 1.5,$ and 2.5 at two different frequencies (a) $\omega = 1.57 \times 10^{-2}$ and (b) $\omega = 3.14 \times 10^{-3}$ for the soft-wall ($V = 0.0$) case. The line joining the points in these plots is just a guide for the eye.

$P(Q)$ represents the probability distributions of the dynamical order parameter Q defined in Eq. (2.2). At a fixed frequency ω, the probability distribution $P(Q)$ is obtained by binning the Q values accumulated from 10^6 different cycles of the periodic force for different force amplitudes.

In Fig. 2.10, we have plotted, the normalized $P(Q)$ for polymer of length $N = 128$ for the soft-wall case ($V = 0$) at six different force amplitudes $g_0 = 0.8, 1.0, 1.1, 1.2, 1.5,$ and 2.5 and two different frequencies $\omega = 1.57 \times 10^{-2}$ and $\omega = 3.14 \times 10^{-3}$. In this case, the polymer can cross the wall, for all frequencies and force amplitudes, without any difficulty. Therefore, the distributions $P(Q)$ are

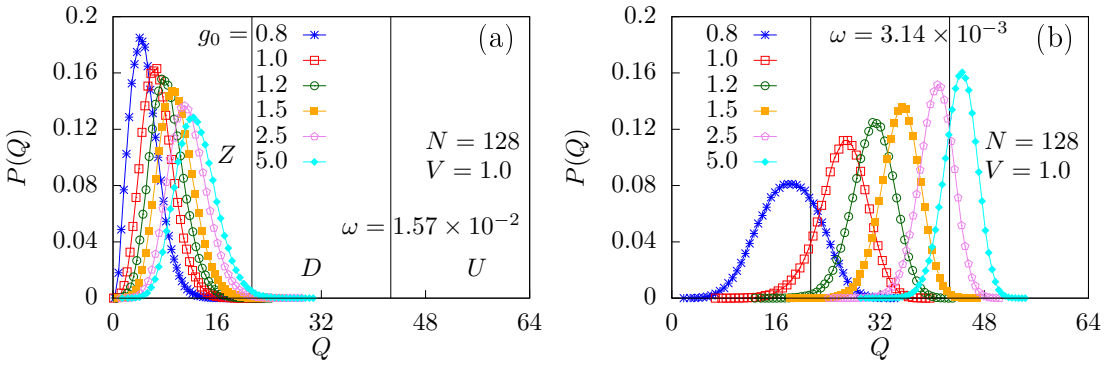

Figure 2.11: The normalized probability distribution $P(Q)$ of order parameter Q of a polymer of length $N = 128$ at various force amplitudes $g_0 = 0.8, 1.0, 1.2, 1.5, 2.5,$ and 5.0 at two different frequencies (a) $\omega = 1.57 \times 10^{-2}$ and (b) $\omega = 3.14 \times 10^{-3}$ for the wall separating two different media ($V = 1.0$) case. The line joining the points in these plots is just a guide for the eye.

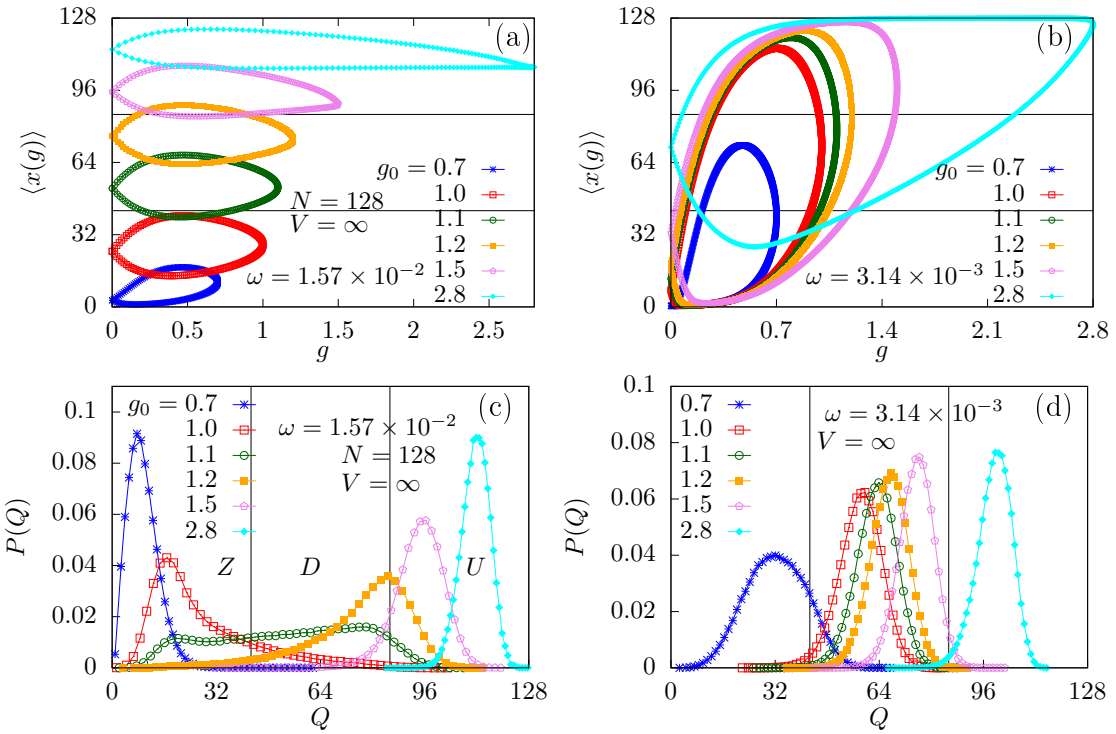

Figure 2.12: Average extension $\langle x(g)\rangle$ as a function of force g of a polymer of length $N = 128$ for various force amplitudes $g_0 = 0.7, 1.0, 1.1, 1.2, 1.5$, and 2.8 at two different frequencies (a) $\omega = 1.57 \times 10^{-2}$ and (b) $\omega = 3.14 \times 10^{-3}$ for hard-wall ($V = \infty$) case. The normalized probability distribution $P(Q)$ of order parameter Q at frequencies (c) $\omega = 1.57 \times 10^{-2}$ and (d) $\omega = 3.14 \times 10^{-3}$. The line joining the points in these plots is just a guide for the eye.

peaked about $Q = 0$ for all force amplitudes at both frequencies [Figs. 2.10(a) and 2.10(b)]. The width of the distribution are found to depend on the frequency. At higher frequencies, the distributions are sharply peaked but their width increases on decreasing the oscillating frequency.

The normalized $P(Q)$ for the wall separating two different media ($V = 1.0$) are plotted in Fig. 2.11. The distributions $P(Q)$, for all the force amplitudes, are peaked at different Q values. At a higher frequency $\omega = 1.57 \times 10^{-2}$ and lower amplitudes (e.g., $g_0 = 0.8$), the peak of the distribution is around $Q = 5$ showing a zipped configuration which implies that the polymer is in the adsorbed phase. On increasing the force amplitude, the distribution starts becoming broader and its peak also shifts towards the higher Q values but is still smaller in magnitude (e.g., $Q \approx 10$ at $g_0 = 2.5$) implying that the polymer is in the adsorbed (Z) phase [Fig. 2.11(a)]. From the figure, it is observed that as the force amplitude g_0 increases, the distribution $P(Q)$ moves slowly towards right and its width increases.

The trend of moving of the distributions towards right side with higher force amplitude is also present in the lower frequency $\omega = 3.14 \times 10^{-3}$, but the distributions become sharper on increasing the force amplitude [see Fig. 2.11(b)].

The normalized probability distributions $P(Q)$ for the hard-wall case ($V = \infty$) for various values of force amplitudes, and corresponding hysteresis loops are plotted in Fig. 2.12. At a higher frequency $\omega = 1.57 \times 10^{-2}$, the distributions $P(Q)$ for the lower values of force amplitude $g_0 = 0.7$ and 1.0 are sharply peaked at lower values of Q implying that the polymer is in the zipped (Z) phase. When the amplitude is increased to $g_0 = 1.1$, the distribution $P(Q)$ becomes broader and spans both the zipped (Z) and dynamic (D) phases (see Fig. 2.12(c)). A similar behavior was earlier found in the unzipping of dsDNA by the periodic force [76, 21]. At an amplitude $g_0 = 1.2$, the distribution starts becoming narrower again with a peak at an intermediate Q value which lies in the boundary of the dynamic (D) and the unzipped (U) phases. On increasing the amplitude further (i.e., $g_0 = 1.5$ and 2.8), the distributions are again sharply peaked at higher Q values indicating that the polymer in in the unzipped (U) phase. However, at a lower frequency $\omega = 3.14 \times 10^{-3}$, the two peak structure in the distribution $P(Q)$, which was present for the intermediate force amplitudes in Fig. 2.12(c)], disappears and we have sharply defined phases (see Fig. 2.12(d)).

2.3 Conclusions

In this chapter, we studied the dynamic transitions in the unzipping of an adsorbed polymer on a attractive surface (or the wall) subjected to a periodic force with amplitude g_0 and frequency ω using Monte Carlo simulations. We considered the three different cases for the walls: the soft-wall, the wall separating two different media, and the hard-wall. We have studied both the static as well as the dynamic force cases. We obtained the force-distance isotherms for various system sizes and extracted the critical values of the unzipping force at various temperatures using finite-size scaling. They are found to match the analytical phase-boundary obtained using the generating function technique. For the dynamic case, the system is not in equilibrium and the results depend on the amplitude g_0 and frequency ω of the periodic force. We observed that the force-distance isotherms show hysteresis loops in all the three cases. The loop depends on the frequency of the force. For

the soft-wall case, as the polymer experiences similar environment on both sides of the wall, the loop is divided about $\langle x(g)\rangle = 0$ axis into two equal and symmetrical parts. Whereas, in case of the wall separating two different media having different affinities for the polymer, loops obtained in the positive and negative cycles are not symmetric. On the other hand, for the hard-wall case, loop is obtained only for the region $x > 0$. The behavior of the loop area, A_{loop}, depends on the force amplitudes. It is found that at lower force amplitudes, loop area exhibits only one peak at resonance frequency $\omega^*(g_0)$, and it decreases monotonically for the frequencies higher than $\omega^*(g_0)$ for all the three cases. However, for higher force amplitudes, it still shows only one peak for the soft-wall and hard-wall cases, respectively, whereas for the wall separating two different types of media, it shows two peaks of different heights. The higher peak occurs at higher frequency. Similar to the case of lower force amplitudes, loop area, for the soft-wall and wall separating two different media, decreases monotonically for the frequencies higher than the $\omega^*(g_0)$, while for the hard-wall it shows oscillatory behavior in the regime $\omega \to \infty$. The number of secondary peaks increases with the length of the polymer. For the hard-wall case, it is observed that the steady state configuration of the polymer at higher frequencies and lower values of force amplitude is a zipped (Z) state. At higher frequencies and higher values of force amplitude, the steady state configuration of the polymer is completely stretched state, i.e., the unzipped (U) state.

Chapter 3

Unzipping of a Block Copolymer DNA by Periodic Force

In this chapter, we study the unzipping of a block copolymer DNA. We consider a hetero-polymer DNA as a block copolymer DNA, in which the heterogeneity is considered in the form of repeated blocks, A_nB_n or B_nA_n, where $2n$ is the block length, A and B are different types of base pairs with two- and three-hydrogen bonds, respectively. One end of this DNA sequence is subjected to a pulling force while the other end is kept anchored. We considered both the constant and the periodic pulling force cases. The unzipping of a block copolymer DNA by a constant pulling force is found to be a first-order phase transition. The equilibrium phase boundary separating the zipped and the unzipped phases does not depend on the DNA sequence and is found to follow the same exact expression, as obtained for the homo-polymer DNA case [17, 99, 19], but with a different effective base pair energy. The results for the unzipping of a block copolymer DNA subjected to a periodic force are however found to be sequence dependent. For sequences of higher block lengths, the results also depend on whether the periodic force is acting on A type or B type base-pairs.

The chapter is organized as follows: In Sec. 3.1 we define our model and simulation details. Section 3.2 is devoted for discussions on our results for both the static and the periodic pulling force cases. We finally summarize the results in Sec. 3.3.

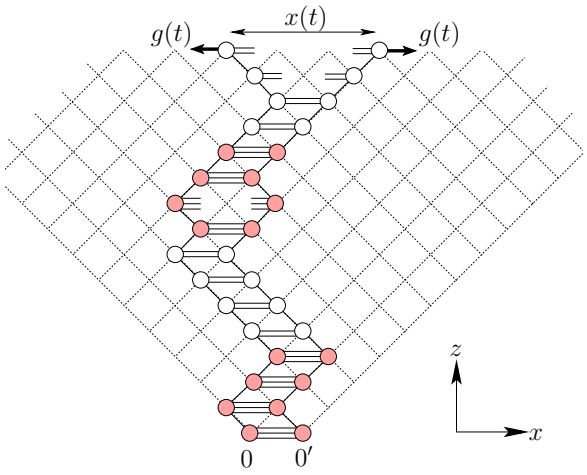

Figure 3.1: Schematic diagram of a heterogeneous dsDNA of the type $(B_4A_4)_2$, where A and B represents base pairs having three and two hydrogen bonds, respectively. One end of the DNA is anchored at the origin (O and O'), and the strands on the free end are subjected to a time-dependent periodic force with frequency ω and amplitude g_0.

3.1 Model

We define hetero-polymer DNA as a block copolymer DNA of type $(A_nB_n)_M$, where A and B are two different types of base pairs, $2n$ is the total number of base pairs in a block unit, also be called as block length, and $M = N/2n$ represents the total number of blocks in the DNA of length N. We consider block lengths $2n = 4, 8, 16, 32, 64, 128$ and 256. The two strands of the DNA are represented by two directed self-avoiding random walks on a $(d = 1 + 1)$ dimensional square lattice. The walks starting from the origins O and O', which are unit distance apart, are restricted to go towards the positive direction of the diagonal axis (z direction) without crossing each other. The directional nature of the walks take care of the self-avoidance. Whenever the complementary bases are unit distance apart they gain energy of -2ϵ ($\epsilon > 0$) for the base pair of type A and -3ϵ for the base pair of type B. Here we have assumed that ϵ ($\epsilon > 0$), represents the strength of a hydrogen bond.

Two strands of the DNA at one end are always kept fixed at origins O and O' and the other end monomers are subjected to a time-dependent periodic force $g(t)$

$$g(t) = g_0 \mid \sin(\omega t) \mid, \tag{3.1}$$

where g_0 is the amplitude and ω is the frequency. The schematic diagram of the model is shown in Fig. 3.1.

We consider the following two cases: (i) the base pairs having two hydrogen bonds are anchored at the origins and the time varying force is applied on the base pairs that are bound by three hydrogen bonds, represented by $(A_nB_n)_M$, and (ii) the opposite case, i.e., the base pairs having three hydrogen bonds are anchored at the origins and the force is acting on monomers that are bound by two hydrogen bonds (represented by $(B_nA_n)_M$). While the equilibrium results for both the cases are found to be the same, the nonequilibrium results show marked differences.

We perform Monte Carlo simulations of the model using the Metropolis algorithm. The strands of the DNA undergo Rouse dynamics that consists of local corner-flip or end flip moves that do not violate mutual avoidance [3]. The elementary move consists of selecting a random monomer from a strand, which itself is chosen at random, and flipping it. If move results in the overlapping of two complementary monomers, thus forming a base-pair between the strands, it is always accepted as a move. The opposite move (i.e., unbinding of monomers) is chosen with the Boltzmann probabilities $\eta = \exp(-2\epsilon/k_BT)$ or $\eta = \exp(-3\epsilon/k_BT)$ for base pairs of types A and B, respectively. If the chosen monomer is from the unbound base-pair, which remains unbound even after the move is perform (thus no change in the energy), is always accepted. The time is measured in units of Monte Carlo steps (MCSs). One MCS consists of $2N$ flip attempts, which means that on average, every monomer is given a chance to flip. Throughout the simulation, the detailed balance is always satisfied and the algorithm is ergodic in nature. It is always possible, from any starting DNA configuration, to reach any other configuration by using the above moves.

We let the simulation run for $2000\pi/\omega$ MCSs, so that system reaches the stationary state before taking measurements. Throughout this chapter, we have chosen dimensionless quantities. The quantities having dimensions of energy are measured in units of ϵ and the quantities that have dimensions of length are measured in terms of the lattice constant a. We have taken $k_B = 1$, $\epsilon = 1$, and $a = 1$.

The separation between the end monomers of the two strands, $x(t)$, changes under the influence of the applied external force $g(t)$, is monitored as a function of

time t. The time averaging of $x(t)$ over a complete period

$$Q = \frac{\omega}{\pi} \oint x(t)dt \tag{3.2}$$

can be used as a dynamical order parameter[162]. From the time series $x(t)$, we obtain the extension $x(g)$ as a function of force g and average it over 10000 cycles to obtain the average extension $\langle x(g) \rangle$ as a function of g. For systems far away from equilibrium, the average extension, $\langle x(g) \rangle$, for the forward and backward paths for the periodic force is not the same, and we see a hysteresis loop. The area of hysteresis loop, A_{loop}, is defined by

$$A_{loop} = \oint \langle x(g) \rangle dg \tag{3.3}$$

depends upon the frequency ω and the amplitude g_0 of the oscillating force. This quantity also serves as another dynamical order parameter.

3.2 Results and Discussions

In this section we discuss the results obtained for both the static and the dynamic cases. Let us first take the static case.

3.2.1 Static Case ($\omega = 0$)

In the static case, this model can be solved exactly using the generating function and the exact transfer matrix techniques. If the partition function of the dsDNA of length n with separation x between monomers of the strands is represented by $\mathcal{D}_n(x)$, in the fixed distance ensemble, then $\mathcal{D}_n(x)$ satisfies the recursion relation:

$$\mathcal{D}_{n+1}(x) = [\mathcal{D}_n(x+1) + 2\mathcal{D}_n(x) + \mathcal{D}_n(x-1)] \times \mathcal{C}, \tag{3.4}$$

where

$$\mathcal{C} = \begin{cases} 1 + \left(e^{2\beta\epsilon} - 1\right) \delta_{x,1}, & \text{for base pair type } A \\ 1 + \left(e^{3\beta\epsilon} - 1\right) \delta_{x,1}, & \text{for base pair type } B. \end{cases} \tag{3.5}$$

The above recursion relation can be iterated N times, with an initial condition $\mathcal{D}_0(x) = \delta_{x,1}$ to obtain the partition function of the DNA of length N. The recursion relation (Eq. (3.4)) with a single base pairing energy (say ε) for each base pair such that $\mathcal{C} = \left[1 + \left(e^{\beta\varepsilon} - 1\right)\delta_{x,1}\right]$ has been solved exactly via the generating function technique [17, 18, 99] to obtain the exact unzipping phase diagram. In this method, the singularities of the generating function are calculated. The phase of the DNA is given by the singularity closest to the origin and when the two singularities cross each other a phase transition takes place. Taking the following form for the generating function for $\mathcal{D}_n(x)$,

$$\hat{\mathcal{D}}(z,x) = \sum_n z^n \mathcal{D}_n(x) = \kappa^x(z) Y(z), \tag{3.6}$$

and used in the above recursion relation (Eq.(3.4) with initial condition $\mathcal{D}_0(x) = \delta_{x,1}$), we obtain $\kappa(z) = (1-2z-\sqrt{1-4z})/(2z)$ and $Y(z) = 1/\left[1 - z\left(2 + \kappa(z)\right)e^{\beta\varepsilon}\right]$. The singularities of $\kappa(z)$ and $Y(z)$ are $1/2$ and $z_2 = \sqrt{1-e^{-\beta\varepsilon}} - 1 + e^{-\beta\varepsilon}$, respectively. The zero force melting, which comes from $z_1 = z_2$, takes place at a temperature $T_m = \varepsilon/\ln(4/3)$. In the large length limit, $D_n(x)$ can be approximated as $D_N(x) \approx \kappa^x(z_2)/z_2^{N+1}$, with the free energy $\beta F = N \ln z_2 - x \ln \kappa(z_2)$. The average force required to maintain the separation x, in a fixed distance ensemble, is then given by

$$g(T) = \frac{\partial F}{\partial x} = -k_B T \ln \kappa(z_2). \tag{3.7}$$

In the fixed force ensemble, the generating function can be written as

$$\begin{aligned} \mathcal{G}(z,\beta,g_0) &= \sum_x e^{2\beta g_0 x} \sum_n z^n \mathcal{D}_n(x) = \sum_x e^{2\beta g_0 x} \kappa^x(z) Y(z) \\ &= \frac{Y(z)}{1 - \kappa(z) e^{2\beta g_0}}, \end{aligned} \tag{3.8}$$

which has an additional force-dependent singularity $z_3 = 1/[2 + 2\cosh(2\beta g_0)]$. The phase boundary comes from $z_2 = z_3$, and is given by

$$g_c(T) = k_B T \cosh^{-1}\left[\frac{1}{2}\frac{1}{\sqrt{1-e^{-\beta\varepsilon}} - 1 + e^{-\beta\varepsilon}} - 1\right], \tag{3.9}$$

which is same as the phase boundary obtained in the fixed distance ensemble [Eq. (3.7)]. In the above expression, ε is the only free parameter, which can be tuned. For the block copolymer DNA case, in every block, we have n base pairs each of types A and B, giving the total base pairing energy $(2\epsilon + 3\epsilon)n$. Since the

total energy of the block remains the same irrespective of the sequence $(A_nB_n)_M$ or $(B_nA_n)_M$, we seek if an effective base pairing energy $\varepsilon = 5\epsilon/2$ in Eq. (3.9) can give us the exact phase boundary for the block copolymer DNA as obtained by iterating the recursion relation Eq. (3.4). The phase diagram of unzipping of a block copolymer DNA (with $\varepsilon = 5\epsilon/2$) is shown in Fig. 3.5 by solid line.

The exact transfer matrix technique can be used to obtain many other equilibrium properties which are based on thermal averaging for a finite system size. In this technique, the partition function $\mathcal{D}_N(x)$ for the DNA of length N, at any temperature, can be obtained numerically by iterating the above recursion relation [i.e. Eq.(3.4)] N times, with an initial condition $\mathcal{D}_0(1) = 1$. The equilibrium average separation between the end monomers, $\langle x \rangle_{\rm eq}$, can then be obtained by

$$\langle x \rangle_{\rm eq} = \frac{\sum_x x\ \mathcal{D}_N(x) e^{\beta g_0 x}}{\sum_x \mathcal{D}_N(x) e^{\beta g_0 x}}. \tag{3.10}$$

In Fig. 3.2, we have plotted the scaled extension $\langle x \rangle / N$, as a function of constant pulling force g for different chain lengths $N = 256, 512$, and 1024 at $T = 1.5$ obtained by iterating the recursion relation Eq. (3.4) for the heterogeneous sequences $(A_{16}B_{16})_M$ [Fig. 3.2(a)], in which the base pair of type A is anchored at the origin and an external force g is applied on the base pair type B, and $(B_{16}A_{16})_M$ [Fig. 3.2(c)], which is the opposite of the above. From the figure, we can clearly see that the DNA is in the zipped phase at lower g values and in the unzipped phase when g exceeds a critical value g_c. Furthermore, as the length N of DNA increases, the transition becomes sharper. In the thermodynamic limit, it would become a step function at a critical value g_c. The point of intersection of these isotherms for various lengths is very close to the critical force g_c. We use chain lengths $N = 256, 512$, and 1024, and the finite-size scaling of the form

$$\langle x \rangle = N^p \mathcal{F}\Big((g - g_c) N^q \Big), \tag{3.11}$$

to extract the critical force g_c. A nice collapse is obtained for $p = 0.97 \pm 0.02$, $q = 1.0 \pm 0.02$ and $g_c = 3.31 \pm 0.05$ for sequence $(A_{16}B_{16})_M$ [shown in Fig. 3.2(b)] and for $p = 1.0 \pm 0.02$, $q = 1.0 \pm 0.02$ and $g_c = 3.31 \pm 0.05$ for sequence $(B_{16}A_{16})_M$ [shown in Fig. 3.2(d)]. The critical force, $g_c = 3.31 \pm 0.05$ (at $T = 1.5$), is found to be same for both the sequences $(A_{16}B_{16})_M$ and $(B_{16}A_{16})_M$ implying that, at equilibrium, it does not matter whether the DNA is unzipped from the end having

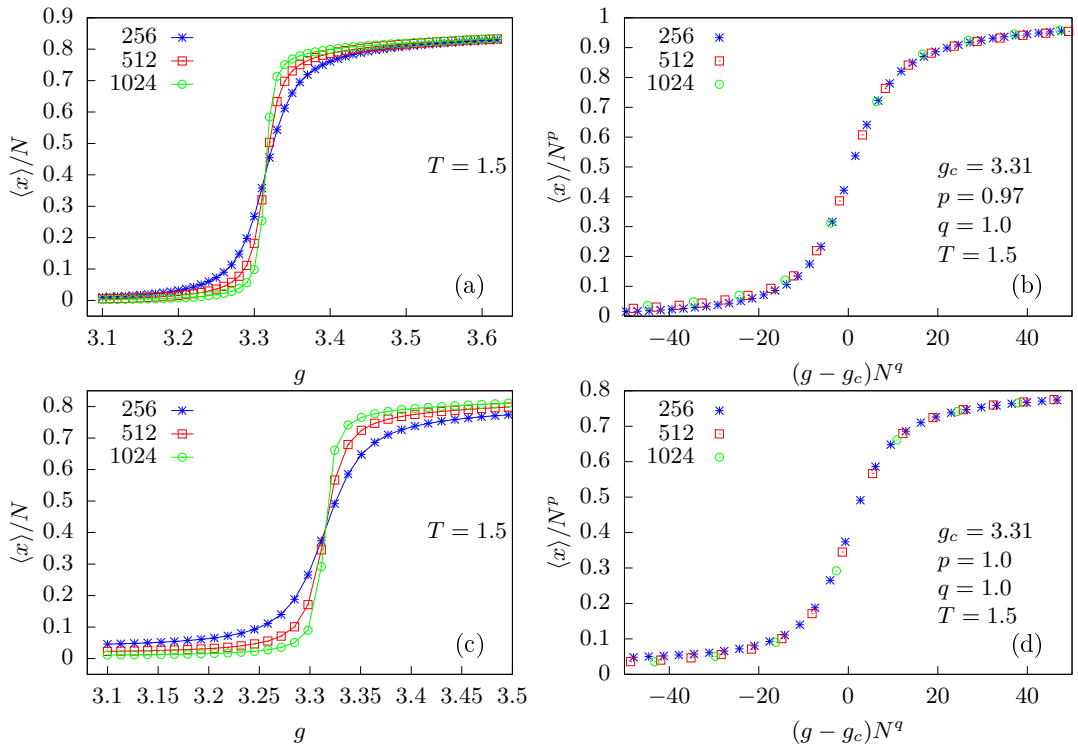

Figure 3.2: Scaled extension $\langle x\rangle/N$, as a function of constant pulling force g, obtained using the exact transfer matrix approach, for different chain lengths $N = 256, 512$, and 1024 at $T = 1.5$ for (a) the heterogeneous sequence $(A_{16}B_{16})_M$. (b) $\langle x\rangle/N^p$ as a function of $(g - g_c)N^q$ showing a nice collapse of data for $g_c = 3.31 \pm 0.05$, $p = 0.97 \pm 0.05$, and $q = 1.0 \pm 0.02$. (c) For the heterogeneous sequence $(B_{16}A_{16})_M$. (d) Collapse of data shown in (c) for $g_c = 3.31 \pm 0.05$, $p = 1.0 \pm 0.05$, and $q = 1.0 \pm 0.02$. The line joining the data points in plots (a) and (c) is just a guide for the eye.

base pairing with three hydrogen bonds (stronger) or the base pairing with two hydrogen bonds (weaker). This is because the unzipping transition is a first-order phase transition. We have obtained the same behavior for various other sequences. In Fig. 3.3, this is shown for sequences $(A_4B_4)_M$ and $(B_4A_4)_M$ at $T = 1.0$ for chain lengths $N = 256, 512$, and 1024, and in Fig. 3.4 for sequences $(A_{64}B_{64})_M$ and $(B_{64}A_{64})_M$ at $T = 2.0$ for chain lengths $N = 512, 1024$, and 2048. The critical forces obtained at various temperatures using the transfer matrix method are shown in Fig. 3.5 by points for the sequences $(A_{16}B_{16})_M$. They match exactly with the analytical results given by Eq. (3.7). The same exact transfer matrix technique could also be used to obtain the melting temperature of the DNA. We again iterate the recursion relations now at zero force value $g = 0$ and obtain the equilibrium separation between strands at the free end as a function of temperature. We use

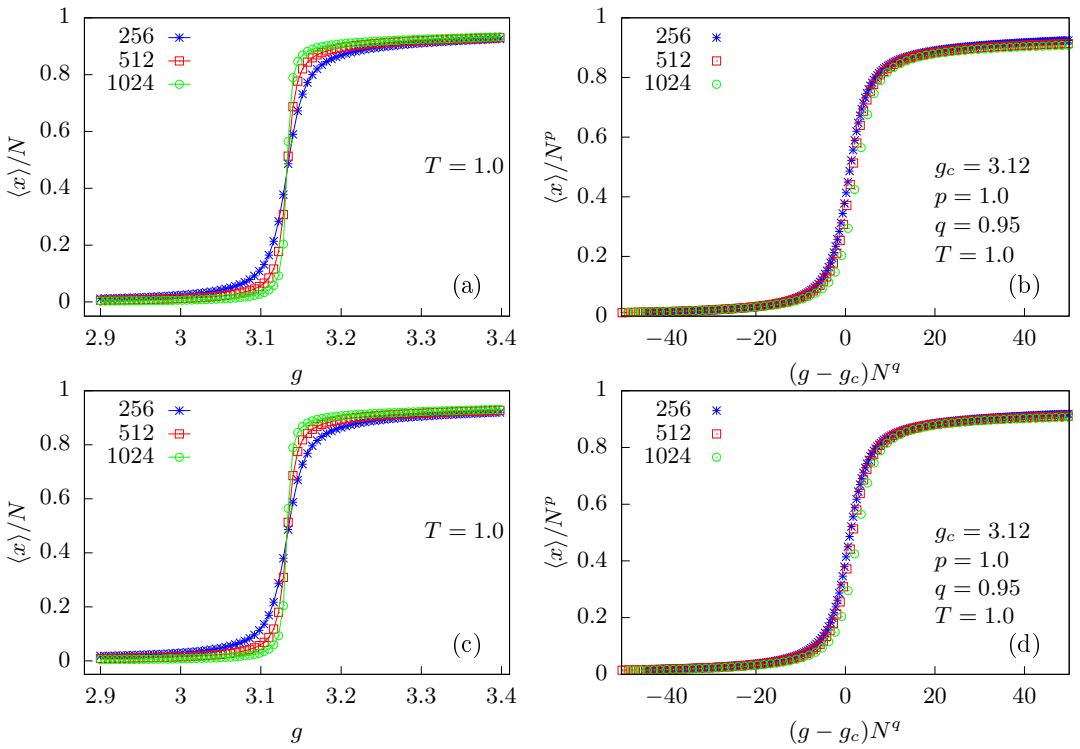

Figure 3.3: Scaled extension $\langle x\rangle/N$, as a function of constant pulling force g, obtained using the exact transfer matrix approach, for different chain lengths $N = 256, 512$, and 1024 at $T = 1.0$ for (a) the heterogeneous sequence $(A_4B_4)_M$. (b) $\langle x\rangle/N^p$ as a function of $(g - g_c)N^q$ showing a nice collapse of data for $g_c = 3.12 \pm 0.05$, $p = 1.0 \pm 0.02$, and $q = 0.95 \pm 0.05$. (c) For the heterogeneous sequence $(B_4A_4)_M$. (d) Collapse of data shown in (c) for $g_c = 3.12 \pm 0.05$, $p = 1.0 \pm 0.02$, and $q = 0.95 \pm 0.05$. The line joining the data points in plots (a) and (c) is just a guide for the eye.

chain lengths $N = 1024, 2048$, and 4096, and the finite-size scaling of the form

$$\langle x\rangle = N^{d_m}\mathcal{G}\Big((T - T_m)N^{\phi_m}\Big), \tag{3.12}$$

to obtain the melting temperature T_m. A nice collapse is obtained for $d_m = 0.52 \pm 0.02$, $\phi_m = 0.48 \pm 0.02$ and $T_m = 8.45 \pm 0.25$ for sequence $(A_{16}B_{16})_M$ [shown in Fig. 3.6(a)]. The melting temperature obtained by the transfer matrix method is also shown in Fig. 3.5 by a diamond. We have tried various other sequences [see Fig. 3.6(b) for sequence $(A_{64}B_{64})_M$] and found that the melting temperatures for all the heterogeneous sequences allowed in our model are the same.

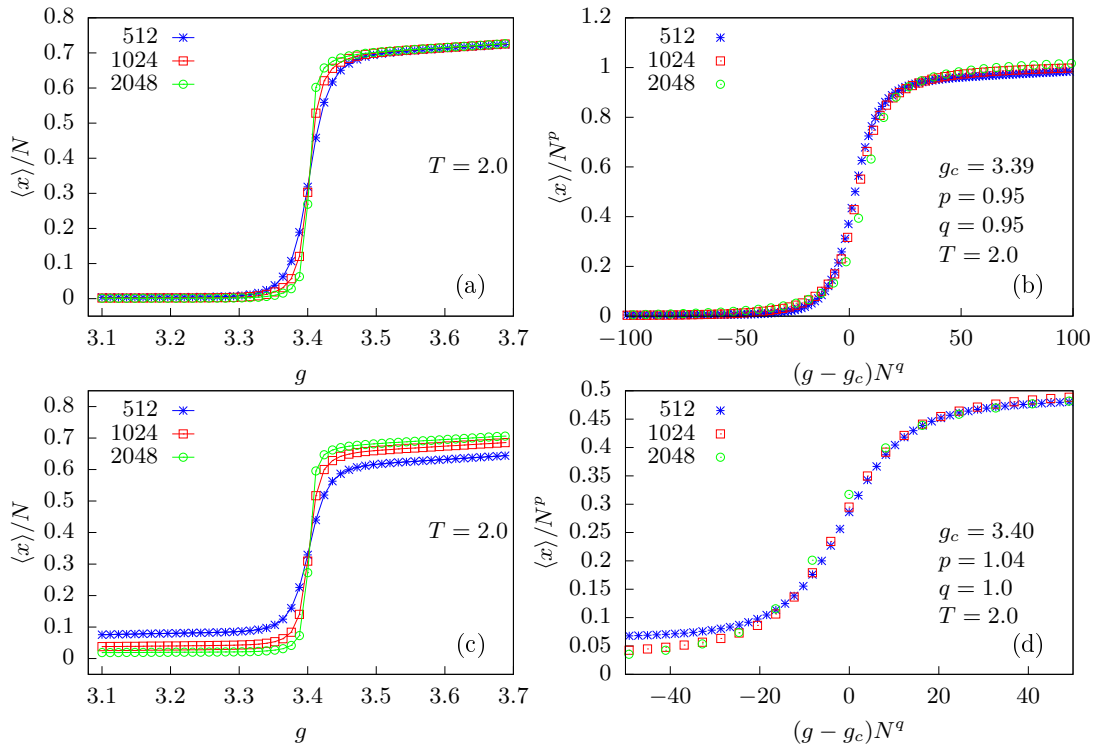

Figure 3.4: Scaled extension $\langle x\rangle/N$, as a function of constant pulling force g, obtained using the exact transfer matrix approach, for different chain lengths $N = 256, 512$, and 1024 at $T = 2.0$ for (a) the heterogeneous sequence $(A_{64}B_{64})_M$. (b) $\langle x\rangle/N^p$ as a function of $(g - g_c)N^q$ showing a nice collapse of data for $g_c = 3.39 \pm 0.05$, $p = 0.95 \pm 0.05$, and $q = 0.95 \pm 0.05$. (c) For the heterogeneous sequence $(B_{64}A_{64})_M$. (d) Collapse of data shown in (c) for $g_c = 3.40 \pm 0.05$, $p = 1.04 \pm 0.05$, and $q = 1.0 \pm 0.05$. The line joining the data points in plots (a) and (c) is just a guide for the eye.

3.2.2 Dynamic Case

In the previous section, we have seen that the unzipping of a block copolymer DNA in equilibrium does not depend on whether the force acts on the base pairs of type A or type B. However, for the time-dependent periodic force, we find that the unzipping depends on which base pairs are unzipped first.

A. Scaled extension

In Fig. 3.7, we have plotted the time variation of external force $g(t)$ and scaled extension $x(t)/N$ for the DNA of length $N = 256$ with respect to time t for five consecutive cycles when it is subjected to a periodic force of amplitude $g_0 = 5$

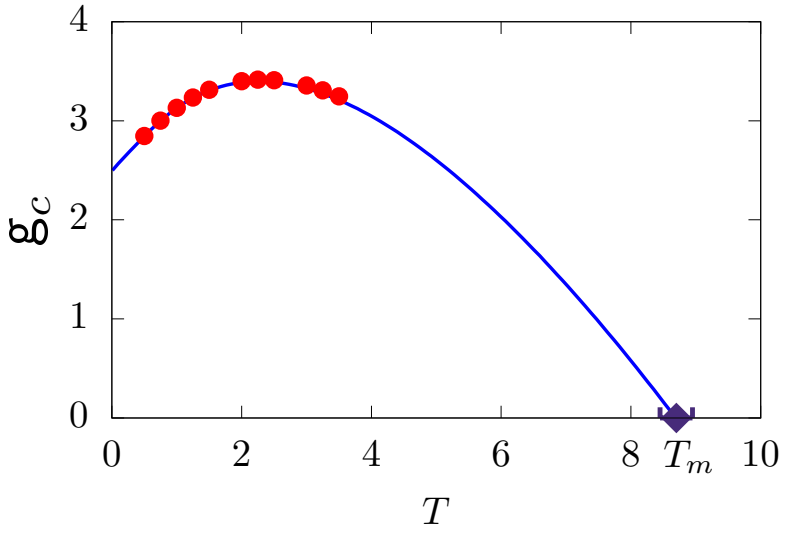

Figure 3.5: Critical unzipping force g_c as a function of temperature T for the heterogeneous sequence $(A_{16}B_{16})_M$. The line is the exact result obtained from the generating function approach [Eq. (3.9)], and the points are obtained by using finite-size scaling of the force-distance isotherms [Eq. (3.10)] as obtained from the exact transfer matrix approach

.

at two different frequencies $\omega = 6.28 \times 10^{-3}$ and 1.57×10^{-3} at $T = 4$. The force increases from zero to a maximum value of g_0, which is much larger than the critical force g_c needed to unzip the DNA at equilibrium, and then decreases to zero again. The DNA responds to this external force and starts unzipping slowly. We can see that there is always a lag between the scaled extension and the force. It is easy to understand that, for a homopolymer DNA, the time required to unzip a dsDNA is directly proportional to its length. The larger the length of the DNA, the more is the unzipping time. However, for a block copolymer DNA, the unzipping time for the DNA of same length can be quite different as it also depends on its sequence. Figure 3.7(a) shows the time variation of the distance between end monomers of the two strands for sequences of smaller block sizes 8 [$(A_4B_4)_{32}$ and $(B_4A_4)_{32}$]. The scaled extension for both sequences is almost the same. Other sequences of smaller block sizes such as 16, 32 and 64, which are shown in Figs. 3.8(a), 3.8(b) and 3.8(c), respectively, show the similar behavior. However, on increasing the block sizes to 128 but keeping the frequency and amplitude same, the scaled extension for the sequence $(B_{64}A_{64})_2$ is more than that for the opposite sequence $(A_{64}B_{64})_2$ [Fig. 3.7(b)]. On increasing the block size further to 256, the scaled extension for the sequence $(B_{128}A_{128})_1$ becomes almost double that for the opposite sequence $(A_{128}B_{128})_1$ as shown in Fig. 3.7(c). This can be understood as

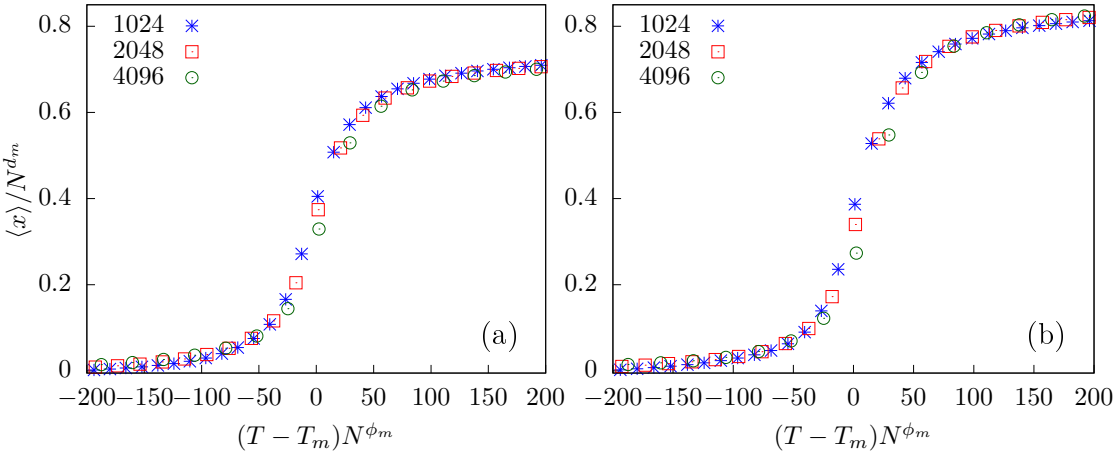

Figure 3.6: Data collapse of the average distance, $\langle x \rangle$, for the chain lengths $N = 1024, 2048$, and 4096. (a) of the heterogeneous sequence $(A_{16}B_{16})_M$. The exponents are $d_m = 0.52 \pm 0.02$, $\phi_m = 0.48 \pm 0.02$ with melting temperature $T_m = 8.45 \pm 0.25$. (b) of the heterogeneous sequence $(A_{64}B_{64})_M$. The exponents are $d_m = 0.50 \pm 0.02$, $\phi_m = 0.48 \pm 0.02$ with melting temperature $T_m = 8.45 \pm 0.25$.

follows. In one cycle of the periodic force with higher frequency ($\omega = 6.28 \times 10^{-3}$), the force changes faster and the system gets less time to relax. Since it is easier to break base pairs with two hydrogen bonds (type A) in comparison with base pairs with three hydrogen bonds (type B), more base pairs are broken for the sequence $(B_{128}A_{128})_1$ than for the sequence $(A_{128}B_{128})_1$, and we see the higher extension. However, on lowering the frequency of the external force to 1.57×10^{-3}, the system gets enough time to relax, and the extension between the strands become almost comparable for both the sequences for all block sizes as shown in Figs. 3.7(d)-3.7(f) and Figs. 3.8(d)-3.8(f).

B. Hysteresis loops

We have seen that the extension $x(t)$ follows the driving force $g(t)$ with a lag. When it is averaged over various cycles, we obtain the average extension $\langle x(g) \rangle$ as a function of force g showing a closed loop. The shape of a loop tells much about the dynamics of the system and depends on the frequency ω and the force amplitude g_0. For the present problem, the hysteresis loop also depends on the sequence of the block copolymer DNA. In Fig. 3.9, we have plotted $\langle x(g) \rangle$ as a function of force g at four different frequencies $\omega = 6.28 \times 10^{-3}$, 1.57×10^{-3}, 3.14×10^{-4}, and 3.49×10^{-5} at force amplitude $g_0 = 5$ for the DNA of length $N = 256$ with block

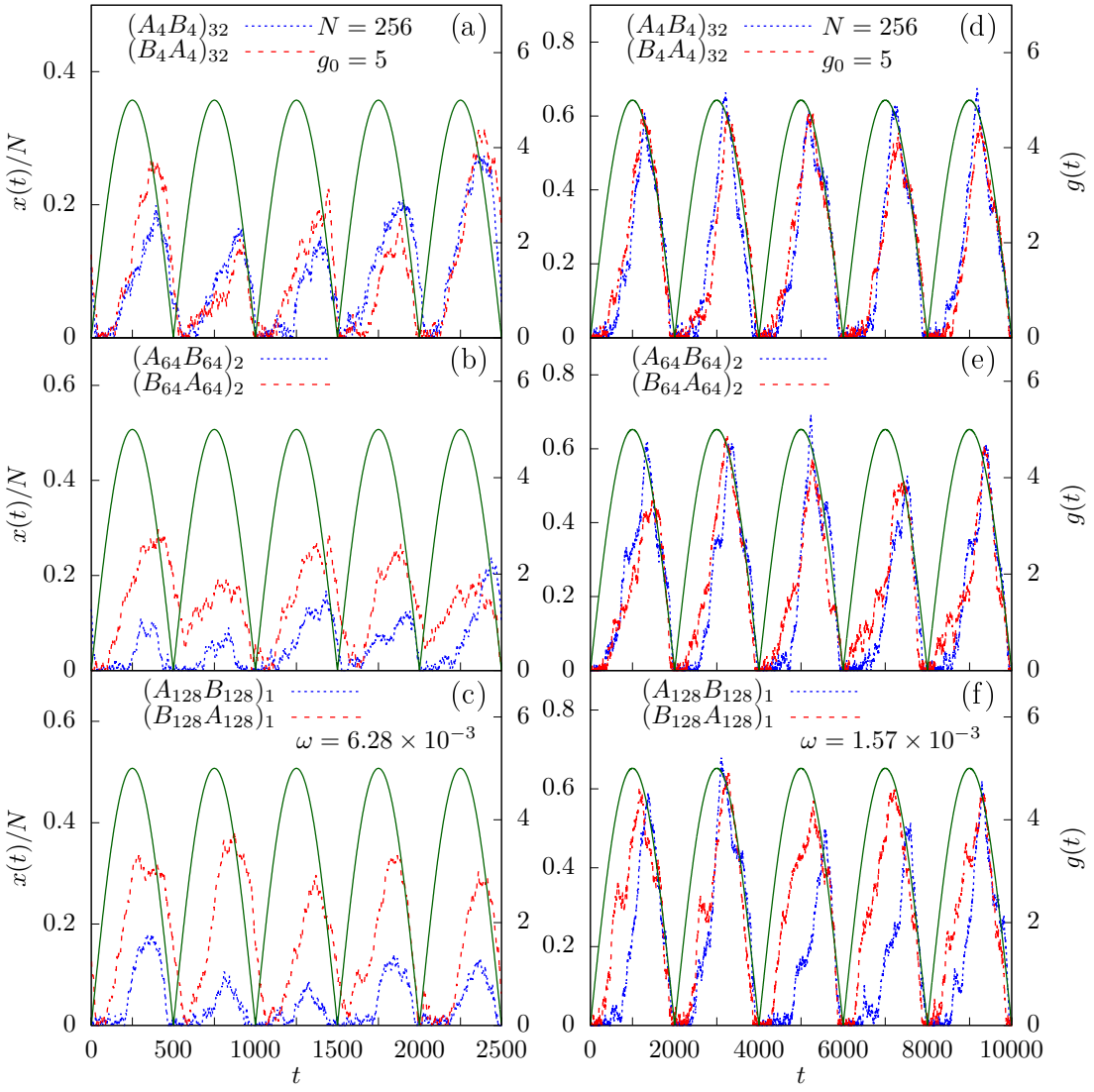

Figure 3.7: The extension $x(t)$ between the end monomers of the two strands of the block copolymer DNA of length $N = 256$ as a function of time t when it is subjected to a periodic force of amplitude $g_0 = 5$ at frequency $\omega = 6.28 \times 10^{-3}$. For the sequences (a) $(A_4B_4)_{32}$ and $(B_4A_4)_{32}$, (b) $(A_{64}B_{64})_2$ and $(B_{64}A_{64})_2$, and (c) $(A_{128}B_{128})_1$ and $(B_{128}A_{128})_1$. Plots (d), (e), and (f) are same as plots (a), (b), and (c) at frequency $\omega = 1.57 \times 10^{-3}$. The variation of force with time, $g(t)$, is represented by solid lines.

sizes 8, 128, and 256 at $T = 4$, and with block sizes 16, 32, and 64 in Fig. 3.10. All of them show hysteresis loops but with different shapes. The loops for DNA of smaller block sizes, e.g., $(A_4B_4)_{32}$ and $(B_4A_4)_{32}$ [Figs. 3.9(a)-3.9(d)], are almost the same, irrespective of which base pair is acted upon by the driving force. To understand the shapes of the loop, we first note that at higher frequency, i.e., $\omega = 6.28 \times 10^{-3}$, the stationary state of the DNA at $g = 0$ is a partially unzipped

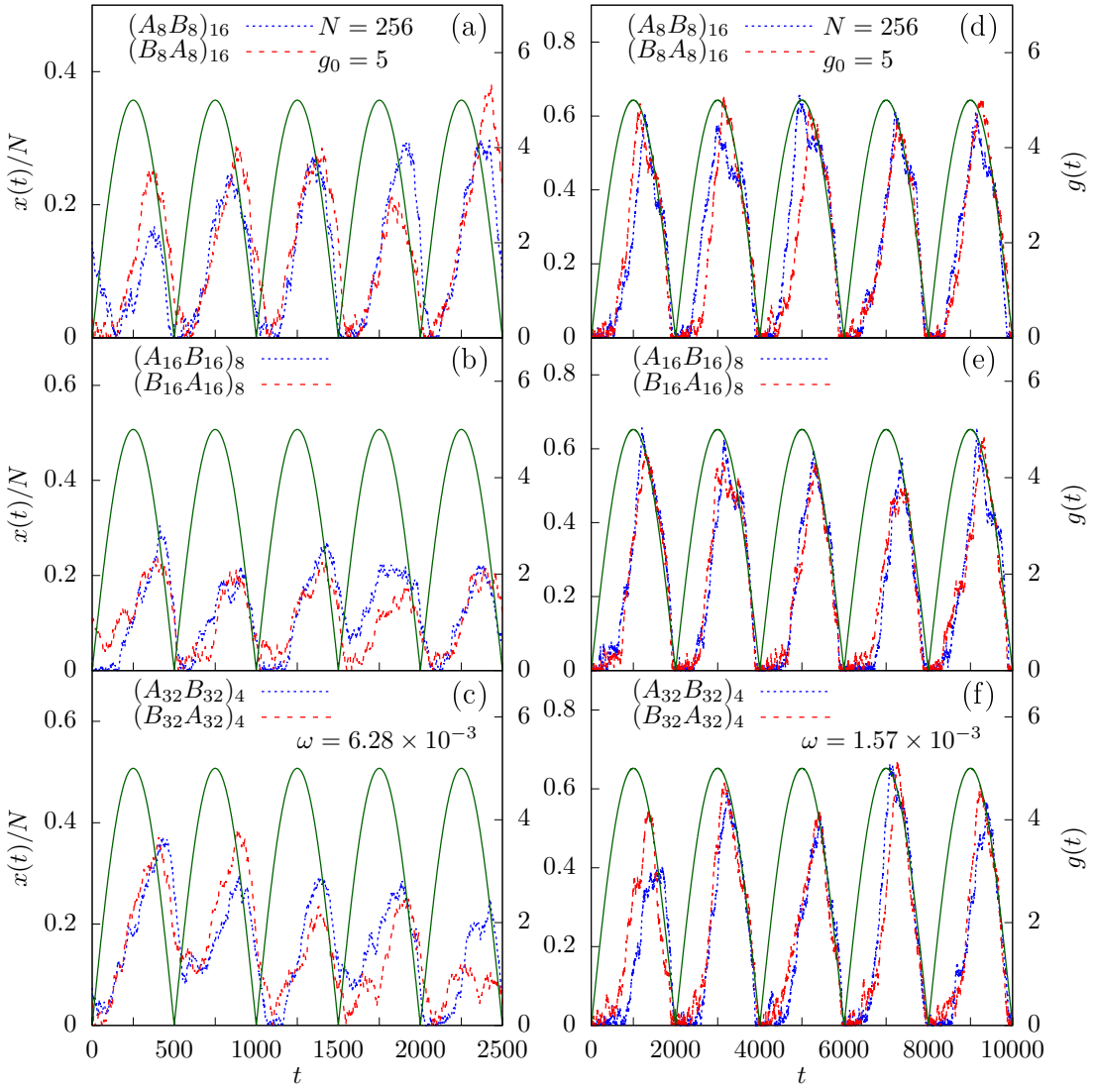

Figure 3.8: The extension $x(t)$ between the end monomers of the two strands of the block copolymer DNA of length $N = 256$ as a function of time t when it is subjected to a periodic force of amplitude $g_0 = 5$ at frequency $\omega = 6.28 \times 10^{-3}$. For the sequences (a) $(A_8B_8)_{16}$ and $(B_8A_8)_{16}$, (b) $(A_{16}B_{16})_8$ and $(B_{16}A_{16})_8$, and (c) $(A_{32}B_{32})_8$ and $(B_{32}A_{32})_8$. Plots (d), (e), and (f) are same as plots (a), (b), and (c) at frequency $\omega = 1.57 \times 10^{-3}$. The variation of force with time, $g(t)$, is represented by solid lines.

state with an average extension $\langle x(g) \rangle = 35$. At this frequency, the force changes very rapidly and the strands of the DNA do not get enough time to relax, and only a small loop is traced by the extension between them. However, for a relatively lower frequency $\omega = 1.57 \times 10^{-3}$, the stationary state of the DNA at $g = 0$ is a fully zipped configuration with an average extension $\langle x(0) \rangle = 0$. The strands now get relatively more time to relax, and the loop area increases. Even at this frequency,

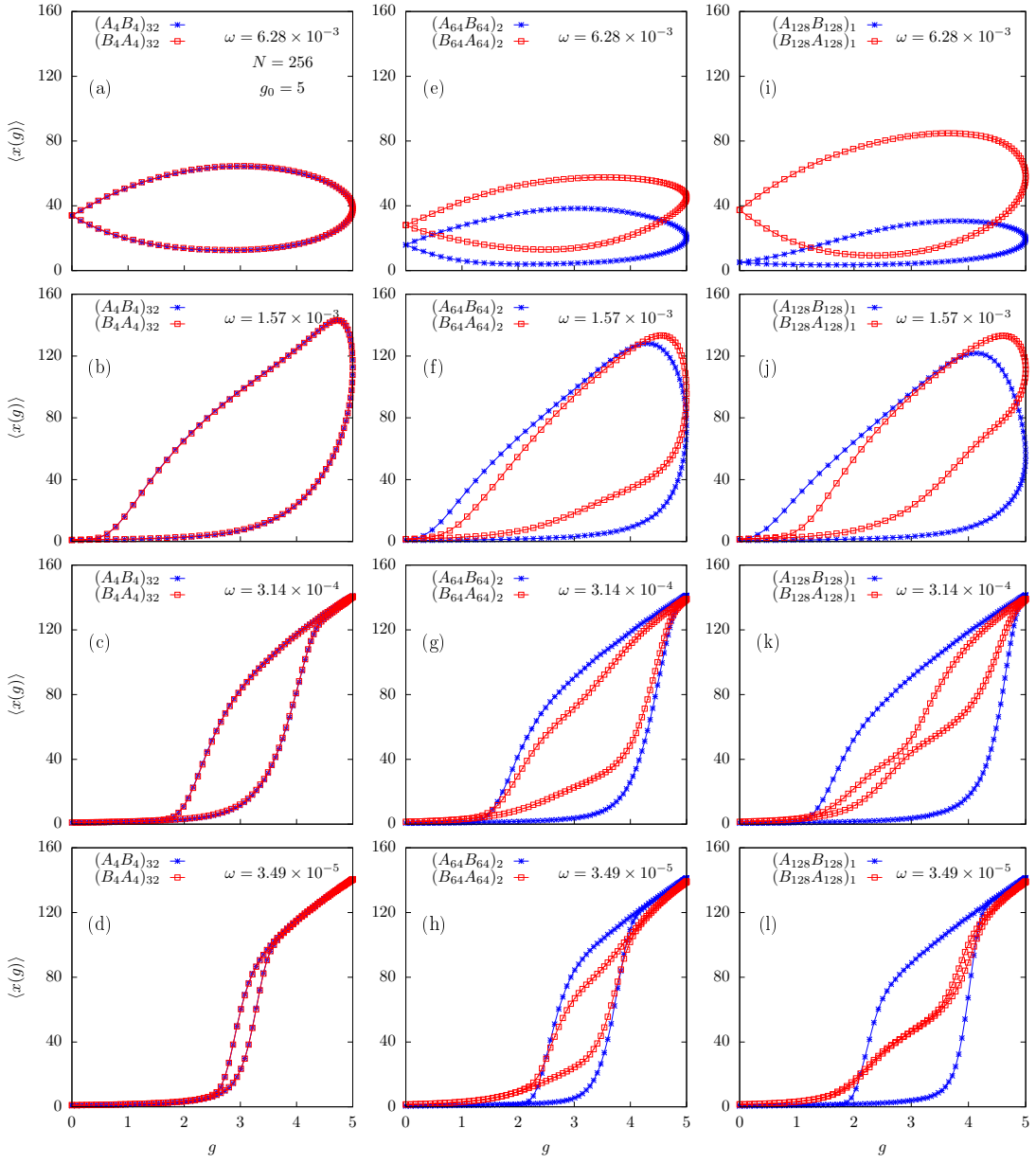

Figure 3.9: The force g vs extension $\langle x(g)\rangle$ curves averaged over 10^4 cycles for the block copolymer DNA of length $N = 256$ and block sizes 8 (first column), 128 (second column), and 256 (third column) at frequencies $\omega = 6.28\times10^{-3}$ (first row), $\omega = 1.57 \times 10^{-3}$ (second row), $\omega = 3.14 \times 10^{-4}$ (third row), and $\omega = 3.49 \times 10^{-5}$ (fourth row) at force amplitude $g_0 = 5$ and temperature $T = 4$. The data shown in this plot are obtained using Monte Carlo simulations. The line joining the points is just a guide for the eye.

the DNA does not get fully unzipped at the maximum force value. This is shown by the rounding of the loop at the maximum force value. The extension increases even though the force decreases. It reaches a maximum for some lower force value,

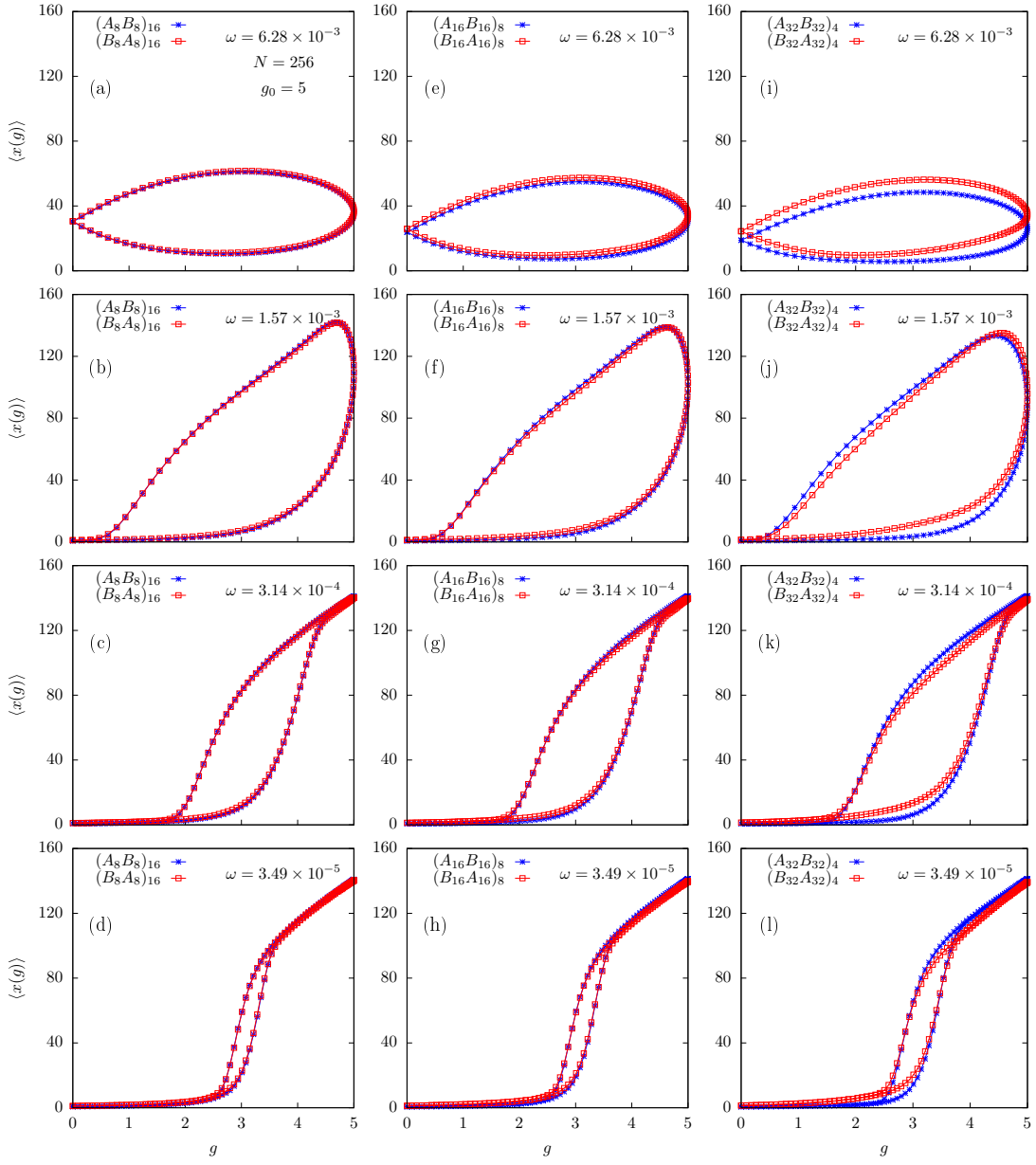

Figure 3.10: The force g vs extension $\langle x(g) \rangle$ curves averaged over 10^4 cycles for the block copolymer DNA of length $N = 256$ and block sizes 16 (first column), 32 (second column), and 64 (third column) at frequencies $\omega = 6.28 \times 10^{-3}$ (first row), $\omega = 1.57 \times 10^{-3}$ (second row), $\omega = 3.14 \times 10^{-4}$ (third row), and $\omega = 3.49 \times 10^{-5}$ (fourth row) at force amplitude $g_0 = 5$ and temperature $T = 4$. The data shown in this plot are obtained using Monte Carlo simulations. The line joining the points is just a guide for the eye.

in the backward cycle, and then decreases to zero when $g = 0$. On decreasing the frequency further, the isotherms at higher and lower force values start following the same curve for the forward and backward cycles but with a loop in between whose

area decreases with decreasing frequency. A similar trend can be seen in the closed loops of sequences of block sizes 16, 32 and 64 [Figs. 3.10(a)-3.10(l)]. The situation for the higher block lengths are, however, different. For the sequence $(A_{128}B_{128})_1$ (third column in Fig. 3.9), the stationary state at frequency $\omega = 6.28 \times 10^{-3}$ is a completely zipped configuration with an average extension $\langle x(g)\rangle \approx 0$ at $g = 0$ [see Fig. 3.9(i)]. This is because the driving force is acting on base pairs with three hydrogen bonds having higher strength, and hence only a few base pairs are broken. Therefore the area of the loop traced by the extension between the strands is also small. In contrast, for the sequence $(B_{128}A_{128})_1$, the stationary state (at the same frequency) is a partially unzipped DNA. In this case, the driving force can break more bonds as it is acting on the base pairs with two hydrogen bonds and therefore is weaker than the previous case. Therefore, the average extension $\langle x(g)\rangle$ traces a loop with larger area. On decreasing the frequency to $\omega = 1.57 \times 10^{-3}$, the stationary state (at $g = 0$) for the sequence $(B_{128}A_{128})_1$ changes to a fully zipped configuration [see Fig. 3.9(j)] as the strands now get enough time to relax and get re-zipped again for forces far below the critical value. On decreasing the frequency further to $\omega = 3.14 \times 10^{-4}$ [Fig. 3.9(k)], the strands get equilibrated for smaller and larger force values, and therefore the extension starts following the equilibrium curve at these force values. However, there is still a hysteresis curve at the transition region that decreases on decreasing the frequency of the force. It is found that the size of the hysteresis loop for the sequence $(B_{128}A_{128})_1$ decreases much faster. The shape of the loop for this sequence starts closing at the center, and the loop divides into two smaller loops and a plateau starts emerging [see Fig. 3.9(k)]. At frequency $\omega = 3.49 \times 10^{-5}$, one of the smaller loop completely disappears, and the other loop is also very small [Fig. 3.9(l)]. The shape of loop is markedly different for the opposite sequence $(A_{128}B_{128})_1$ at the same frequency with considerable loop area. For sequences of intermediate block lengths, for example, $(A_{64}B_{64})_2$ and $(B_{64}A_{64})_2$ with block length 128 [Figs. 3.9(e)-3.9(h)], the hysteresis loops show mixed features as seen for sequences with smaller and larger block lengths (columns one and three of Fig. 3.9).

C. Loop area

We calculate the area of the hysteresis loops, shown in Figs. 3.9 and 3.10 , numerically using the trapezoidal rule. For the trapezoidal rule to work properly, the intervals should be uniformly spaced. For the problem considered in this chapter,

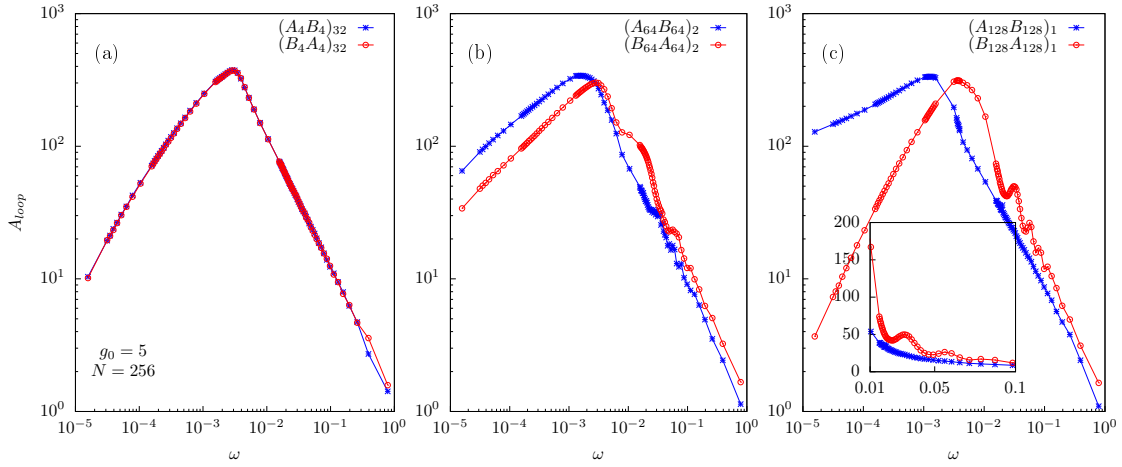

Figure 3.11: Area of the hysteresis loop A_{loop} as a function of frequency ω (in log-log scale) at force amplitude $g_0 = 5$ and length $N = 256$ for the block copolymer DNA sequences (a) $(A_4B_4)_{32}$ and $(B_4A_4)_{32}$, (b) $(A_{64}B_{64})_2$ and $(B_{64}A_{64})_2$, and (c) $(A_{128}B_{128})_1$ and $(B_{128}A_{128})_1$. The inset shows the higher frequency region (in linear scale), where secondary peaks are visible in A_{loop} for the sequence $(B_{128}A_{128})_1$ but are absent for the opposite sequence. In all the plots, the line joining the points is just a guide for the eye.

the force increases as sine function which gives us non uniformly spaced force values. To convert it into a uniformly spaced interval, we divide the force interval $g \in [0, g_0]$, for both the rise and fall of the cycle, into 1000 equal intervals, and then obtain the value of $\langle x(g) \rangle$ at the end points of these intervals by interpolation using cubic splines of the GNU Scientific Library [163]. The loop area, A_{loop}, is then evaluated numerically by using the trapezoidal rule on these intervals.

In Figs. 3.11 and 3.12, the area of the hysteresis loop, A_{loop}, is plotted as a function of the frequency, ω, of the external pulling force for sequences of various block sizes 8, 128, and 256 of block copolymer DNA of length $N = 256$ at force amplitude $g_0 = 5$ and temperature $T = 4$. On decreasing the frequency of the pulling force, it is found that the loop area first increases, reaches a maximum value at some frequency ω^*, and then decreases with decreasing the frequency further, similar to the hysteresis loop area behavior for a homopolymer DNA under periodic forcing [20]. At a frequency ω^*, the natural frequency of the block copolymer DNA matches the frequency of the externally applied force, and we have a resonance with a maximum loop area. For the block copolymer DNA case, the behaviour of A_{loop} also depends on the DNA sequence used. For sequences of smaller block lengths, e.g., $(A_4B_4)_{32}$ and $(B_4A_4)_{32}$, the loop area is same, and hence ω^* is same for both

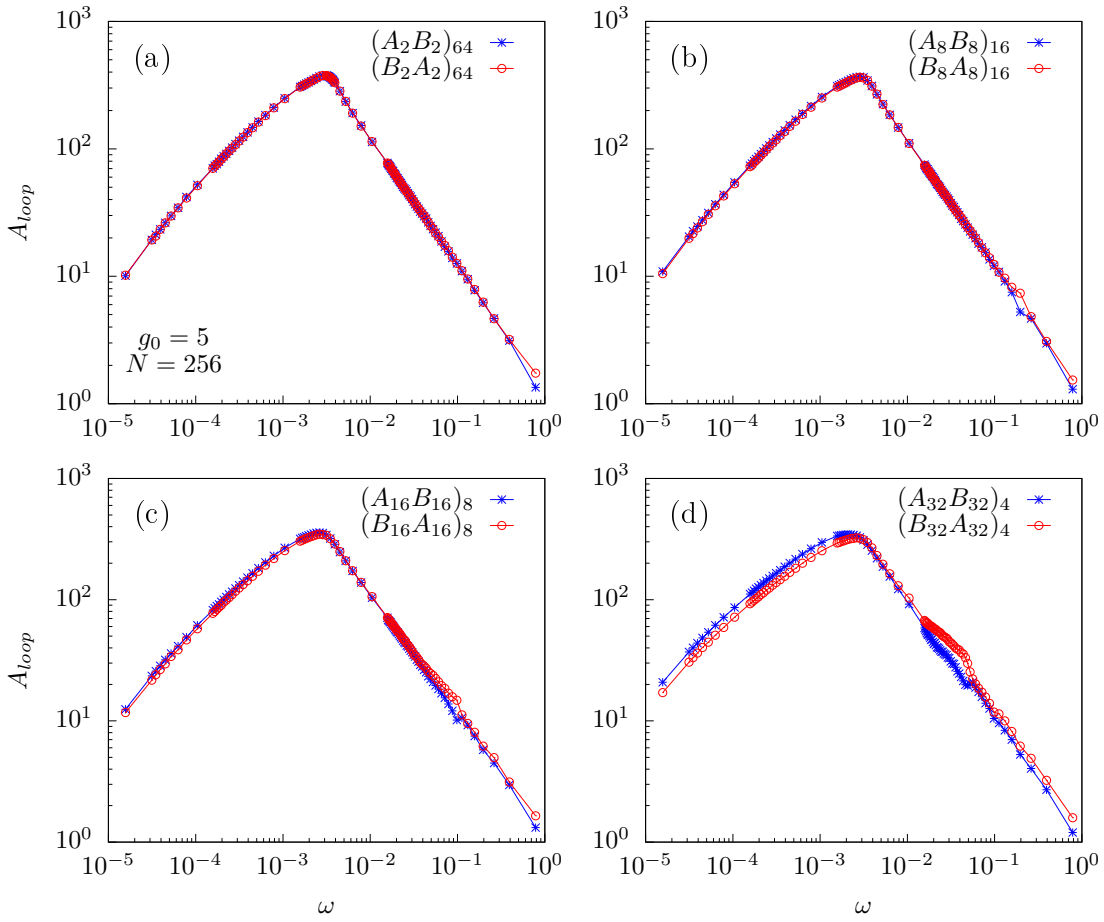

Figure 3.12: Area of the hysteresis loop A_{loop} as a function of frequency ω (in log-log scale) at force amplitude $g_0 = 5$ and length $N = 256$ for the block copolymer DNA sequences (a) $(A_2B_2)_{64}$ and $(B_2A_2)_{64}$, (b) $(A_8B_8)_{16}$ and $(B_8A_8)_{16}$, (c) $(A_{16}B_{16})_8$ and $(B_{16}A_{16})_8$, and (d) $(A_{32}B_{32})_4$ and $(B_{32}A_{32})_4$. In all the plots, the line joining the points is just a guide for the eye.

the sequences [see Fig. 3.11(a)]. Sequences of block sizes 4, 16, 32, and 64, behave in similar fashion as it can be seen in Fig. 3.12. However, this is no longer true for sequences of higher block sizes, where clear differences are seen for the opposite sequences. For example, for block length 256, we can observe that the frequency ω^* is higher for the sequence $(B_{128}A_{128})_1$ than its opposite sequence $(A_{128}B_{128})_1$ [see Fig. 3.11(c)]. At frequencies higher than ω^*, the former sequence shows secondary peak structures, whereas the sequence $(A_{128}B_{128})_1$ falls off smoothly without showing any such peaks [see inset of Fig. 3.11(c)]. On the lower side of frequency ω^*, the loop area A_{loop} falls sharply to zero for the sequence $(B_{128}A_{128})_1$, whereas it decreases very slowly for the opposite sequence $(A_{128}B_{128})_1$. The secondary peaks in A_{loop} are the frequencies $\omega_p = (2p-1)\pi/2N$, with $p = 1, 2, \ldots$ as integers, and

are higher Rouse modes [20]. These modes are more pronounced for the sequence $(B_{128}A_{128})_1$, where the pulling force is applied to A type base pairs that can be broken at relatively lower force values than B type base pairs, and hence more base pairs are broken. The two strands thus separated with each other can explore more configurations and can trace a hysteresis loop [See Fig. 3.9(l)]. This loop has larger area whenever the frequency of the periodic force is ω_p, i.e., higher harmonics of the natural frequency of the DNA. In contrast, for the opposite sequence $(A_{128}B_{128})_1$, more force is required to break B type of base pairs where force is applied, and at higher frequencies only a few base pairs are broken, and the loop traced by unzipped strands is very small and hence no secondary peaks are visible.

We have plotted A_{loop}, vs ω for various sequences at force amplitude $g_0 = 5$ for block copolymer DNA of three different lengths $N = 512$, 768, and 1024 in Figs. 3.13(a) and 3.13(b). The maximum value of the loop area A_{loop} is directly proportional to the length of the DNA used in the simulation. Furthermore, the resonance frequency ω^*, where A_{loop} is maximum, decreases with the length of the DNA, suggesting the scaling form

$$A_{loop} = N^d \mathcal{F}(\omega N^z), \tag{3.13}$$

where d and z are exponents, for the loop area A_{loop}. When A_{loop}/N, is plotted with the scaled frequency ωN (i.e., for exponents $d = 1$ and $z = 1$) , we find a nice data collapse for sequences of all the block sizes [Figs. 3.13(c) and 3.13(d)], implying that the loop area for the block copolymer DNA decreases with frequency ω as $A_{loop} \sim 1/\omega$ at higher frequencies (i.e., $\omega \to \infty$), similar to the homopolymer case [20].

To obtain the scaling behavior at lower frequencies, we have plotted A_{loop}, for sequences of various block lengths obtained for a block copolymer DNA of length $N = 512$, with respect to $(g_0 - g_c)^\alpha \omega^\beta$, at three different force amplitudes $g_0 = 5.0$, 6.5, and 8 in the low-frequency regime (i.e., $\omega \to 0$). In the above expression we have subtracted the critical force g_c needed to unzip the block copolymer DNA for the static force case [$g_c(T = 4) = 3.0467..$]. A similar type of scaling was found earlier for the unzipping of a homopolymer DNA using Brownian dynamics [75, 78] and Monte Carlo simulations [20]. The exponents α and β are, however, found to be different for these studies. The earlier studies on Brownian dynamics simulations suggested $\alpha = 1/2$ and $\beta = 1/2$ [75], which were later modified to $\alpha = 0.33$ and $\beta = 1/2$ [78]. On the other hand, the exponents obtained for the Monte Carlo

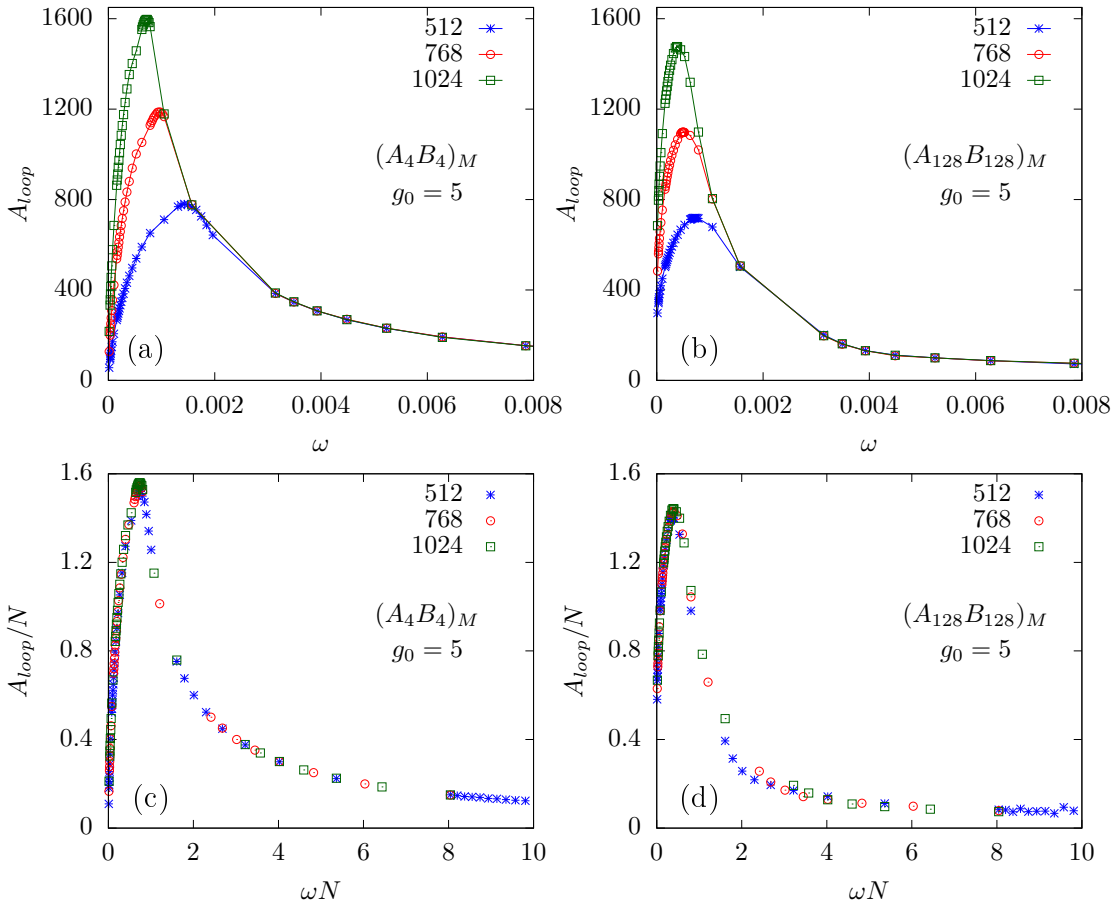

Figure 3.13: Area of the hysteresis loop A_{loop} as a function of frequency ω for the block copolymer DNA of lengths $N = 512, 768, 1024$ at force amplitude $g_0 = 5$ for sequences (a) $(A_4B_4)_M$ and (b) $(A_{128}B_{128})_M$. Plots (c) and (d) are A_{loop}/N vs ωN for respective sequences in (a) and (b). The line joining the points in these plots is just a guide for the eye.

studies were $\alpha = 1$ and $\beta = 5/4$ [20]. In Figs. 3.14(a) and 3.14(b), we have plotted the scaled data for three sequences $(A_4B_4)_{64}$, $(A_{64}B_{64})_4$, and $(A_{128}B_{128})_2$ and the data for the opposite sequences $(B_4A_4)_{64}$, $(B_{64}A_{64})_4$, and $(B_{128}A_{128})_2$, respectively. For all these sequences, we obtain a nice collapse for values $\alpha = 1.0 \pm 0.05$ and $\beta = 1.25 \pm 0.05$, the same as the exponents obtained in earlier Monte Carlo studies for the unzipping of a homopolymer DNA by a periodic force [20].

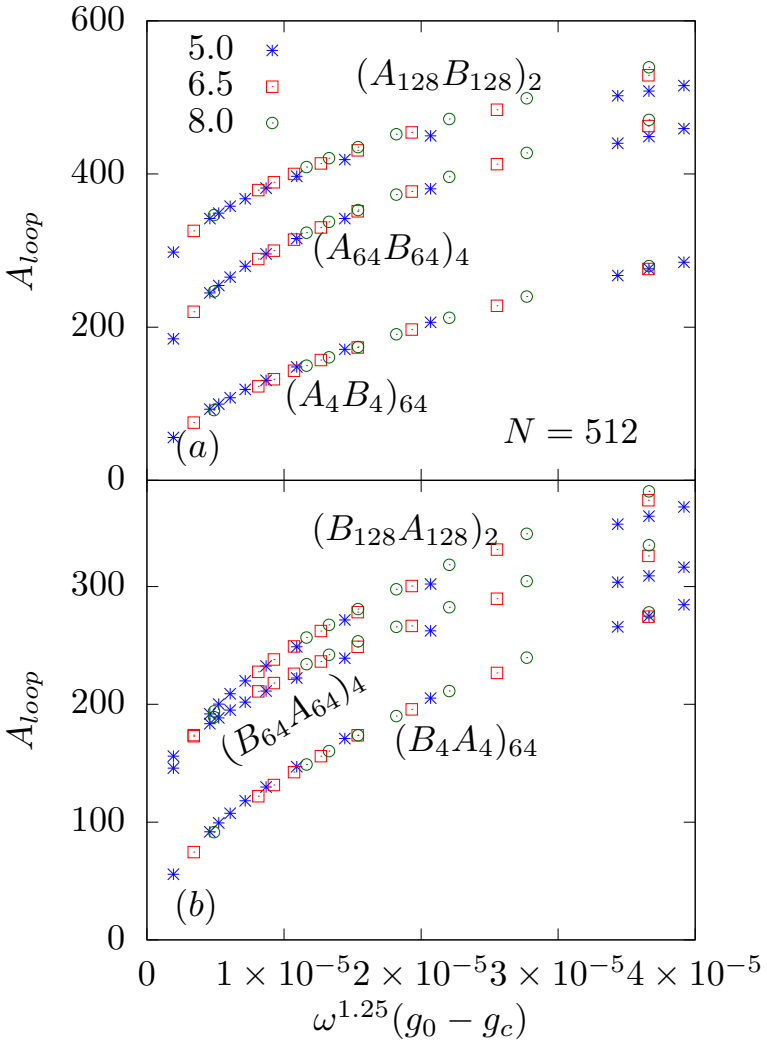

Figure 3.14: Scaling of A_{loop} with respect to $\omega^{1.25}(g_0 - g_c)$ in the low-frequency regime at force amplitudes $g_0 = 5.0, 6.5, 8.0$ of a block copolymer DNA of length $N = 512$ for the sequences (a) $(A_4B_4)_{64}$, $(A_{64}B_{64})_4$, and $(A_{128}B_{128})_2$ and (b) $(B_4A_4)_{64}$, $(B_{64}A_{64})_4$, and $(B_{128}A_{128})_2$.

D. Order parameter

In this section, we study the unzipping transition in the DNA block copolymer achieved by keeping the frequency fixed and varying the force amplitude. As defined in the previous chapter, let $P(Q)$ represents the probability distributions of the dynamical order parameter Q. At a fixed frequency ω, the probability distribution $P(Q)$ is obtained by binning the Q values accumulated from 10^6 different cycles of the periodic force at different force amplitudes.

In Figs. 3.15 (a) and 3.15(b), we have plotted the average extension $\langle x(g) \rangle$ as a

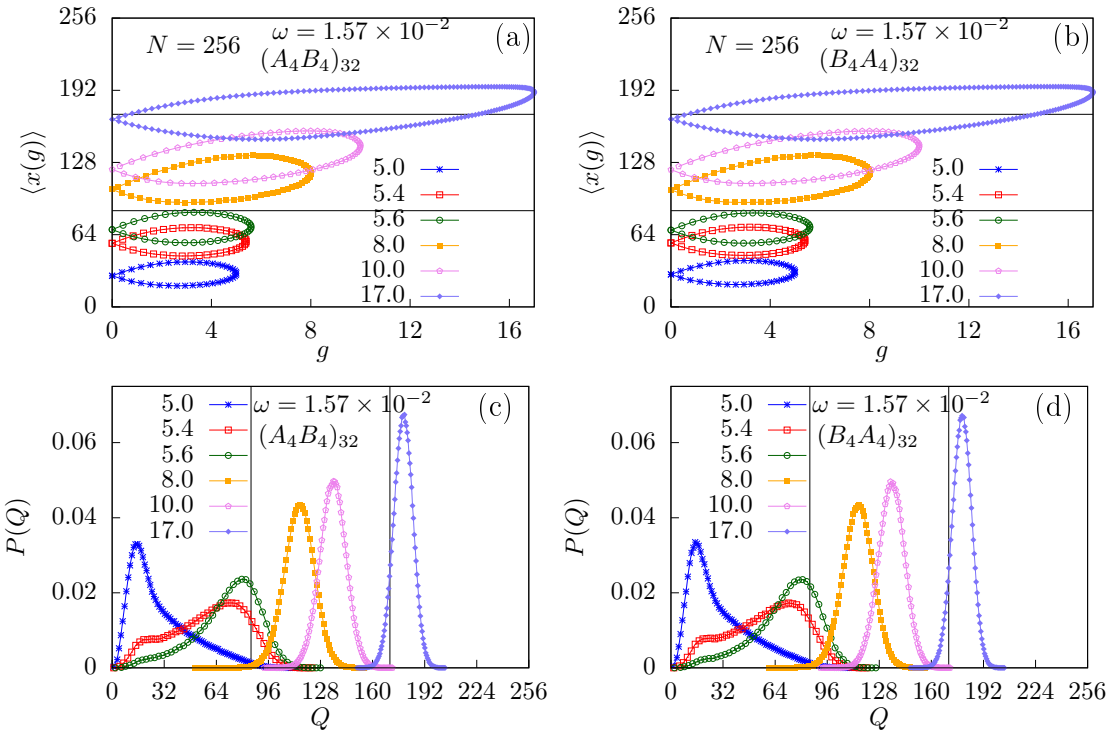

Figure 3.15: Average extension $\langle x(g)\rangle$ as a function of force g of a block copolymer DNA of length $N = 256$ for various force amplitudes $g_0 = 5.0, 5.4, 5.6, 8.0, 10.0$, and 17.0 at frequency $\omega = 1.57 \times 10^{-2}$ for the sequences (a) $(A_4B_4)_{32}$ and (b) $(B_4A_4)_{32}$ respectively. The normalized probability distribution $P(Q)$ of order parameter Q for the sequences (c) $(A_4B_4)_{32}$ and (d) $(B_4A_4)_{32}$ respectively. The line joining the points in these plots is just a guide for the eye.

function of g for various force amplitudes $g_0 = 5.0, 5.4, 5.6, 8.0, 10.0$ and 17.0 at frequency $\omega = 1.57 \times 10^{-2}$ for the block copolymer sequences $(A_4B_4)_{32}$ and $(B_4A_4)_{32}$, respectively. The length of the DNA is taken as $N = 256$. The corresponding probability distributions $P(Q)$ for the two sequences are shown in Figs. 3.15 (c) and 3.15(d) respectively. From the figure, it can be seen that the distributions $P(Q)$ are the same for both the sequences. For a lower force amplitude $g_0 = 5.0$, the distribution $P(Q)$ is sharply peaked at lower Q value implying that block copolymer DNA is in the zipped (Z) phase. At amplitudes $g_0 = 5.4$ and 5.6, $P(Q)$ becomes broader and its peak moves towards right, but DNA is still in zipped (Z) phase. As amplitude increases to $g_0 = 8.0$ and 10.0, the distribution $P(Q)$ again starts becoming narrower and is peaked at intermediate Q values in the dynamic (D) phase. When the amplitude is increased further to $g_0 = 17.0$, the distribution $P(Q)$ is sharply peaked at higher Q value showing that the DNA is in the unzipped (U) phase (see Figs. 3.15(c) and 3.15(d)).

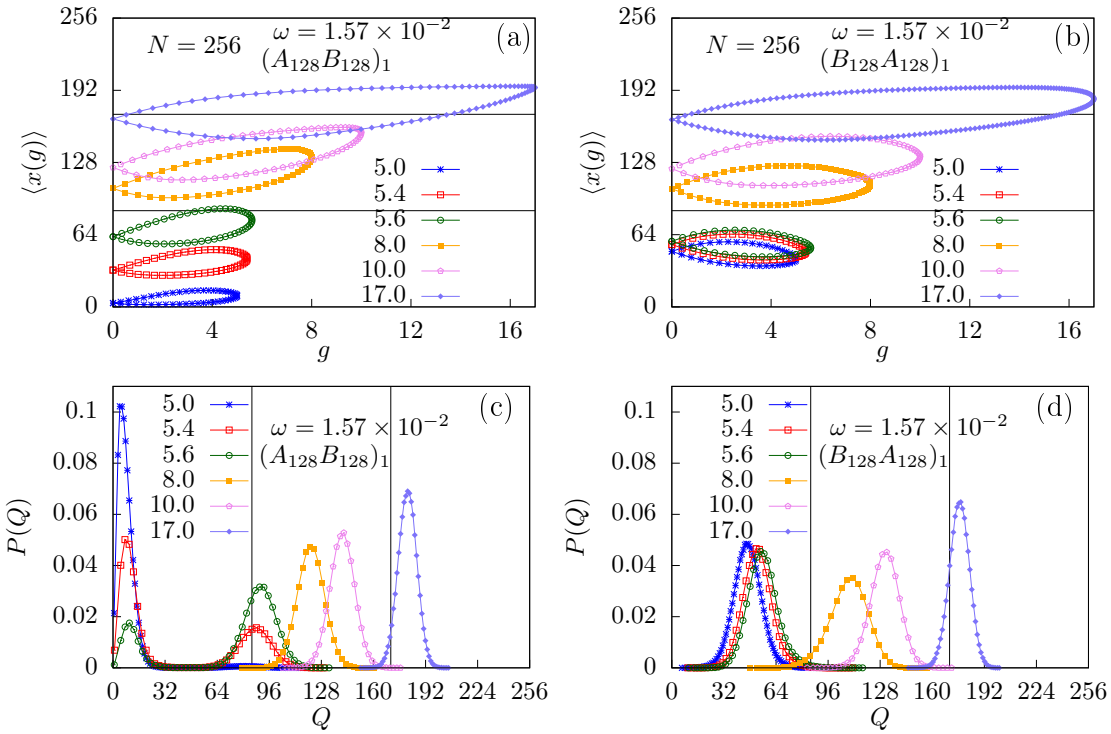

Figure 3.16: Average extension $\langle x(g)\rangle$ as a function of force g of a block copolymer DNA of length $N = 256$ for various force amplitudes $g_0 = 5.0, 5.4, 5.6, 8.0, 10.0,$ and 17.0 at frequency $\omega = 1.57 \times 10^{-2}$ for the sequences (a) $(A_{128}B_{128})_1$ and (b) $(B_{128}A_{128})_1$ respectively. The normalized probability distribution $P(Q)$ of order parameter Q for the sequences (c) $(A_{128}B_{128})_1$ and (d) $(B_{128}A_{128})_1$ respectively. The line joining the points in these plots is just a guide for the eye.

The average extension $\langle x(g)\rangle$ as a function of g for the block copolymer sequences $(A_{128}B_{128})_1$ and $(B_{128}A_{128})_1$ at frequency $\omega = 1.57 \times 10^{-2}$ for various force amplitudes $g_0 = 5.0, 5.4, 5.6, 8.0, 10.0$ and 17.0 are plotted in Figs. 3.16(a) and 3.16(b), and the corresponding probability distributions $P(Q)$ are shown in Figs. 3.16 (c) and 3.16(d), respectively. At a lower force amplitude $g_0 = 5.0$, the distribution $P(Q)$ for the sequence $(A_{128}B_{128})_1$ is sharply peaked at a very low value of Q which shows that DNA is in zipped (Z) state. When the amplitude is slightly increased to values $g_0 = 5.4$ and 5.6, $P(Q)$ becomes broader and shows two peak structures which are peaked at lower and intermediate Q values respectively. In this scenario DNA is said to coexist in the zipped (Z) and the dynamic (D) phases. As the amplitude is increased further (i.e., $g_0 = 8.0$ and 10.0), the distributions become narrower again with peaks at intermediate Q values which are in the dynamic (D) phase. On increasing the amplitude further to $g_0 = 17.0$, the distribution $P(Q)$ is peaked at a higher Q value showing that the DNA is in the unzipped (U) phase (see Fig. 3.16(c)). The situation for the opposite sequence, i.e.,

$(B_{128}A_{128})_1$ as shown in Fig. 3.16(d), is slightly different. The two peak structure from the distribution at intermediate force amplitudes ($g_0 = 5.4$ and 5.6) disappear and for these amplitudes the DNA lies purely in the zipped phase. However, for the higher force amplitudes $g_0 = 8.0, 10.0$ and 17.0, the behavior of the distribution $P(Q)$ is very similar to distribution for the sequence $(A_{128}B_{128})_1$.

3.3 Conclusions

In this chapter, we have studied the unzipping of a block copolymer DNA subjected to a periodic force with amplitude g_0 and frequency ω using Monte Carlo simulations. We obtained results for the static force case and found that the equilibrium results do not depend on the block copolymer DNA sequence and, the temperature-dependent phase boundary $g_c(T)$, separating the zipped and the unzipped phases, could be obtained by replacing the binding energy in the exact expression previously obtained for the homopolymer DNA case, by an effective average binding energy per block of the block copolymer DNA sequence. For the dynamic case, the system, however, is not in equilibrium, and results depend on the amplitude and frequency of the periodic force as well as on the DNA sequence. We monitor the separation between the strands of the block copolymer DNA as a function of time at various frequencies and force amplitudes. The averaged separation $\langle x \rangle$ plotted as a function of force value g shows a hysteresis loop. The shape of the hysteresis loops is found to be dependent on the frequency of the periodic force and the sequence of block copolymer DNA. For sequences of shorter block lengths, e.g., $(A_4B_4)_{32}$ and $(B_4A_4)_{32}$, the loops are found to be the same, with equal area, irrespective of periodic force acting on A- or B-type base pairs at all frequencies. However, for longer block lengths, e.g., $(A_{128}B_{128})_1$ and $(B_{128}A_{128})_1$, the shape of the loops strongly depends on whether the periodic force is applied on A- or B-type base pairs. We also obtain the area of the hysteresis loops, A_{loop} as a function of frequency ω. The resonance frequency, ω^*, at which the loop area A_{loop} is maximum is higher for the sequence $(B_{128}A_{128})_1$. For frequencies higher than ω^*, the loop area for the sequence $(B_{128}A_{128})_1$ is always more than that for the opposite sequence $(A_{128}B_{128})_1$. Another difference is the oscillatory behavior of the A_{loop} seen for the sequence $(B_{128}A_{128})_1$, whereas it is absent for the opposite sequence. For frequencies lower than ω^*, we find that the rate at which A_{loop} decreases with frequency also depends on the block length. The loop area for the sequence $(B_{128}A_{128})_1$ is

found to decrease much faster than the sequence $(A_{128}B_{128})_1$. In the lower frequency regime A_{loop} scales as $A_{loop} \sim (g_0 - g_c)^{\alpha}\omega^{\beta}$ with exponents $\alpha = 1$ and $\beta = 5/4$ same as the exponents obtained for periodic forcing of a homopolymer DNA studied earlier [20], whereas in the higher frequencies, the loop area A_{loop} is found to scale with frequency as $A_{loop} \sim 1/\omega$ [76, 20]. The differences in exponents observed in Brownian dynamics simulations and the current study requires further investigation and will be the subject of a future study.

Chapter 4

Stochastic Resonance in the Unzipping of a DNA by Periodic Force

In this chapter, we study the stochastic resonance in a periodically driven homopolymer double-stranded DNA (dsDNA) and a block copolymer DNA by using Monte Carlo simulations. We obtain $T - G - \omega_{\text{res}}$ phase diagram by performing the simulations at different force amplitudes and temperatures. We observe that the resonance frequency increases as the temperature or amplitude increases. We observe that the resonance frequencies obtained at $G = 1$, $T = 1$ and $G = 3$, $T = 1$ are same as the frequencies at which the area of the hysteresis loop is maximum reported in [20].

This chapter is organized as follows: in section 4.1, we describe our model and define resonance quantifiers that are used to identify the stochastic resonance. We discuss our results in section 4.2 and give concluding remarks in section 4.3.

4.1 Model

The model used in this chapter has been used previously to study periodically driven DNA [20, 21, 22]. In this model, the two strands of a homopolymer DNA are represented by two directed self-avoiding walks on a $(d = 1 + 1)$-dimensional

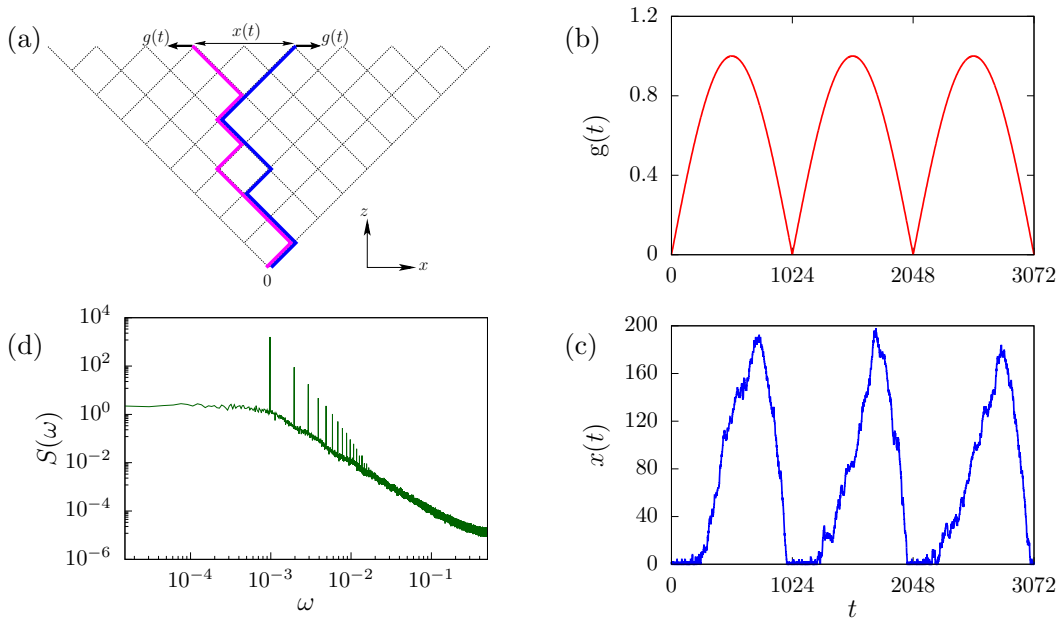

Figure 4.1: (a) Schematic diagram of the model. The strands of the DNA are shown by thick solid lines. The one end of the DNA is anchored at origin (O), and the free end monomers of the strands are pulled along $x-$ direction with a periodic force $g(t) = G\,|\sin(\omega_0 t)|$, where ω_0 is the frequency and G is the amplitude of the force. (b) Variation of the force $g(t)$ as a function of the time t for the three consecutive cycles at a frequency $\omega_0 = 3.06 \times 10^{-3}$ and amplitude $G = 1.0$. (c) The separation between the end monomers, $x(t)$, follows the external force $g(t)$ with a lag. The length of the DNA is taken as $N = 128$. (d) Power spectral density $S(\omega)$ of the extension $x(t)$ obtained using the TISEAN package for a DNA of length $N = 128$.

square lattice. The walks, which start from the origin, are restricted to go towards the positive direction of the diagonal axis (z-direction) without crossing each other. The self-avoidance and the correct base pairing of the DNA are taken care of by the directional nature of walks. The complementary monomers of the strands are allowed to occupy the same lattice site. For each such overlap there is a gain in energy $-\epsilon$ ($\epsilon > 0$). One end of the DNA is anchored at the origin and a time-dependent periodic force

$$g(t) = G\,|\sin(\omega_0 t)| \tag{4.1}$$

with angular frequency ω_0 and amplitude G acts along the transverse direction ($x-$ direction) at the free end. Throughout the chapter, by frequency we mean the angular frequency. The schematic diagram of the model is shown in Fig. 4.1(a).

Although the above model ignores finer details such as bending rigidity of the

dsDNA, sequence heterogeneity, stacking of base pairs, etc., it was found that the basic features, such as the first order nature of the unzipping transition and the existence of a re-entrant region allowing unzipping by decreasing temperature, are preserved by this two dimensional model [17, 18]. For this model the zero force melting takes place at a temperature $T_m = \varepsilon/\ln(4/3)$ [19]. In this chapter, we work on temperatures which are lower than the melting temperature $T_m \approx 3.476$. We present most of the results at a temperature $T = 1.0$, for which the critical force $g_c(1) = 0.6778...$

We perform Monte Carlo simulations of the model by using the Metropolis algorithm. In our model, the directional nature of the walks prevents the self-crossing of strands. To avoid mutual crossing of strands, we allow strands to undergo Rouse dynamics with local corner-flip or end-flip moves [3] that do not violate mutual avoidance. The elementary move consists of selecting a random monomer, from a randomly chosen strand, and flipping it. If the move results in the overlapping of two complementary monomers, thus forming a base-pair between the strands, it is always accepted as a move. The opposite move, i.e., the unbinding of monomers, is chosen with the Boltzmann probability $\xi = \exp(-\varepsilon/k_BT)$. If the chosen monomer is unbound, and it remains unbound after the move is performed, is always accepted. The time is measured in units of Monte Carlo Steps (MCS). One MCS consists of $2N$ flip attempts, i.e., every monomer is given a chance to flip on average. Throughout the simulation, the detailed balance is always satisfied. From any starting configuration, it is possible to reach any other configuration by using the above moves. Throughout this chapter, we have chosen $\varepsilon = 1$ and $k_B = 1$.

At any given force amplitude G and frequency ω_0, as the time t is increased by unity, the external force $g(t)$ changes, according to Eq. (4.1), from 0 to a maximum value G and then decreases to 0. Between each time increment, the system is relaxed by a unit time (1 MCS). Upon increasing t further, the above cycle gets repeated again and again. The simulation is run for 2000 cycles to allow the system to reach the stationary state and then measurements are done.

In our simulations, the distance between the end monomers of the two strands, $x(t)$, as a function of time for various force amplitudes G and frequencies ω_0 is monitored. From the time series $x(t)$, we then obtain the power spectral density,

$S(\omega)$, defined as the Fourier transform of auto-correlation function of $x(t)$,

$$S(\omega) = \int_{-\infty}^{\infty} \langle x(t)x(t+\tau)\rangle \exp^{-i\omega\tau}\, d\tau. \tag{4.2}$$

Here $\langle\cdot\rangle$ denotes time average over the series. $S(\omega)$ can be described as the superposition of a background power spectral density $S_N(\omega)$ and a structure of delta spikes centred at $\omega = (2n+1)\omega_0$ with $n = 0, 1, 2, ..$ and ω_0 being the frequency of applied force [164, 165]. From the power spectral density $S(\omega)$, we can define resonance quantifier output signal (OS) as,

$$\eta = \int_{\omega_0-\Delta\omega}^{\omega_0+\Delta\omega} S(\omega)d\omega, \tag{4.3}$$

where $\Delta\omega$ is taken as half of the full width at half maximum.

In case of few bistable systems, η does not show a peak at resonance frequency for which, we need to calculate SNR (signal-to-noise ratio) to identify stochastic resonance [166]. SNR is defined as

$$\xi = \eta/S_N(\omega_0) \tag{4.4}$$

where $S_N(\omega_0)$ is background noise at ω_0 [165]. However, both η and ξ are equally valid to identify stochastic resonance. In our system however, η proves to be an excellent quantifier to identify stochastic resonance.

We performed Monte Carlo simulations by considering DNA of various chain lengths at various frequencies and amplitudes of force at different temperatures. We monitored the extension x, and calculated the power spectral density using TISEAN 3.0.1 software package [167]. We repeated the whole process with 50 different initial stationary states for each set of frequency, amplitude and temperature values and obtained the average power spectral density.

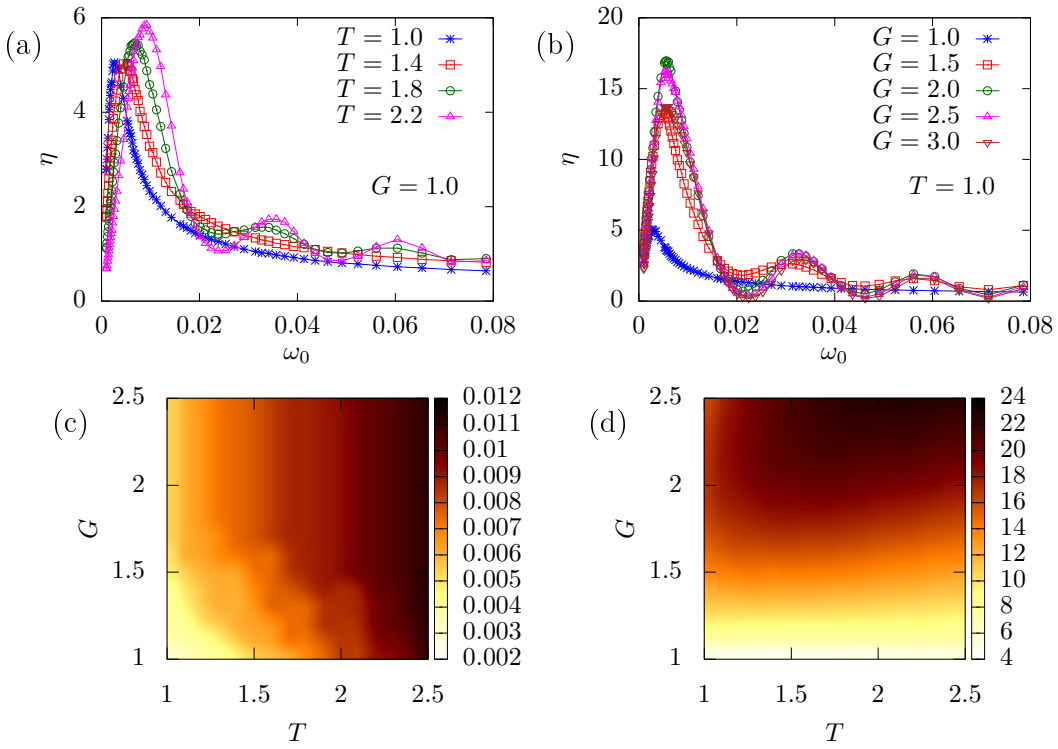

Figure 4.2: Variation of η as a function of applied force frequency of a DNA of length $N = 128$ for (a) force amplitude $G = 1.0$ at various temperatures $T = 1.0, 1.4, 1.8$ and 2.2. (b) η as a function of the applied frequency ω_0 for various force amplitudes $G = 1.0, 1.5, 2.0, 2.5$ and 3.0 at temperature $T = 1$, (c) The $T - G - \omega_{\rm res}$ phase diagram mapped on a two dimensional space. (d) The $T - G - \eta_{\omega_{res}}$ phase diagram mapped on a two dimensional space.

4.2 Results

4.2.1 Influence of force amplitude and temperature

In Fig. 4.1(b), we have plotted the time variation of the external periodic force $g(t)$ for the DNA of length $N = 128$ at a given value of G and ω_0 for three consecutive cycles. In Fig. 4.1(c), the corresponding time variation of the extension $x(t)$ captures the folding and unfolding dynamics of the DNA with a largely unzipped state at the maximum of $x(t)$ and a zipped state when $x(t) \approx 0$. The Fourier transform of the stationary correlation function of $x(t)$ gives the power spectral density $S(\omega)$. As shown in Fig. 4.1(d), $S(\omega)$ can be described as the superposition of a background spectral density and delta peaks at frequencies which are multiples of ω_0. We then calculate the output signal using Eq. (4.3). The resulting η as a function of the oscillating frequency are depicted in Figs. 4.2(a,b) for various values

of force amplitude and temperatures. We observe that as the frequency increases, the η increases up to a frequency and decreases on further increment in frequency confirming stochastic resonance in DNA on periodic forcing. We have observed how both effects change the resonance frequency of the system. The output signal shows a peak for all the different variations of G and T. The position and strength of the peak however varies across the different parameter values. At a given temperature, the strength of the peak increases with increasing force amplitude. Further, the peak frequency ω^* shifts to higher frequencies with increasing force amplitudes. In Fig. 4.2(c,d), we show the detailed phase diagram in the $G-T$ plane of the η peak positions and magnitudes respectively. As seen in Fig. 4.2(a), the peak position is at lower frequencies for low values of G and T. For a fixed G, increasing T shifts peak to higher frequencies. The peak values of the output signal increases monotonically with increasing force amplitude at a fixed temperature (Fig. 4.2(d)).

The presence of multiple peaks in the η /ξ indicates multiple stable and metastable states in the system and transitions between them. For $G = 1$ (see Fig. 4.3(a-c)), which lies slightly above the critical force g_c needed to unzip the DNA, the majority of the beads of the DNA are in the zipped state. At very high frequencies ω_0, the fluctuating force opens only a few of the base pairs. With decreasing frequencies, the possibility of the DNA to relax to the fluctuating force increases, leading to more base pair openings. At a certain critical frequency, we observe a peak in η signalling stochastic resonance (Fig. 4.3(a)). For very low frequencies, the system is nearly in the equilibrium state and the η is low.

The situation for $G = 3$ (see Fig. 4.3(b-d)), is very different. Starting at high frequencies, as we lower ω_0, we see the appearance of a small peaks in η, signifying stochastic resonance. The appearance of the smaller peaks signifies that at high G there are multiple dynamical states. At this force value which lies far above the phase boundary, the steady state of the system is an unzipped one at a constant force. As the frequency is decreased and the DNA gets time to relax, it settles into metastable states of partially zipped conformations. This shows up as multiple peaks in the η versus ω_0 plot. While multiple peaks in stochastic resonance have been observed earlier in FPU chains [168] and arrays of monostable oscillators [169], we believe this is the first report of the same in a periodically driven DNA system.

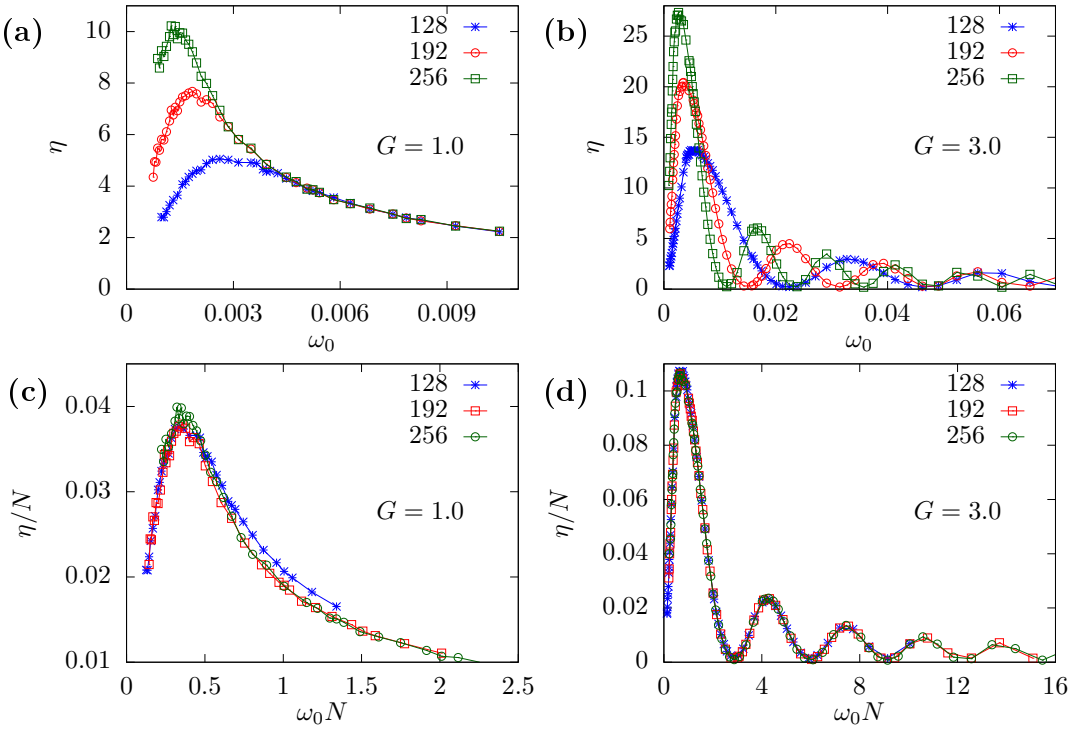

Figure 4.3: Variation of η as a function of applied force frequency ω_0 for three different chain lengths $N = 128, 192$, and 256 at force amplitudes (a) $G = 1.0$ and (b) $G = 3.0$. When the scaled η/N for various chain lengths are plotted as $\omega_0 N$, we get a nice data collapse for (c) $G = 1.0$ and (d) $G = 3.0$.

4.2.2 Influence of changing DNA lengths

In order to see what happens when we vary the length of the DNA, we observed the response of the system to periodic driving as N is increased. For both $G = 1$ and $G = 3$, we find a shift of the resonance peak(s) towards lower frequencies as we increase the length. Further, the peak value also increases with increasing length. These features suggests a scaling of η as

$$\eta \sim N^{\delta} \mathcal{G}(\omega_0 N^{z}), \tag{4.5}$$

similar to scaling of hysteresis loop area in earlier theoretical studies of periodically driven DNA. Here δ and z are critical exponents. Data collapse for both $G = 1$ and $G = 3$ is achieved for $\delta \approx 1$ and $z \approx 1$.

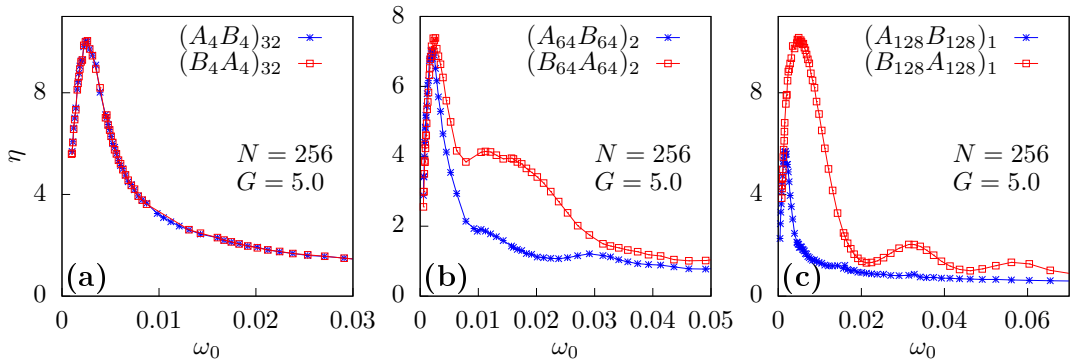

Figure 4.4: Optical signal, η, as a function of frequency ω_0 of the driving force for a block copolymer DNA of length $N = 256$ at force amplitude $G = 5.0$ for the opposite sequences (a) $(A_4B_4)_{32}$ and $(B_4A_4)_{32}$, (b) $(A_{64}B_{64})_2$ and $(B_{64}A_{64})_2$, and (c) $(A_{128}B_{128})_1$ and $(B_{128}A_{128})_1$ at temperature $T = 4.0$.

4.2.3 Influence of heterogeneity on DNA

To see if the above features are preserved for hetero-polymer DNA, we consider the periodic forcing of a block copolymer DNA. The heterogeneity on the DNA chain is introduced in the form of repeated blocks, $-A_nB_n-$ or $-B_nA_n-$, where $2n$ is the block length, and A and B are different types of base pairs with two- and three-hydrogen bonds, respectively. The variation of η as a function of frequency at a force amplitudes $G = 5.0$ for different block lengths ($(A_4B_4)_{32}$, $(A_{64}B_{64})_2$, and $(A_{128}B_{128})_1$ and its opposite sequence) are plotted in Fig. 4.4. The length of the DNA is taken as $N = 256$.

In the presence of static force it has been found that the critical force required to unzip the DNA is enhanced for block copolymer DNA. Further, the critical force is independent of the sequence of the DNA i.e. it does not matter whether the DNA is unzipped from the end having base pairing with three hydrogen bonds (stronger) or the base pairing with two hydrogen bonds. For periodic forcing with $G = 5$, we find that for smaller block sizes like $(A_4B_4)_{32}$, the η shows a single resonance peak at lower frequency. For these block sizes, it again does not matter which end is being unzipped first (see Fig. 4.4(a)). However, as the block sizes increase, η starts showing additional peaks at higher frequencies and there is a strong dependence on which end is unzipped first. For $G = 5$, multiple peaks are observed for sequences $-B_nA_n-$ (see Fig. 4.4(b-c)). At these G values, the steady state of the polymer is a zipped one at constant forces. With periodic forcing, it is easier to unzip the polymer end if the bonding is weaker. This is true where

the pulling force is applied to A-type base pairs i.e. for the $-B_nA_n-$ sequences. The strands are therefore separated easier and these separated strands can explore more configurations. Again the peaks are observed whenever the frequency of the periodic force is ω_p which are the higher harmonics.

4.3 Conclusions

We have studied stochastic resonance phenomenon in a double stranded DNA subjected to a periodic force. Power spectral density of extension $x(t)$ is calculated by using TISEAN package. From the power spectral density, we have measured the resonance quantifier η as a function of applied force frequency at different amplitudes and different temperatures. For a given amplitude and temperature, η increases upto a frequency and decreases as the frequency decreased. The frequency where we get maximum η is taken as resonance frequency. We have inferred that at the resonance frequencies, the area of the hysteresis loop that formed due to the lag between the response of the system and the applied force will be maximum. We also obtained a phase $T - G - \omega_{\text{res}}$ by measuring resonance frequencies at different amplitudes and temperatures and observed that resonance frequency increases as the amplitude or temperature is increases.

Chapter 5

Summary

To summarize, in this thesis, we have studied the dynamic transitions in the unzipping of an adsorbed polymer from an attractive surface (or the wall) and a double-stranded block copolymer DNA under the influence of a time-dependent periodic force. We have also studied the stochastic resonance phenomenon in the unzipping of a homopolymer dsDNA and a block copolymer DNA by a periodic force. For the investigation of these problems in details, we have used three different techniques like generating function, exact transfer matrix, and the Monte Carlo simulations and a software package TISEAN (acronym for Time Series Analysis).

At the very first, we have defined the polymer and its different types in details. Polymer as a statistical mechanical model in physics has been also described. We then introduced the DP model and highlighted its various applications as a model system in statistical physics. We gave a brief introduction about the polymer adsorption on a surface. We talked about adsorption-desorption transition and unzipping transition which are two different types of the transitions that a polymer undergoes. We discussed both of them with examples. After that we gave a short introduction about the copolymer and block copolymer. We then gave an introduction to DNA and mentioned its different structures. We discussed the DNA replication and RNA transcription in brief. We introduced the DNA block copolymer and highlighted its some applications. We also discussed different melting processes of DNA, like chemical denaturation, thermal denaturation and the force induced unzipping, in which two strands of the DNA are separated. Several theoretical models which are used to investigate the dynamic transitions in the force induced unzipping of DNA were discussed. To study the unzipping of DNA

experimentally, various single molecule micro-manipulation techniques were also discussed. Lastly, we introduced the stochastic resonance phenomenon and described different theories which explain it. To quantify the SR, we have discussed about the different quantifier.

In the first problem of the thesis, we have studied the dynamic transitions in the unzipping of an adsorbed polymer from an attractive surface (or the wall) by a periodic force with frequency ω and amplitude g_0. We have considered three different types of surfaces:

1. The surface is impenetrable, i.e., the polymer is allowed to stay only on one side of the wall. We refer such a surface as *hard-wall* in the thesis.

2. The surface is penetrable, i.e., the polymer is allowed to cross the surface, and the polymer has an equal affinity on either sides of the surface. We call such a surface as *soft-wall*.

3. The surface is penetrable but the polymer has different affinities on either sides of the surface. This can be thought of as an interface between the two immiscible liquids in which the polymer has different degrees of solubility.

We first reproduced the results of static force case using Monte Carlo simulations and studied the response of the polymer in the presence of a periodic force. We observed that the force-distance isotherms show hysteresis loops in all the three cases. It was found that the shape and the size of the loop depends on the frequency of the periodic force. For the softwall case, as the polymer experiences similar environment on both sides of the wall, the loop is divided about $\langle x(g)\rangle = 0$ axis into two equal and symmetrical parts. Whereas, in case of the wall separating two different media having different affinities for the polymer, loops obtained in the positive and negative cycles are not symmetric. On the other hand, for the hardwall case, the hysteresis loops are possible only in the region $x > 0$. The behavior of the loop area, A_{loop}, depends on both the frequency and the amplitude of the force. We found that A_{loop} shows nonmonotonic behavior as the frequency is varied keeping the amplitude constant. On increasing the frequency, the loop area first increases, it reaches a maximum at frequency $\omega^*(g_0)$, and then decreases on increasing the frequency further. For small force amplitudes, A_{loop} shows only one peak at a resonance frequency $\omega^*(g_0)$, and it decreases monotonically on increasing the frequencies for all the three cases. However, for higher force amplitudes, the

A_{loop} still shows only one peak for the softwall and hardwall cases, whereas, it shows two peaks of different height for the wall separating two different types of media. Furthermore, secondary peaks are also present at higher frequencies. For all the three cases, we found that A_{loop} scales as $1/\omega$ in the higher frequency regime, and as $g_0^\alpha \omega^\beta$ with exponents $\alpha = 1$ and $\beta = 1.25$ in the lower frequency regime.

We studied the unzipping of a block copolymer DNA. We considered a heteropolymer DNA as a block copolymer DNA, in which the heterogeneity is considered in the form of repeated blocks, A_nB_n or B_nA_n , where $2n$ is the block length, and A and B are different types of base pairs with two- and three-hydrogen bonds, respectively. One end of this DNA sequence is subjected to a pulling force while the other end is kept anchored. We have considered both the constant and the periodic pulling force cases. The unzipping of a block copolymer DNA by a constant pulling force was found to be a first-order phase transition. The equilibrium phase boundary separating the zipped and the unzipped phases does not depend on the DNA sequence and is found to follow the same exact expression, as obtained for the homopolymer DNA case, but with a different effective base pair energy. The results for the unzipping of a block copolymer DNA subjected to a periodic force were, however, found to be sequence dependent. For sequences of higher block lengths, the results also depend on whether the periodic force is acting on A-type or B-type base pairs. The force-distance isotherms again show hysteresis loops. It was found that A_{loop} scales as $1/\omega$ in the higher frequency regime, and as $g_0^\alpha \omega^\beta$ with exponents $\alpha = 1$ and $\beta = 1.25$ in the lower frequency regime.

We have also studied the stochastic resonance phenomenon in the unzipping of a homopolymer double-stranded DNA (dsDNA) and a block copolymer DNA by a periodic force using Monte Carlo simulations at different force amplitudes (G) and temperatures (T). We measured the resonance quantifier, output signal(OS) from power spectral density of extension (distance between the end monomers of two strands) as a function of applied force frequency ω. We found that the output signal increases as a function of frequency up to a certain frequency $\omega_{\rm res}$ which is called the resonance frequency and decreases as we increase the frequency further. We obtained $T-G-\omega_{\rm res}$ phase diagram by measuring the resonance frequencies at different applied force amplitudes and temperatures and observe that the resonance frequency increases as we increase the amplitude or temperature.

Bibliography

[1] Paul J Flory. *Principles of polymer chemistry*. Cornell University Press, 1953.

[2] Pierre-Gilles De Gennes and Pierre-Gilles Gennes. *Scaling concepts in polymer physics*. Cornell university press, 1979.

[3] M Doi and SF Edwards. The theory of polymer dynamics oxford university press (clarendon) london new york. 1986.

[4] Berenike Maier and Joachim O Rädler. Conformation and self-diffusion of single dna molecules confined to two dimensions. *Physical review letters*, 82(9):1911, 1999.

[5] Jeffrey J Prentis and Daniel R Sisan. Granular polymer solution. *Physical Review E*, 65(3):031306, 2002.

[6] Alberto Berretti and Alan D Sokal. New monte carlo method for the self-avoiding walk. *Journal of Statistical Physics*, 40(3):483–531, 1985.

[7] Carlo Vanderzande. *Lattice models of polymers*. Number 11. Cambridge University Press, 1998.

[8] SM Bhattacharjee. Statistics of linear polymers in disordered media ed bk chakrabarti, 2005.

[9] BK Chakrabarti and SS Manna. Critical behaviour of directed self-avoiding walks. *Journal of Physics A: Mathematical and General*, 16(4):L113, 1983.

[10] AM Szpilka. The asymptotic behaviour of directed self-avoiding walks. *Journal of Physics A: Mathematical and General*, 16(12):2883, 1983.

[11] JL Cardy. Critical exponents of directed self-avoiding walks. *Journal of Physics A: Mathematical and General*, 16(11):L355, 1983.

[12] Pierre-Gilles de Gennes. Exponents for the excluded volume problem as derived by the wilson method. *Physics Letters A*, 38(5):339–340, 1972.

[13] V Privman and NM Švrakić. Restoration of universality for the rod-to-coil transition scaling in the infinite-dimensionality limit: Exact results for directed walks. *Journal of statistical physics*, 50(1):81–89, 1988.

[14] Timothy Halpin-Healy and Yi-Cheng Zhang. Kinetic roughening phenomena, stochastic growth, directed polymers and all that. aspects of multidisciplinary statistical mechanics. *Physics reports*, 254(4-6):215–414, 1995.

[15] Somendra M Bhattacharjee. Unzipping dnas: towards the first step of replication. *Journal of Physics A: Mathematical and General*, 33(45):L423, 2000.

[16] Enzo Orlandini, Somendra M Bhattacharjee, Davide Marenduzzo, Amos Maritan, and Flavio Seno. Mechanical denaturation of dna: existence of a low-temperature denaturation. *Journal of Physics A: Mathematical and General*, 34(50):L751, 2001.

[17] D Marenduzzo, A Trovato, and A Maritan. Phase diagram of force-induced dna unzipping in exactly solvable models. *Physical Review E*, 64(3):031901, 2001.

[18] Davide Marenduzzo, Somendra M Bhattacharjee, Amos Maritan, Enzo Orlandini, and Flavio Seno. Dynamical scaling of the dna unzipping transition. *Physical review letters*, 88(2):028102, 2001.

[19] Rajeev Kapri. Hysteresis and nonequilibrium work theorem for dna unzipping. *Physical Review E*, 86(4):041906, 2012.

[20] Rajeev Kapri. Unzipping dna by a periodic force: Hysteresis loop area and its scaling. *Physical Review E*, 90(6):062719, 2014.

[21] M Suman Kalyan and Rajeev Kapri. Unzipping dna by a periodic force: Hysteresis loops, dynamical order parameter, correlations, and equilibrium curves. *The Journal of chemical physics*, 150(22):224903, 2019.

[22] Ramu Kumar Yadav and Rajeev Kapri. Unzipping of a double-stranded block copolymer dna by a periodic force. *Physical Review E*, 103(1):012413, 2021.

[23] RAL JONES and RW Richards. Polymers at interfaces, 1999.

[24] Roland R Netz and David Andelman. Neutral and charged polymers at interfaces. *Physics reports*, 380(1-2):1–95, 2003.

[25] PHL Martins, JA Plascak, and M Bachmann. Adsorption of flexible polymer chains on a surface: Effects of different solvent conditions. *The Journal of chemical physics*, 148(20):204901, 2018.

[26] Robert J Rubin. Random-walk model of chain-polymer adsorption at a surface. *The Journal of Chemical Physics*, 43(7):2392–2407, 1965.

[27] Pierre-Gilles De Gennes. *Simple views on condensed matter*, volume 8. World scientific, 1998.

[28] V Privman, G Forgacs, and HL Frisch. New solvable model of polymer-chain adsorption at a surface. *Physical Review B*, 37(16):9897, 1988.

[29] G Forgacs, V Privman, and HL Frisch. Adsorption–desorption transition of polymer chains interacting with surfaces. *The Journal of Chemical Physics*, 90(6):3339–3345, 1989.

[30] G Forgacs and M Semak. Adsorption of a directed polymer chain in the presence of monomer attraction: analytical results. *Journal of Physics A: Mathematical and General*, 24(14):L779, 1991.

[31] R Rajesh, Deepak Dhar, Debaprasad Giri, Sanjay Kumar, and Yashwant Singh. Adsorption and collapse transitions in a linear polymer chain near an attractive wall. *Physical Review E*, 65(5):056124, 2002.

[32] Yashwant Singh, Sanjay Kumar, and Debaprasad Giri. Surface adsorption and collapse transition of a linear polymer chain in three dimensions. *Journal of Physics A: Mathematical and General*, 32(36):L407, 1999.

[33] Yashwant Singh, Debaprasad Giri, and Sanjay Kumar. Crossover of a polymer chain from bulk to surface states. *Journal of Physics A: Mathematical and General*, 34(8):L67, 2001.

[34] Pramod Kumar Mishra, Debaprasad Giri, Shamantha Kumar, and Yashwant Singh. Does a surface attached globule phase exist? *Physica A: Statistical Mechanics and its Applications*, 318(1-2):171–178, 2003.

[35] Rajeev Kapri and Somendra M Bhattacharjee. Unzipping an adsorbed polymer in a dirty or random environment. *Physical Review E*, 72(5):051803, 2005.

[36] E Orlandini, MC Tesi, and SG Whittington. Adsorption of a directed polymer subject to an elongational force. *Journal of Physics A: Mathematical and General*, 37(5):1535, 2004.

[37] G Iliev, E Orlandini, and SG Whittington. Adsorption and localization of random copolymers subject to a force: The morita approximation. *The European Physical Journal B-Condensed Matter and Complex Systems*, 40(1):63–71, 2004.

[38] PK Mishra, Sanjay Kumar, and Yashwant Singh. Force-induced desorption of a linear polymer chain adsorbed on an attractive surface. *EPL (Europhysics Letters)*, 69(1):102, 2004.

[39] S Bhattacharya, VG Rostiashvili, A Milchev, and Thomas A Vilgis. Polymer desorption under pulling: A dichotomic phase transition. *Physical Review E*, 79(3):030802, 2009.

[40] KL Sebastian, VG Rostiashvili, and Thomas A Vilgis. Dynamics of pulled desorption with effects of excluded-volume interaction: The p-laplacian diffusion equation and its exact solution. *EPL (Europhysics Letters)*, 95(4):48006, 2011.

[41] Ian W Hamley. *Developments in block copolymer science and technology*. John Wiley & Sons, 2004.

[42] James D Watson. *Molecular biology of the gene*. Pearson Education India, 2004.

[43] Helen M Berman, John Westbrook, Zukang Feng, Gary Gilliland, Talapady N Bhat, Helge Weissig, Ilya N Shindyalov, and Philip E Bourne. The protein data bank. *Nucleic acids research*, 28(1):235–242, 2000.

[44] Jason P Weisenseel, G Ramachandra Reddy, Lawrence J Marnett, and Michael P Stone. Structure of an oligodeoxynucleotide containing a 1, n 2-propanodeoxyguanosine adduct positioned in a palindrome derived from the salmonella typhimurium hisd3052 gene: Hoogsteen pairing at ph 5.2. *Chemical research in toxicology*, 15(2):127–139, 2002.

[45] Arthur Kornberg, Tania A Baker, et al. *DNA replication*, volume 3. Wh Freeman New York, 1992.

[46] Daniel S Johnson, Lu Bai, Benjamin Y Smith, Smita S Patel, and Michelle D Wang. Single-molecule studies reveal dynamics of dna unwinding by the ring-shaped t7 helicase. *Cell*, 129(7):1299–1309, 2007.

[47] Aakash Basu, Allyn J Schoeffler, James M Berger, and Zev Bryant. Atp binding controls distinct structural transitions of escherichia coli dna gyrase in complex with dna. *Nature structural & molecular biology*, 19(5):538–546, 2012.

[48] Natali Fili, Gregory I Mashanov, Christopher P Toseland, Christopher Batters, Mark I Wallace, Joseph TP Yeeles, Mark S Dillingham, Martin R Webb, and Justin E Molloy. Visualizing helicases unwinding dna at the single molecule level. *Nucleic acids research*, 38(13):4448–4457, 2010.

[49] Piotr Szymczak and Harald Janovjak. Periodic forces trigger a complex mechanical response in ubiquitin. *Journal of molecular biology*, 390(3):443–456, 2009.

[50] Ilker Donmez and Smita S Patel. Mechanisms of a ring shaped helicase. *Nucleic acids research*, 34(15):4216–4224, 2006.

[51] Sameer S Velankar, Panos Soultanas, Mark S Dillingham, Hosahalli S Subramanya, and Dale B Wigley. Crystal structures of complexes of pcra dna helicase with a dna substrate indicate an inchworm mechanism. *Cell*, 97(1):75–84, 1999.

[52] Margaret E Fairman-Williams and Eckhard Jankowsky. Unwinding initiation by the viral rna helicase nph-ii. *Journal of molecular biology*, 415(5):819–832, 2012.

[53] Robert J White. *RNA polymerase III transcription*. Springer Science & Business Media, 2013.

[54] Fikri E Alemdaroglu, N Ceren Alemdaroglu, Peter Langguth, and Andreas Herrmann. Cellular uptake of dna block copolymer micelles with different shapes. *Macromolecular rapid communications*, 29(4):326–329, 2008.

[55] Marc Lemaitre, Bernard Bayard, and Bernard Lebleu. Specific antiviral activity of a poly (l-lysine)-conjugated oligodeoxyribonucleotide sequence complementary to vesicular stomatitis virus n protein mrna initiation site. *Proceedings of the National Academy of Sciences*, 84(3):648–652, 1987.

[56] Ankit Agarwal, Robert C Unfer, and Surya K Mallapragada. Dual-role self-assembling nanoplexes for efficient gene transfection and sustained gene delivery. *Biomaterials*, 29(5):607–617, 2008.

[57] Chao Chen, Ross AL Wylie, Daniel Klinger, and Luke A Connal. Shape control of soft nanoparticles and their assemblies. *Chemistry of Materials*, 29(5):1918–1945, 2017.

[58] Roger M Wartell and Albert S Benight. Thermal denaturation of dna molecules: a comparison of theory with experiment. *Physics Reports*, 126(2):67–107, 1985.

[59] Bruno H Zimm. Theory of"melting"of the helical form in double chains of the dna type. *The Journal of Chemical Physics*, 33(5):1349–1356, 1960.

[60] Douglas Poland and Harold A Scheraga. Phase transitions in one dimension and the helix—coil transition in polyamino acids. *The Journal of chemical physics*, 45(5):1456–1463, 1966.

[61] Michael E Fisher. Effect of excluded volume on phase transitions in biopolymers. *The Journal of Chemical Physics*, 45(5):1469–1473, 1966.

[62] Michel Peyrard and Alan R Bishop. Statistical mechanics of a nonlinear model for dna denaturation. *Physical review letters*, 62(23):2755, 1989.

[63] Yariv Kafri, David Mukamel, and Luca Peliti. Why is the dna denaturation transition first order? *Physical Review Letters*, 85(23):4988, 2000.

[64] Y Kafri, D Mukamel, and L Peliti. Melting and unzipping of dna. *The European Physical Journal B-Condensed Matter and Complex Systems*, 27(1):135–146, 2002.

[65] Maria Serena Causo, Barbara Coluzzi, and Peter Grassberger. Simple model for the dna denaturation transition. *Physical Review E*, 62(3):3958, 2000.

[66] Vassili Ivanov, Yan Zeng, and Giovanni Zocchi. Statistical mechanics of base stacking and pairing in dna melting. *Physical Review E*, 70(5):051907, 2004.

[67] Dinko Cule and Terence Hwa. Denaturation of heterogeneous dna. *Physical Review Letters*, 79(12):2375, 1997.

[68] Yan Zeng, Awrasa Montrichok, and Giovanni Zocchi. Length and statistical weight of bubbles in dna melting. *Physical review letters*, 91(14):148101, 2003.

[69] Nikos Theodorakopoulos, Thierry Dauxois, and Michel Peyrard. Order of the phase transition in models of dna thermal denaturation. *Physical Review Letters*, 85(1):6, 2000.

[70] Thomas Garel, Cécile Monthus, and Henri Orland. A simple model for dna denaturation. *EPL (Europhysics Letters)*, 55(1):132, 2001.

[71] Somendra M Bhattacharjee. Comment on" a simple model for dna denaturation". *arXiv preprint cond-mat/0203155*, 2002.

[72] Ralf Blossey and Enrico Carlon. Reparametrizing the loop entropy weights: effect on dna melting curves. *Physical Review E*, 68(6):061911, 2003.

[73] Amar Singh and Navin Singh. Dna melting in the presence of molecular crowders. *Physical Chemistry Chemical Physics*, 19(29):19452–19460, 2017.

[74] Arghya Maity and Navin Singh. Melting of dna in confined geometries. *European Biophysics Journal*, 49(7):561–569, 2020.

[75] Sanjay Kumar and Garima Mishra. Statistical mechanics of dna unzipping under periodic force: scaling behavior of hysteresis loops. *Physical review letters*, 110(25):258102, 2013.

[76] Garima Mishra, Poulomi Sadhukhan, Somendra M Bhattacharjee, and Sanjay Kumar. Dynamical phase transition of a periodically driven dna. *Physical Review E*, 87(2):022718, 2013.

[77] Rakesh Kumar Mishra, Garima Mishra, Debaprasad Giri, and Sanjay Kumar. Scaling of hysteresis loop of interacting polymers under a periodic force. *The Journal of chemical physics*, 138(24):244905, 2013.

[78] Sanjay Kumar, Ravinder Kumar, and Wolfhard Janke. Periodically driven dna: Theory and simulation. *Physical Review E*, 93(1):010402, 2016.

[79] Tanmoy Pal and Sanjay Kumar. Dna unzipping with asymmetric periodic forces: Robustness of the scaling behavior of hysteresis loop. *EPL (Europhysics Letters)*, 121(1):18001, 2018.

[80] Rajeev Kapri. Hysteresis loop area scaling exponents in dna unzipping by a periodic force: A langevin dynamics simulation study. *arXiv preprint arXiv:2104.07170*, 2021.

[81] E Yeramian. Genes and the physics of the dna double-helix. *Gene*, 255(2):139–150, 2000.

[82] Andreas Hanke, Martha G Ochoa, and Ralf Metzler. Denaturation transition of stretched dna. *Physical review letters*, 100(1):018106, 2008.

[83] Thierry Dauxois, Michel Peyrard, and Alan R Bishop. Entropy-driven dna denaturation. *Physical Review E*, 47(1):R44, 1993.

[84] Michel Peyrard, Santiago Cuesta-Lopez, and Guillaume James. Nonlinear analysis of the dynamics of dna breathing. *Journal of biological physics*, 35(1):73–89, 2009.

[85] Titus S Van Erp, Santiago Cuesta-Lopez, and Michel Peyrard. Bubbles and denaturation in dna. *The European Physical Journal E*, 20(4):421–434, 2006.

[86] Naomichi Hatano and David R Nelson. Localization transitions in non-hermitian quantum mechanics. *Physical review letters*, 77(3):570, 1996.

[87] Naomichi Hatano and David R Nelson. Vortex pinning and non-hermitian quantum mechanics. *Physical Review B*, 56(14):8651, 1997.

[88] Naomichi Hatano and David R Nelson. Non-hermitian delocalization and eigenfunctions. *Physical Review B*, 58(13):8384, 1998.

[89] David K Lubensky and David R Nelson. Pulling pinned polymers and unzipping dna. *Physical review letters*, 85(7):1572, 2000.

[90] David K Lubensky and David R Nelson. Single molecule statistics and the polynucleotide unzipping transition. *Physical Review E*, 65(3):031917, 2002.

[91] Jeff ZY Chen. Unzipping double-stranded dna with a force: Numerical results. *Physical Review E*, 66(3):031912, 2002.

[92] Pui-Man Lam, JCS Levy, and Hanchen Huang. Excluded volume effect in unzipping dna with a force. *Biopolymers: Original Research on Biomolecules*, 73(3):293–300, 2004.

[93] Pui-Man Lam and JC Levy. Unzipping dna from the condensed globule state—effects of unraveling. *Biopolymers: Original Research on Biomolecules*, 79(6):287–291, 2005.

[94] Nikos K Voulgarakis, Amaia Redondo, Alan R Bishop, and KØ Rasmussen. Probing the mechanical unzipping of dna. *Physical review letters*, 96(24):248101, 2006.

[95] Simona Cocco, Rémi Monasson, and John F Marko. Force and kinetic barriers to unzipping of the dna double helix. *Proceedings of the National Academy of Sciences*, 98(15):8608–8613, 2001.

[96] KL Sebastian. Pulling a polymer out of a potential well and the mechanical unzipping of dna. *Physical Review E*, 62(1):1128, 2000.

[97] Somendra M Bhattacharjee and Flavio Seno. Helicase on dna: a phase coexistence based mechanism. *Journal of Physics A: Mathematical and General*, 36(13):L181, 2003.

[98] Somendra M Bhattacharjee. Helicase activity on dna as a propagating front. *EPL (Europhysics Letters)*, 65(4):574, 2004.

[99] Rajeev Kapri, Somendra M Bhattacharjee, and Flavio Seno. Complete phase diagram of dna unzipping: Eye, y fork, and triple point. *Physical review letters*, 93(24):248102, 2004.

[100] Sanjay Kumar, Debaprasad Giri, and Somendra M Bhattacharjee. Force-induced triple point for interacting polymers. *Physical Review E*, 71(5):051804, 2005.

[101] Navin Singh and Yashwant Singh. Statistical theory of force-induced unzipping of dna. *The European Physical Journal E*, 17(1):7–19, 2005.

[102] Rajeev Kapri and Somendra M Bhattacharjee. Unzipping dna by force: thermodynamics and finite size behaviour. *Journal of Physics: Condensed Matter*, 18(14):S215, 2006.

[103] Debaprasad Giri and Sanjay Kumar. Effects of the eye phase in dna unzipping. *Physical Review E*, 73(5):050903, 2006.

[104] Sanjay Kumar and Debaprasad Giri. Does changing the pulling direction give better insight into biomolecules? *Physical review letters*, 98(4):048101, 2007.

[105] J Kierfeld. Force-induced desorption and unzipping of semiflexible polymers. *Physical review letters*, 97(5):058302, 2006.

[106] Rajeev Kapri and Somendra M Bhattacharjee. Randomly forced dna. *Physical review letters*, 98(9):098101, 2007.

[107] Rajeev Kapri and Somendra M Bhattacharjee. Bubbles in dna by random force. *Physica A: Statistical Mechanics and its Applications*, 384(1):10–14, 2007.

[108] Somendra M Bhattacharjee and D Marenduzzo. Dna sequence from the unzipping force? one mutation problem. *Journal of Physics A: Mathematical and General*, 35(26):L349, 2002.

[109] Valentina Baldazzi, Simona Cocco, Enzo Marinari, and Remi Monasson. Inference of dna sequences from mechanical unzipping: an ideal-case study. *Physical review letters*, 96(12):128102, 2006.

[110] Valentina Baldazzi, Serena Bradde, Simona Cocco, Enzo Marinari, and Remi Monasson. Inferring dna sequences from mechanical unzipping data: the large-bandwidth case. *Physical Review E*, 75(1):011904, 2007.

[111] K Hatch, C Danilowicz, V Coljee, and M Prentiss. Measurements of the hysteresis in unzipping and rezipping double-stranded dna. *Physical Review E*, 75(5):051908, 2007.

[112] Raymond W Friddle, Paul Podsiadlo, Alexander B Artyukhin, and Aleksandr Noy. Near-equilibrium chemical force microscopy. *The Journal of Physical Chemistry C*, 112(13):4986–4990, 2008.

[113] Zion Tshiprut and Michael Urbakh. Exploring hysteresis and energy dissipation in single-molecule force spectroscopy. *The Journal of chemical physics*, 130(8):084703, 2009.

[114] Pan TX Li, Carlos Bustamante, and Ignacio Tinoco. Real-time control of the energy landscape by force directs the folding of rna molecules. *Proceedings of the National Academy of Sciences*, 104(17):7039–7044, 2007.

[115] Adam Yasunaga, Yousif Murad, and Isaac TS Li. Quantifying molecular tension—classifications, interpretations and limitations of force sensors. *Physical biology*, 17(1):011001, 2019.

[116] Ulrich Bockelmann, Ph Thomen, B Essevaz-Roulet, Virgile Viasnoff, and Francois Heslot. Unzipping dna with optical tweezers: high sequence sensitivity and force flips. *Biophysical journal*, 82(3):1537–1553, 2002.

[117] Claudia Danilowicz, Vincent W Coljee, Cedric Bouzigues, David K Lubensky, David R Nelson, and Mara Prentiss. Dna unzipped under a constant force exhibits multiple metastable intermediates. *Proceedings of the National Academy of Sciences*, 100(4):1694–1699, 2003.

[118] C Danilowicz, Y Kafri, RS Conroy, VW Coljee, J Weeks, and M Prentiss. Measurement of the phase diagram of dna unzipping in the temperature-force plane. *Physical review letters*, 93(7):078101, 2004.

[119] Felix Ritort. Single-molecule experiments in biological physics: methods and applications. *Journal of Physics: Condensed Matter*, 18(32):R531, 2006.

[120] Carlos Bustamante, Steven B Smith, Jan Liphardt, and Doug Smith. Single-molecule studies of dna mechanics. *Current opinion in structural biology*, 10(3):279–285, 2000.

[121] Carlos Bustamante, Jed C Macosko, and Gijs JL Wuite. Grabbing the cat by the tail: manipulating molecules one by one. *Nature Reviews Molecular Cell Biology*, 1(2):130–136, 2000.

[122] Jordanka Zlatanova and Sanford H Leuba. Magnetic tweezers: a sensitive tool to study dna and chromatin at the single-molecule level. *Biochemistry and cell biology*, 81(3):151–159, 2003.

[123] Paolo Polimeno, Alessandro Magazzu, Maria Antonia Iati, Francesco Patti, Rosalba Saija, Cristian Degli Esposti Boschi, Maria Grazia Donato, Pietro G Gucciardi, Philip H Jones, Giovanni Volpe, et al. Optical tweezers and their applications. *Journal of Quantitative Spectroscopy and Radiative Transfer*, 218:131–150, 2018.

[124] Baptiste Essevaz-Roulet, Ulrich Bockelmann, and Francois Heslot. Mechanical separation of the complementary strands of dna. *Proceedings of the National Academy of Sciences*, 94(22):11935–11940, 1997.

[125] U Bockelmann, B Essevaz-Roulet, and F Heslot. Molecular stick-slip motion revealed by opening dna with piconewton forces. *Physical review letters*, 79(22):4489, 1997.

[126] U Bockelmann, B Essevaz-Roulet, and F Heslot. Dna strand separation studied by single molecule force measurements. *Physical Review E*, 58(2):2386, 1998.

[127] Hong Yin, Michelle D Wang, Karel Svoboda, Robert Landick, Steven M Block, and Jeff Gelles. Transcription against an applied force. *Science*, 270(5242):1653–1657, 1995.

[128] Miklós SZ Kellermayer, Steven B Smith, Henk L Granzier, and Carlos Bustamante. Folding-unfolding transitions in single titin molecules characterized with laser tweezers. *Science*, 276(5315):1112–1116, 1997.

[129] Jin-Der Wen, Maria Manosas, Pan TX Li, Steven B Smith, Carlos Bustamante, Felix Ritort, and Ignacio Tinoco Jr. Force unfolding kinetics of rna using optical tweezers. i. effects of experimental variables on measured results. *Biophysical journal*, 92(9):2996–3009, 2007.

[130] Maria Manosas, J-D Wen, Pan TX Li, Steven B Smith, Carlos Bustamante, Ignacio Tinoco Jr, and Felix Ritort. Force unfolding kinetics of rna using optical tweezers. ii. modeling experiments. *Biophysical journal*, 92(9):3010–3021, 2007.

[131] Michelle D Wang, Steven J Koch, Alla Shundrovsky, and Benjamin C Jantzen. Unzipping force analysis of protein association (ufapa): a novel technique to probe protein-dna interactions. In *Fluctuations and Noise in Biological, Biophysical, and Biomedical Systems*, volume 5110, pages 22–27. International Society for Optics and Photonics, 2003.

[132] K Hayashi, S de Lorenzo, M Manosas, JM Huguet, and F Ritort. Single-molecule stochastic resonance. *Physical Review X*, 2(3):031012, 2012.

[133] M Hashemi Shabestari, AEC Meijering, WH Roos, GJL Wuite, and EJG Peterman. Recent advances in biological single-molecule applications of optical

tweezers and fluorescence microscopy. *Methods in enzymology*, 582:85–119, 2017.

[134] Gil U Lee, Linda A Chrisey, and Richard J Colton. Direct measurement of the forces between complementary strands of dna. *Science*, 266(5186):771–773, 1994.

[135] Matthias Rief, Hauke Clausen-Schaumann, and Hermann E Gaub. Sequence-dependent mechanics of single dna molecules. *Nature structural biology*, 6(4):346–349, 1999.

[136] Dario Anselmetti, Jürgen Fritz, Benjamin Smith, and Xavier Fernandez-Busquets. Single molecule dna biophysics with atomic force microscopy. *Single Molecules*, 1(1):53–58, 2000.

[137] Christopher P Calderon, Wei-Hung Chen, Kuan-Jiuh Lin, Nolan C Harris, and Ching-Hwa Kiang. Quantifying dna melting transitions using single-molecule force spectroscopy. *Journal of Physics: Condensed Matter*, 21(3):034114, 2008.

[138] Matthias Rief, Mathias Gautel, Filipp Oesterhelt, Julio M Fernandez, and Hermann E Gaub. Reversible unfolding of individual titin immunoglobulin domains by afm. *science*, 276(5315):1109–1112, 1997.

[139] Rainer Eckel, Robert Ros, Alexandra Ros, Sven David Wilking, Norbert Sewald, and Dario Anselmetti. Identification of binding mechanisms in single molecule–dna complexes. *Biophysical journal*, 85(3):1968–1973, 2003.

[140] Thi-Huong Nguyen, Sang-Myung Lee, Kyounghwan Na, Sungwook Yang, Jinseok Kim, and Eui-Sung Yoon. An improved measurement of dsdna elasticity using afm. *Nanotechnology*, 21(7):075101, 2010.

[141] Terence R Strick, J-F Allemand, David Bensimon, Aaron Bensimon, and Vincent Croquette. The elasticity of a single supercoiled dna molecule. *Science*, 271(5257):1835–1837, 1996.

[142] Terence R Strick, Vincent Croquette, and David Bensimon. Single-molecule analysis of dna uncoiling by a type ii topoisomerase. *Nature*, 404(6780):901–904, 2000.

[143] Steven B Smith, Laura Finzi, and Carlos Bustamante. Direct mechanical measurements of the elasticity of single dna molecules by using magnetic beads. *Science*, 258(5085):1122–1126, 1992.

[144] Min Ju Shon, Sang-Hyun Rah, and Tae-Young Yoon. Submicrometer elasticity of double-stranded dna revealed by precision force-extension measurements with magnetic tweezers. *Science advances*, 5(6):eaav1697, 2019.

[145] Hang Fu, Chen Zhang, Xiao-Wei Qiang, Ya-Jun Yang, Liang Dai, Zhi-Jie Tan, and Xing-Hua Zhang. Opposite effects of high-valent cations on the elasticities of dna and rna duplexes revealed by magnetic tweezers. *Physical review letters*, 124(5):058101, 2020.

[146] Jan Liphardt, Bibiana Onoa, Steven B Smith, Ignacio Tinoco, and Carlos Bustamante. Reversible unfolding of single rna molecules by mechanical force. *Science*, 292(5517):733–737, 2001.

[147] Andrey Revyakin, Richard H Ebright, and Terence R Strick. Promoter unwinding and promoter clearance by rna polymerase: detection by single-molecule dna nanomanipulation. *Proceedings of the National Academy of Sciences*, 101(14):4776–4780, 2004.

[148] Roberto Benzi, Alfonso Sutera, and Angelo Vulpiani. The mechanism of stochastic resonance. *Journal of Physics A: mathematical and general*, 14(11):L453, 1981.

[149] Roberto Benzi, Giorgio Parisi, Alfonso Sutera, and Angelo Vulpiani. Stochastic resonance in climatic change. *Tellus*, 34(1):10–16, 1982.

[150] Adam Simon and Albert Libchaber. Escape and synchronization of a brownian particle. *Physical review letters*, 68(23):3375, 1992.

[151] Carmen Schmitt, Bartlomiej Dybiec, Peter Hänggi, and Clemens Bechinger. Stochastic resonance vs. resonant activation. *EPL (Europhysics Letters)*, 74(6):937, 2006.

[152] Pierre Jop, Artyom Petrosyan, and Sergio Ciliberto. Work and dissipation fluctuations near the stochastic resonance of a colloidal particle. *EPL (Europhysics Letters)*, 81(5):50005, 2008.

[153] David F Russell, Lon A Wilkens, and Frank Moss. Use of behavioural stochastic resonance by paddle fish for feeding. *Nature*, 402(6759):291–294, 1999.

[154] Mark D McDonnell and Derek Abbott. What is stochastic resonance? definitions, misconceptions, debates, and its relevance to biology. *PLoS computational biology*, 5(5):e1000348, 2009.

[155] D Petracchi, M Pellegrini, Mario Pellegrino, M Barbi, and F Moss. Periodic forcing of a k+ channel at various temperatures. *Biophysical journal*, 66(6):1844–1852, 1994.

[156] Milena Grifoni and Peter Hänggi. Coherent and incoherent quantum stochastic resonance. *Physical review letters*, 76(10):1611, 1996.

[157] Dirk Witthaut, F Trimborn, and S Wimberger. Dissipation-induced coherence and stochastic resonance of an open two-mode bose-einstein condensate. *Physical Review A*, 79(3):033621, 2009.

[158] Hendrik Anthony Kramers. Brownian motion in a field of force and the diffusion model of chemical reactions. *Physica*, 7(4):284–304, 1940.

[159] Thomas Wellens, Vyacheslav Shatokhin, and Andreas Buchleitner. Stochastic resonance. *Reports on progress in physics*, 67(1):45, 2003.

[160] Norbert Wiener. Generalized harmonic analysis. *Acta mathematica*, 55(1):117–258, 1930.

[161] Mark EJ Newman and Gerard T Barkema. *Monte Carlo methods in statistical physics*. Clarendon Press, 1999.

[162] Bikas K Chakrabarti and Muktish Acharyya. Dynamic transitions and hysteresis. *Reviews of Modern Physics*, 71(3):847, 1999.

[163] Mark Galassi, Jim Davies, James Theiler, Brian Gough, Gerard Jungman, Michael Booth, and Fabrice Rossi. Gnu scientific library reference manual (network theory ltd., 2009). *URL http://www. gnu. org/s/gsl*, 103, 2009.

[164] Peter Jung and Peter Hänggi. Stochastic nonlinear dynamics modulated by external periodic forces. *EPL (Europhysics Letters)*, 8(6):505, 1989.

[165] Luca Gammaitoni, Peter Hänggi, Peter Jung, and Fabio Marchesoni. Stochastic resonance. *Reviews of modern physics*, 70(1):223, 1998.

[166] NG Stocks. A theoretical study of the non-linear response of a periodically driven bistable system. *Il Nuovo Cimento D*, 17(7):925–940, 1995.

[167] Rainer Hegger, Holger Kantz, and Thomas Schreiber. Practical implementation of nonlinear time series methods: The tisean package. *Chaos: An Interdisciplinary Journal of Nonlinear Science*, 9(2):413–435, 1999.

[168] George Miloshevich, Ramaz Khomeriki, and Stefano Ruffo. Stochastic resonance in the fermi-pasta-ulam chain. *Physical review letters*, 102(2):020602, 2009.

[169] John F Lindner, Barbara J Breen, Meghan E Wills, Adi R Bulsara, and William L Ditto. Monostable array-enhanced stochastic resonance. *Physical Review E*, 63(5):051107, 2001.